UNIVERSITY OF CAPE COAST

NUMERICAL STUDIES OF TEMPERATURE CHANGES IN ADULT

AND PAEDIATRIC PATIENTS IN BRAIN MAGNETIC RESONANCE

IMAGING

CHRISTIANA SUBAAR

2019

© Christiana Subaar

University of Cape Coast

UNIVERSITY OF CAPE COAST

NUMERICAL STUDIES OF TEMPERATURE CHANGES IN ADULT

AND PAEDIATRIC PATIENTS IN BRAIN MAGNETIC RESONANCE

IMAGING

BY

CHRISTIANA SUBAAR

Thesis submitted to the Department of Physics of the School of Physical Sciences, College of Agriculture and Natural Sciences, University of Cape Coast, in partial fulfilment of the requirements for the award of Doctor of Philosophy degree in Physics

DECEMBER 2019

DECLARATION

Candidate's Declaration

I hereby declare that this thesis is the result of my own original research and that no part of it has been presented for another degree in this university or elsewhere.

Candidate's Signature................................   Date:.............................

 Name: Christiana Subaar

Supervisors' Declaration

We hereby declare that the preparation and presentation of the thesis were supervised in accordance with the guidelines on supervision of thesis laid down by the University of Cape Coast.

Principal Supervisor's Signature...................................   Date:..................

Name: Dr. Joseph Kwabena Amoako

Co-Supervisor's Signature..   Date:…................

Name: Dr. Alfred Owusu

ABSTRACT

Magnetic Resonance Imaging (MRI) of the brain has seen a rising clinical request during diagnosis. The ohmic heating of tissue results in rising human temperature during MRI. This may be as a result of the unintentional heating which seems to be an under-appreciated risk especially of high-field-strength MRI. This study modelled Penne's bio-heat equation and used Matlab programming language to predict in-vivo power deposition in brain tissues during brain MRI of Radiofrequency (RF) above 100 kHz. Experimental thermal dosimetry was carried out on 114 patients. These patients were referred for (head) brain MRI at field strength of 0.3 tesla and 1.5 tesla at the same scanning protocols of specific absorption rate (SAR) of 3.2 W/kg. The experimental results showed that the highest change in temperature of 0.3 tesla is 1.2 °C and 1.5 tesla is 1.9 °C. The average change confirmed that the temperature distributions during MRI do not correlate well with SAR limit but rather showed a positive correlation with patients' body mass index, scan duration and the field strength. The lowest temperature during MRI from the simulated results was 37.5 °C and the highest temperature was 42.5 °C during brain scan of duration less than sixty minutes; this revealed that brain temperature increased as scan duration increased. The highest estimated brain temperature during brain MRI of the study was 43 °C and this depicted brain hyperthermia since the temperature value was above 41 °C. This might contribute to the causes of profuse localize sweating of some patients during MRI in the acceptable ambient MRI environment. It is, therefore, recommended that continuous temperature monitoring during MRI scan should be the most paramount, particularly if the scan durations are prolonged.

KEY WORDS

Brain

Hyperthermia

Imaging

Magnetic resonance

Patients

Temperature

ACKNOWLEDGEMENTS

I am indebted to the Ghana Education Trust Fund (GETFund) for the financial support to this work. My heart felt gratitude goes to my Principal Supervisor, Dr. J. K. Amoako, the Deputy Director of Radiation Protection Institute for his mentorship since my master's degree. I would like to thank my Co-Supervisor, Dr. A. Owusu, Senior Lecturer at the University of Cape Coast for his professional guidance, encouragements and the goodwill with which he guided this work. Without my supervisors' guidance and advice, it would not have been possible to complete this Doctoral studies. I would like to thank the current Head of the Department of Physics, Prof G. Amoako and the former Heads of the Department of Physics, Prof. M. J. Eghan and Dr. B. Anderson in the course of my Doctoral studies for their advice and directions. Not forgetting, Dr. K. A. Dompreh for his suggestions and encouragement, Prof. J. J. Fletcher for his advice, and Prof. Mary Boadu, the Director of Radiological and Medical Sciences Research Institute at Ghana Atomic Energy Commission for her directions and motherly love showed to me during my studies.

I would also like to thank my family for their support, my friends and loved ones, especially, Mr. Stephen Dery Ziniyel, Rev. Fr. Beyuo Christopher, Rev. Fr. Akapata Isaac Anyayanibe Gaylord for their support. Last but not the least, my special thanks go to the staff of the MRI Unit at the 37 Military Hospital and Diagnostic Centre Limited, East Legon, Ghana. I would also like to thank the entire staff of St. John Bosco's College of Education, Navrongo for their encouragement and support, and all my other family members at Nandom-Poffien in the Upper West Region for their financial support.

DEDICATION

To all my family members and loved ones

TABLE OF CONTENTS

LIST OF TABLES

LIST OF FIGURES

LIST OF ACRONYMS

3D	Three Dimensional
ACR	America College of Radiology
BBB	Blood-Brain Barrier
BMI	Body Mass Index
BTBS	Brain Temperature Before MRI Scan
BTDS	Brain Temperature During MRI Scan
CNS	Central Nervous System
CSF	Cerebrospinal Fluid
DNA	Deoxyribonucleic Acid
ECC	Eddy Current Correction
EM	Electromagnetic
EMR	Electromagnetic Radiation
FDA	Food and Drug Administration
FDM	Finite Difference Method
FDTD	Finite-Difference Time-Domain
FH TBS	Forehead Temperature Before MRI Scan;
FH TDS	Forehead Temperature During MRI Scan
FH TDS	Temperature During MRI Scan
FLAIR	Fluid Attenuated Inversion Recovery
IRT	Infrared Thermography
LCT	Liquid Crystal Thermometer
LCTG	Liquid Crystal Thermograph
MHRA	Medicine and Healthcare Product Regulatory Agency

MR	Magnetic Resonance
MRI	Magnetic Resonance Imaging
NRPB	National Radiological Protection Board
NSA	Number of Signal Average
PBHE	Penne's Bio-Heat Equation
RF	Radiofrequency
SAR	Specific Absorption Rate
SCENIHR	Scientific Committee on Emerging and Newly Identified Health Risks
SD	Scan Duration
SNR	Signal-to-Noise Ratio
TAS	Temperature After MRI Scan
TBR	Temperature Before Recovery
TBS	Temperature Before MRI Scan
TBS	Temperature Before Scan
TBS	Temperature Before Scan
USFDA	United State Food and Drug Administration
WHO	World Health Organization
ΔFHT	Change in Forehead Temperature

LIST OF SYMBOLS

A_{eff}	effective area
B_1	radiofrequency magnetic fields
C_t	specific heat capacity of tissue (J/kg K)
ΔE	atomic energy difference
σ	conductivity in (S/m)
∂	rate of change
$\dfrac{\partial T}{\partial t}$	rate of temperature rise
E	electric field (V/m)
hf	radiofrequency pulse energy
S	rate of energy storage
ARF	rate of heat entering bounding surface
C_{bl}	specific heat of the blood (J/kg $^{o}C^{-1}$)
$\dfrac{\partial B}{\partial t}$	time-varying magnetic field gradients
γ	gyromagnetic ratio
T_{art}	arterial temperature
T_{en}	environmental temperature
V_b	volumetric flow rate of blood (m^3 s)
W_b	energy transported by bloodstream
ρ_{bl}	density of blood (kg/m^3)
ρ_t	density of tissue (kg/m^3)
f	frequency

H_{lost}	total heat lost due to the environment
h	heat transfer coefficient
h_C	heat convection
h_E	heat evaporation
h_R	heat radiation
B_o	main magnetic field
∂T_{max}	maximum rise in temperature
H_{lost}	total heat lost
p_{air}	partial pressure of water vapour
p_{skin}	vapour pressure of sweat at skin temperature
T	temperature of patients (^{o}C)
T_{air}	ambient air temperature
T_{skin}	temperature ofd the skin
ΔT	Change in temperature (^{o}C)
C	Specific capacity of head tissues (Jkg^{-1} ^{o}C^{-1})
C_{pbl}	specific capacity of the blood (Jkg^{-1} ^{o}C^{-1})
k_t	thermal conductivity of head tissues (Wm^{-1} ^{o}C^{-1})
Q_m	metabolic energy generated in the head tissues (W/m^3)
Q_r	external heating source
T	tissue temperature (^{o}C)

LIST OF PHYSICAL CONSTANTS

Planck's constant (h) 6.626×10^{-34} J S

Stefan-Boltzmann (σ) 5.67051×10^{-8} W / (m$^2 \cdot$ K^4)

Emissivity (ε)   0.97

Acceleration due to gravity (g) 9.8 m/s^2

CHAPTER ONE

INTRODUCTION

Magnetic resonance imaging systems provide highly detailed images of tissue in the body. The systems detect and process the signals generated when hydrogen atoms, which are abundant in tissue and have an inherent magnetic moment as a result of their nuclear spin, are placed in a strong magnetic field and excited by a resonant magnetic excitation pulse. For hydrogen nuclei in a typical 0.3 T and 1.5 T magnetic resonance field, the resonant frequency is approximately 12.77 MHz and 63.86 MHz respectively.

Background to the Study

Magnetic resonance imaging has become a significant diagnostic procedure. This is because of its high resolution since Paul Christian Lauterbur and Peter Mansfield, in 1974, independently published work which made the development of MRI possible (Macchia, Termine & Buchen, 2007; Pearson, 2003). Medical imaging is an important component in medicine especially in radiation therapy procedures. The adaptation and integration of imaging into the process of diagnosis in an area of medicine is undergoing rapid development. The use of MRI technique has increased enormously in medical settings among the various imaging modalities such as; X-Ray, Ultrasound, Single Photon Emission Computer Tomography, Computerized Tomography (Kirkham, Emberton & Allen, 2006; Nakada, 2007; Riederer, 2004), since it produces high-quality images of the inside of human body and considerably safer than x-ray or radio-isotopes techniques, despite the risk of MRI thermal injuries have been published (ICNIRP, 2004).

Magnetic resonance imaging have been used in treatment planning processes for better definition of structures and extraction of normal and cancerous organs shape to increase accuracy and precision in the delivery of dose (McRobbie, Moore & Graves, 2017). MRI creates images of human body using the principle of nuclear magnetic resonance. As an imaging technology, MRI has undergone exciting developments of superconductors which make use of strong magnetic fields (Kauffman, 2014). The advance clinical high static magnetic fields for human use are between 0.2 T and 3.0 T (Hoffmann, 2009).

During magnetic resonance imaging, patients are placed in MRI scanner of in-built components which consists of static magnetic fields, faster and stronger gradient magnetic fields, and more powerful radiofrequency transmission coils (McRobbie et al., 2017). Pulsed radiofrequency fields in MRI environment are transmitted readily through free space from the transmitted radiofrequency coil to the patient. The net magnetization vector of the numerous protons in the tissue is excited and rotated based on the relaxation time together with contrast agents to define tumor and organ extent for numerous uses in multiple areas of medicine (McRobbie et al., 2017).

The dangers confronted during MRI emerge primarily from MRI components and some physiological monitoring device of MRI. The radiofrequency coils and the prolonged immobilization of patients to reduce motion artifacts during MRI are also causes of MRI dangers (Shellock, 2000a). During an MRI procedure, most of the transmitted radiofrequency power of MRI of field strength above 100 kHz may increase in concentration of electrical current sufficient to be transformed into heat within the patient's

tissue. This may cause excessive heating and tissue damage as a result of resistive losses since the human body is lossy dielectric by nature (Shellock, 2000b). This tends to absorbed greater portion of radiofrequency fields leading to temperature rise in body (ICNIRP, 2004; Shellock, 2000b) especially if a body part is touching the radiofrequency coil cable.

The primary bio-effects associated with the radiofrequency radiation used for MRI procedures are directly related to the thermogenic qualities of electromagnetic field (Ng, 2003; ICNIRP, 2004; Shellock, 2000b). It is envisage that temperature of body part being scan in MRI environment, due to absorption of Radiofrequency (RF) of Electromagnetic Radiation (EMR), will rise despite the fact that the human body's thermo regulatory mechanism tends to ensure temperature balance in most cases (MHRA, 2015; Ng, 2003). As a result of challenges in measuring temperature increase in-vivo during magnetic resonance imaging, the average change in temperature distribution during MRI is predicted by researchers using numerical method (Kunz & Luebbers, 1993). There are inherent problems associated with recording physiological variables during the operation of MRI scanner. This makes direct measurement of temperature of the human body difficult (Kunz & Luebbers, 1993).

Since magnetic resonance imaging does not use ionizing radiation, it is more suitable for diagnosis in neonates, infants, children and elderly patients. Patients that need magnetic resonance imaging examination present unique problems and are mostly required to stay still for the forty-five to sixty minutes needed to complete one MRI examination. This is a challenge to the requirement of technique in which a drug is used to produce a state of

depression of the central nervous system known as sedation in paediatrics, as well as adults to enable them remain calm during the MRI examination. The number of paediatric and adult patients undergoing MRI as a diagnostic technique has increased dramatically in Ghana with few publications, which includes; temperature changes in the brain of patients undergoing MRI examination and finite difference time domain approach of thermal effects on paediatric patients undergoing MRI in Ghana (Subaar, Amoako, Darko, Ansah-Narh, & Dery, 2014; Dery, Darko, Amoako & Kyere, 2013), available on clinical experience with MRI from Ghana. Temperature increase during MRI as a results of radiofrequency exposure is more directly related to potential hazards (Shellock & Crues, 1988; Ng, 2003). This study therefore numerically predict temperature distribution to create awareness of the potential hazards caused by MRI, one of the electromagnetic device, especially in research setting since 2.5 T field strength is currently in Ghana to be operated.

Statement of the Problem

Magnetic resonance imaging diagnostic test requires prolonged immobilization to acquire images. The total scan time may last less than sixty minutes (Keengwe et al., 1999; Laurence, 2000). The heating effect of radiofrequency fields resulting from induced current can increase body temperature (Shellock, 2000b), especially in children with immature thermoregulation mechanisms (Oh, Webb, Neuberger, Park & Collins, 2010) making them tender to radiofrequency heating. Adult patients with compromised thermoregulatory systems are also at greatest risk. In a worst-

4

case scenario, the heating effect during MRI can cause body part of a patient to burn (Dempsey, Condon & Hadley, 2001; Machata et al., 2009).

The reference levels set on the usage of the RF systems are only external values and do not take account of the way the field develops inside the human body as well as the account of the exposed person during MRI scan (Fields, 1997; Siauve, Scorretti, Burais, Nicolas & Nicolas, 2003). Studies have been conducted on brain temperature changes before and immediately after MRI of the brain, effect of core temperature of paediatrics undergoing MRI (Shellock & Crues, 1988; Subaar, Amoako, Darko, Ansah-Narh & Dery, 2014) and effect of temperature immediately after brain MRI on body core temperature (Dery et al., 2013; Machata et al., 2009). None of the studies, however, examined the real-time measurement of temperature changes during brain MRI in order to justify the relation between the temperature and Specific Absorption Rate (SAR) limits since measurement of the temperature rise in-vivo is difficult.

Electric current produced by the RF pulses has the potential to induce localized burns (Wang et al., 2007), especially, if a body part is touching the RF coil cable during MRI. With the frequency of clinical diagnostic request increasing, it is relevant to continuously show that, there is excessive temperature elevation at the skin surface of the patients due to the ohmic heating of tissue (ICNIRP, 2004). It is also relevant to monitor patients' temperature during MRI scan to avoid hyperthermia that can cause harm by increasing human body temperature and damaging biological organs and tissues of the head.

Purpose of the Study

The numerous methods used in studying temperature change during brain MRI includes experimental temperature measurements of patients undergoing brain MRI (Finelli et al., 2002; Machata et al., 2009; Rezai et al., 2002) and numerical modelling approach to calculate the associated temperature distribution in the brain (Chang & Nguyen, 2004; Collins et al., 2004; Nguyen, Brown, Chang, Krycia & Mirotznik, 2004; Simunic, Wach, Renhart & Stollberger, 1996). The purpose of the study is to numerically model to predict temperature increase in biological tissues of human head during MRI of field strength above 100 kHz. The numerical brain temperature dosimetry will be complemented with the experimental thermal dosimetry carried out at the MRI facilities of field strength 0.3 T (12.77 MHz) and 1.5 T (63.86 MHz) in order to justify the relationship between temperature and SAR limits during MRI.

Main Objective

The main objective of the study is to determine thermal variation of patients undergoing brain MRI examinations.

Specific Objectives

The specific objectives of this thesis are to:

1. Theoretically determine patients temperature using modified classical Penne's Bio-Heat Equation (PBHE)

2. Experimentally measure temperature variation in patients undergoing brain MRI scan at field strength of 0.3 T (12.77 MHz) and 1.5 T (63.86 MHz), respectively.

6

3. Analyze the experimental results graphically and compare with the numerical results.

Significance of the Study

The recommended SAR limitations according to America College of Radiology (ACR) depend on the anatomy being imaged. The SAR limitations during normal mode of MRI operation should not exceed 2 W/kg for whole body and 3.2 W/kg for head, respectively. Also temperature rise due to SAR as a result of pulse sequence should not be more than 1 °C anywhere on the head with the corresponding temperature limit for the torso extremities is 2 °C. Also, pulse sequence must not raise the human core temperature by more than 0.5 °C, as a typical body has daily core temperature fluctuations between 36 to 38 °C (Arens & Zhang, 2006; Athey, 1992; Brück, 1989; Zaremba, 2000), whereas, the body maximum core temperature and local temperature during MRI is 39 °C (Athey, 1992). To accurately measure brain temperature with any non-invasive thermometer, approximately 2 °C must be added to the measured skin temperature in order to estimate core temperature (Dräger, 2014; Liu, Chang & Chang, 2004; Pompei & Pompei, 2004).

The ohmic heating of tissue resulting in rising in human temperature during MRI is greatest at the surface and minimal at the centre of the patient's body (Ng, 2003). This may result in the unintentional heating which seems to be an under-appreciated risk especially of high-field-strength MRI. As a safety issue during brain MRI scan, this work hopes;

I. To modify classical PBHE by taken into account the SAR from MRI scanner.

7

II.   To present numerical estimation of temperature increase during MRI since there are no reliable technique for direct in-vivo temperature measurement during MRI.

III.   To provide real-time information of brain temperature distribution during head MRI and also a better understanding of the relationship between temperature and SAR.

IV.   To obtain data to support the ongoing efforts of the implant industry to produce devices that work in and out of MRI scanners.

Delimitation

This thesis covers only 114 patients undergoing brain MRI in Ghana of field strength 0.3 T and 1.5 T with operating frequencies, 12.77 MHz and 63.86 MHz, respectively, at the 37 Military Hospital and Diagnostic Center Limited both in Accra. A Three-Dimensional (3-D) numerical model will be developed from classical PBHE to predict temperature distribution in patients undergoing brain MRI examinations.

An explicit formula of finite difference time domain and finite difference method equations of classical PBHE will be developed. The central difference will be employed to discretize the heat equations developed whilst Lagrange interpolation scheme will be used to model the time dependence and the time independence equations assuming that the biological tissues of the human brain are homogeneous. The explicit list of element obtained from the linear equations will be solved with a programming language (Matlab version, R2017A) despite the fact that Matlab uses a large amount of memory.

Limitation

According to Nepa (2012) in EMR and biological interactions, the magnetically induced field component of the Electromagnetic (EM) field is size dependent, while the electric coupling is independent of size (Faruque, Islam & Misran, 2010). The temperature distribution along the three dimensions of the head (brain) is size independent. The experimental data were collected from MRI of field strength of 0.3 T and 1.5 T. Physical parameters of the biological tissues that approximate heterogeneous head (brain) structure of a human being will be used in the study, but the solved equations simulated RF of EM field of frequency above 100 kHz of homogeneous tissue inside human brain. Therefore, this study demonstrates that temperature changes by depth within brain depict the heterogeneous nature of head.

Organisation of the Study

The study consists of five chapters. Chapter One gives the introduction of MRI, the operating frequencies of MRI and its heating effects. Chapter Two discusses the basic principles of MRI and reviews the theoretical and experimental methods of thermal dosimetry during brain MRI. Chapter Three deals with brain temperature estimation; this includes the modelled of a 3-D PBHE to predict temperature elevation with the help of appropriate boundary conditions. The forehead and tympanic temperature measurement to validate the numerical study is elaborated. The results and discussions are presented in Chapter Four. Chapter Five provides the summary, conclusions of the study, recommendations and suggestions for further research.

Chapter Summary

Magnetic resonance imaging current operating radiofrequencies are above 100 kHz to energize the magnetization vector in human tissue. The absorption of the radiofrequencies by tissue during MRI converts tissue properties into magnetic resonance images and heat through resistive tissue losses. In Ghana, MRI operating frequencies are 12.77 MHz and 63.86 MHz for 0.3 tesla (T) and 1.5 tesla (T) magnetic fields, respectively, and this leads to significant power absorption and temperature increase in patients. Studies have reported temperature increases after MRI which were all within guidance levels. MRI of the brain has seen a rising clinical request during diagnosis and imaging. This is coupled with a concurring increase in temperature in patients. Temperature increase due to radiofrequency above 100 kHz exposure during MRI is as a result of induced currents. The temperature of patients' brain as a results of induced currents during magnetic resonance imaging of patients placed in MRI scanner of powerful radiofrequency transmission coil will be estimated by accurately measuring brain temperature with any non-invasive thermometer, and approximately 2 °C from literature will be added to the measured forehead skin temperature in order to estimate core brain temperature.

CHAPTER TWO

LITERATURE REVIEW

Introduction

Medical imaging technique, MRI, is an important EM device in medicine which uses RF above 100 KHz. The study quantifies the power deposition in adult and paediatric patients brain MRI by measurement of temperature theoretically and experimentally. In this chapter, the history of MRI, effects of magnetic fields and RF MRI, and thermal effects of MRI will be discussed.

History of Magnetic Resonance Imaging

Magnetic resonance imaging is an imaging technique used primarily in medical settings to produce high-quality images of the inside of the human body. In 2008, magnets of static field strength ranging from 0.3 T to 1.5 T were the clinical standard for routine radiological examinations on humans. Because high-field MRI is a powerful clinical tool for imaging the human body, MRI scan is apparently moving slowly to the use of 3 T magnets (McRobbie et al., 2017; Weiss, Nour & Lewin, 2008).

Today, MRI systems may subject the human body to fields between 3 T and 4 T for a short period of time, although 1.5 T and below 1.5 T MRI systems has been used for clinical imaging for two decades ago (Habash, 2007). Clinical MRI systems with magnetic field (B_o) of 1.5 T and 3 T systems are becoming increasingly widespread in clinical practice, offering a higher Signal-to-Noise Ratio (SNR) and thus higher spatial resolution (Hu & Norris, 2004; Oshinski, Delfino, Sharma, Gharib & Pettigrew, 2010). Commercially available 0.2 T to 0.5 T systems based on permanent magnets

11

offer both lower cost and wider patient aperture than their higher field counterparts at the expense of spatial resolution (Inglis et al., 2013; Macovski & Conolly, 1993).

Despite the fact that an MRI has been in clinical use over thirty years, its use and availability in Ghana, a West Africa state, being the third country to have acquired it in Africa, after Egypt and South Africa, is still extremely low, hence only a few publications are available on clinical experience with MRI from Ghana. Ten MRI centres are established in regional hospitals in Ghana to render health care delivery across the world. This is to benefit most especially neighbouring countries such as Burkina Faso where patients would find it convenient accessing the MRI services than having to travel to South Africa, Egypt or Europe (Mordy, 2012).

Basic Principle of Magnetic Resonance Imaging

Magnetic resonance imaging systems use a magnetic field illustrated by lines of force as shown in Figure 1 and always exists when there is a flow of an electric current. It employs the elementary particles, neutrons and protons of nucleus of an atom that have odd numbers (Bushong & Clarke, 2014; Hartwig et al., 2009).
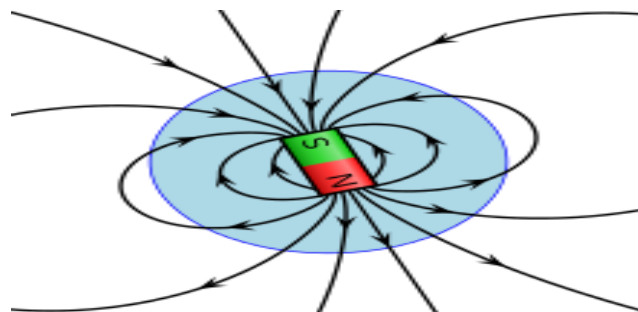
Figure 1: Magnetic Field Illustrated by Lines of Force.

Source: (Bushong & Clarke, 2014).

Nuclear Spin and Magnetic Moment

The common particles used in MRI, includes; ^{1}H, ^{13}C, ^{23}Na, and ^{31}P. These particles have an intrinsic quantum mechanical angular momentum called spin (Blink, 2004; Bushong & Clarke, 2014; De Graaf, 2013; Levitt, 2001; Plewes & Kucharczyk, 2012). Most tissue of the human body is largely composed of 70 % to 90 % of water molecules (Heymsfield, 2005; Moritani, Ekholm & Westesson, 2009; Wang, Pierson & Heymsfield, 1992). The properties and amount of water in tissue can greatly be altered with disease and injury which makes Magnetic Resonance (MR) very tender as a diagnostic technique. MRI detects subtle changes in the magnetism of the nucleus, the tiny entity that lies at the centre of the atom (McRobbie et al., 2017; Hilschenz et al., 2013).

The part of a body (brain) to be imaged is placed in MRI scanner whose B_o is always in the z-direction as shown in Figure 2. (Dechent, Buljubasich, Schreiber, Spiess & Münnemann, 2012; Pacetti, 2003).
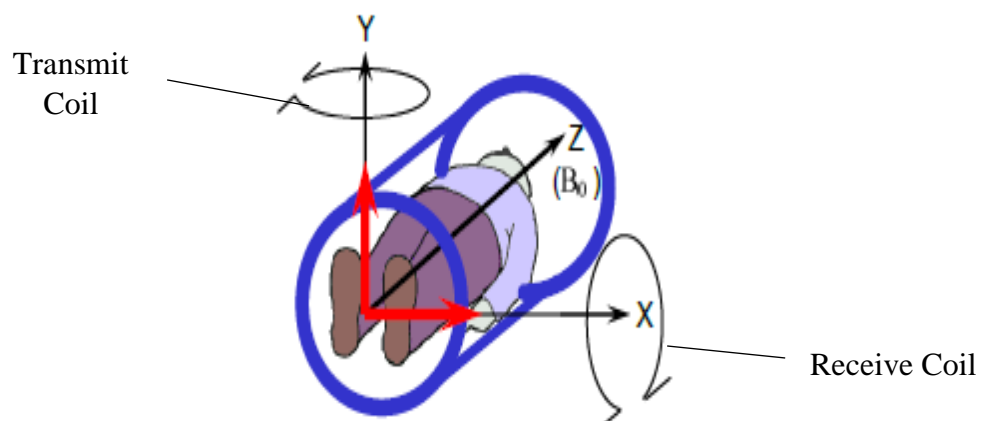
Figure 2: The Human Body to be Imaged is Placed in MRI Scanner.

Source: (Pacetti, 2003).

The hydrogen (^{1}H) nucleus consists of a single proton and has the largest gyromagnetic ratio of 42.57 MHz / Tesla, which is taken as the MR

13

imaging source (Blink, 2004; Dale, Brown & Semelka, 2015; Plewes & Kucharczyk, 2012). Some of the hydrogen protons spin up (parallel to B_o) and some spin down (anti-parallel B_o) when in alignment with B_o. The atomic energy levels at the difference in energy, ΔE, between spin up and spin down is proportional to the total B_o at the nucleus as shown in Equation (1) (Dixon & Ekstrand, 1982; Levitt, 2001)

$$\Delta E = \gamma.B_o \tag{1}$$

Where ΔE, is the atomic energy levels at the difference in energy, γ is the gyromagnetic ratio of the atom and B_o is the main (static) magnetic field.

Magnetic resonance image is obtained by exciting the tissue magnet with an RF pulse through the transmit coil, and the RF pulse is received for image constructions through receive coil as shown in Figure 2 (Callaghan, 1993; Kuperman, 2000). A radiofrequency pulse energy (hf) of EMR frequency (f) that corresponds precisely to the energy difference between the two energy levels as shown in Equation (2), is applied to the body tissue (brain) (Brown, Haacke, Cheng, Thompson & Venkatesan, 2014; McCarthy, 1994)

$$hf = \Delta E = \gamma.B_o \tag{2}$$

The photons of the RF beam are absorbed and exciting many of the nuclei from the lower state to the upper state. When significant absorption of RF occurs the proton precess at Larmor frequency, f, of a given field strength B_o when the applied RF is absorbed as shown in Equation (3).

$$f = \frac{\gamma.B_o}{h} \tag{3}$$

14

where the frequency f is proportional to the magnetic field, B_o and Planck's constant (h) = 6.626 x 10^{-34} J S (Barentsz, Debruyne & Ruijs, 1990; Bushong & Clarke, 2014; Inglis et al., 2013).

The Larmor equation expresses a connection between the resonance frequency and the magnetic field. Therefore, the resonance frequency for protons in 0.3 T scanner is 12.77 MHz and 1.5 T is 63.86 MHz (Bitar et al., 2006; Hansson-Mild et al., 2009).

Magnetic Resonance Imaging of the Brain

Magnetic resonance imaging of the brain is the most commonly performed examination. During brain MRI it requires patients to stay still up to one hour or more in a noisy and claustrophobic environment. High-resolution brain image is achieved to reflect a large amount of information of this complex organ (Földes, 2016; Machata et al., 2009; McRobbie et al., 2017). The contrast in an MR image is controlled by the choice sequence and sequence parameters. The most basic examination consists of a sagittal T1-weighted, axial proton density and axial T2-weighted images. An improvement in T2-weighted images known as FLAIR (Fluid Attenuated Inversion Recovery) has become popular for being able to visualize the periventricular tissues without interference from bright Cerebrospinal Fluid (CSF) (Hansson-Mild et al., 2009; Lu et al., 2005).

Diffusion imaging is also popular because of its exquisite sensitivity to ischaemic injuries. These allow cellular fluids to diffuse through cell membranes. For some specific conditions, it may be useful to obtain additional images at higher resolution through a specific region of interest, such as the brainstem, or specific cranial nerves such as the cochlear nerve or optic nerve

15

(Romero, Schaefer, Grant, Becerra & González, 2002; Schaefer, Grant & Gonzalez, 2000).

Sagittal T2-weighted images are used for the optimal definition of the characteristic T2 bright changes of multiple sclerosis. Post gadolinium T1-weighted images typically acquired in axial and coronal planes give the greatest sensitivity for detecting pathological processes that break down the normal Blood-Brain Barrier (BBB) (Hansson-Mild et al., 2009). Tumours, infection, and inflammation all break down the BBB and light up vividly on post-gadolinium T1-weighted images. Accordingly, gadolinium is particularly useful when these are suspected. For patients with cancer, post-gadolinium imaging is essential for the optimal detection and characterization of metastatic disease. It helps to determine the extent of primary tumour growth and the precise boundary between normal and neoplastic tissue (Hansson-Mild et al., 2009).

Effects of Magnetic Fields during Magnetic Resonance Imaging

Individuals being scanned and those in the immediate vicinity of MRI equipment are exposed to three diverse magnetic fields, simultaneously (Buchli, Saner, Meier, Boskamp & Boesiger, 1989). These are;

I.   The static magnetic field (B_o)

II.   Time-varying magnetic field gradients $\left(\dfrac{\partial B}{\partial t} \right)$

III. Radiofrequency magnetic fields (B_1).

These three different magnetic fields are used in creating an image based on magnetic resonance. Concerns for patients safety have been raised in each of

16

the three distinct fields used in MRI (Crow, 2000; Kanal et al., 2007; MHRA, 2015; Shellock, 2000a).

Safety Issues Concerning Static Magnetic Fields

The magnet is the largest component of an MRI system which creates the external field to align the MR signal from hydrogen nuclei found in the water molecules in patient's body (Bushberg & Boone, 2011; Lucas et al., 2006). A large field produces a high degree of alignment and thus a large magnetization gives better SNR (Hansson-Mild et al., 2009). The strengths of the static magnetic fields used in clinical and research range from 0.012 T to more than 10 T compared to the 50 mT of the earth magnetic field (Ng, 2003). The clinical base for safety is a static magnetic field strength of up to 2 T. However, above this level, facts and proves of safety must be issued by the sponsor or device manufacturer in advance to routine clinical use (Shellock, 1994).

The two major safety issues regarding the use of MRI are the attraction of ferromagnetic material towards the magnet and biological changes (Ng, 2003). The principal interactions of the body and its functions are the creation of electrical potentials resulting currents generated by body movements. Also, there is possible displacement of naturally generated currents within the body (MHRA, 2015; Bryan, Templeton, Nick, Szafran & Tung, 2006; Machata, Willschke, Kabon, Prayer & Marhofer, 2009). Amendment conclusions regarding the static field current information does not indicate any serious health effects resulting from acute exposure to static magnetic fields up to 8 T. It should be noted, however, that such exposures can lead to potentially

17

unpleasant sensory effects such as vertigo during head or body movement (ICNIRP, 2009).

The very high degree of patient safety in strong magnetic fields is attributed to the small value of the magnetic susceptibility of human tissues and to the lack of ferromagnetic components in these tissues. At very high field strengths there is considerable evidence for mild sensory effects such as vertigo, metallic taste, and magnetophosphenes, but there is no evidence that these effects are at all harmful. These effects, vertigo, in particular, can be reduced by moving patients slowly while they are in regions of very strong fields (Schenck, 2000). Physical movement within a static field gradient is reported to induce sensations of vertigo and nausea, and sometimes phosphenes and a metallic taste in the mouth, although only transient, such effects may adversely have effects on eye-hand coordination on people (MHRA, 2015).

Safety Issues Concerning Time-Varying Magnetic Field Gradients

The gradient magnetic field produces different resonant frequencies for aligned protons, depending on their spatial positions on the gradient axes (Hendee & Morgan, 1984). The part of the body to be imaged is exposed to rapid variations of magnetic fields due to the transient application of time-varying gradient magnetic fields during the imaging sequence to obtain three dimensional MRI images (Jagannathan, 1999). In MRI, three orthogonal magnet1ic field gradients are switched on and off to select the region of diagnostic interest and to spatially encode the MR signals. As a general guide, the faster the imaging or spectroscopy sequence, the greater the rate of change

18

of the gradient fields used and the resultant current density induced in the tissue (MHRA, 2015).

The main safety concerns with the time-varying magnetic field gradients are biological effects and acoustic noise (Ng, 2003). As the gradient coils are switched on and off during image acquisition, loud tapping, knocking, or chirping sounds are generated in the core of the magnet. Temporary hearing loss has been reported (McJury & Frank, 2000). Time-varying EM fields exposed to the human body can lead to induced electric currents that probably affects the normal function of nerve cells and muscle (Bourland et al., 1996; MHRA, 2015; Recoskie, Scholl, Zinke-Allmang & Chronik, 2010). The sensation of flashes of light caused by induced electric currents stimulates the retina, peripheral nerves, muscles and blood valves. A more serious response to electric currents flowing through the body is that of cardiac stimulation or even ventricular fibrillation are possible (Jamieson, 2014; Ng, 2003).

The body is most sensitive to fibrillation at frequencies between about 10 Hz and 100 Hz and to peripheral nerve stimulation at up to about 5 kHz. Above these frequencies, nerve and muscle cells become progressively less responsive to electrical stimulation. At frequencies above 1 MHz, a reactive element begins to be significant and at frequencies above about 30 MHz, the wavelength begins to influence the electric field and current distribution (Demers et al., 2014; Ng, 2003). The rapidly changing fields induced by the high rates of gradient field used in MRI systems will preferentially stimulate peripheral nerves. Hence, limiting exposure of patients and volunteers to high

rates of gradient fields can minimize any uncomfortable or painful sensations caused by the field (ICNIRP, 2009; Schaefer, Bourland & Nyenhuis, 2000).

Safety Issues Concerning Radiofrequency Magnetic Fields

During MRI the radiofrequency magnetic field (B_1) is centered at the net magnetization, M, to excite and rotate it away from equilibrium with B_o so that it no longer points along the magnetic field. The net magnetization precess around the field with a frequency of 12.77 million rotations per second at 0.3 tesla and 63.86 million rotations per second at 1.5 tesla which eventually return to equilibrium as soon as the radiofrequency pulse is switched off. The time during which the magnetization vector returns to the equilibrium is different for each tissue (Buonocore & Maddock, 2015; Kuperman, 2000).

Absorption of energy from radiofrequency fields used in MRI results in the increased oscillation of molecules and the generation of heat. The transfer of energy from the RF pulse to the magnetic moments may penetrate the surface of the body and become absorbed by the tissue. The excess energy may be dissipated in the form of heat within the patient's body and, if not regulated, could cause extensive heating. This can results in increasing core body temperature or cause localized heating and possible tissue damage (Adair & Black, 2003; Demers et al., 2014; Schwan & Piersol, 1955; Simon, 1993). Hence the main safety issues for RF fields used in MRI is thermal heating (Repacholi, 1998) leading to heat stress, induced current and contact burns and this can be quantified through theoretical and experimental studies (MHRA, 2015; Schenck, 2000). At all frequencies, induced currents will lead to power dissipation within the body's tissues, which in turn will lead to accumulation of energy with time and a rise in body temperature (MHRA, 2015).

20

Three different quantities are commonly used in dosimetry. At low frequencies below 100 kHz, many biological effects are quantified in terms of the current density. At frequencies above 0.1 MHz, heating effects predominate and this is the major consequence for MRI (Barnes & Greenebaum, 2006; Levine et al., 2007; MHRA, 2015). The RF field distribution is not uniform. The decrease of RF field homogeneity may be as a result of shorter penetration distance or skin depth (Alsop, Connick & Mizsei, 1998), also inhomogeneity increases with increasing field strength and may depend on coil design (Nepa, 2012).

The thermal characteristics differ in different organs. The actual temperature rise at any time will depend on the balance between the energy absorbed and the energy transferred from the region of the body concerned (MHRA, 2015). Normal brain functioning largely depends on maintaining brain temperature. A study conducted by Zhu, Ackerman, Sukstanskii & Yablonskiy, (2006) on how the body controls brain temperature reported that brain-temperature profile is exponentially defined by a characteristic temperature shielding length, with cooler peripheral areas and a warmer brain core approaching body temperature. Also Mcilvoy (2004) study conducted on comparison of brain temperature to core temperature; a review of the article, demonstrated that brain temperatures have been found to be higher than core temperatures. According to Mellergård (1994, 1995), Mellergard and Norstrom (1990), Mellergård & Nordström, (1991), the temperature within brain varies by depth and temperature measured in epidural space is lower than temperatures measured in lateral ventricle. Also, the eyes are organs that

have very little blood flow. The lens of the eyes have no blood flow and therefore takes time to disperse thermal energy (MHRA, 2015).

The BBB physiologically, is a barrier that serves as an interface between the brain and the blood (Hitchcock & Patterson, 1995) which separates the brain and cerebral spinal fluid of the Central Nervous System (CNS) from the blood. Permeability of BBB is highly temperature dependent (Kiyatkin & Sharma, 2009). Brain cells are exceptionally sensitive to thermal damage. Normothermic values of brain cell is in the range of 34.2–38 ^{o}C, slightly higher 2–4 fold at hypothermic values 32.2–34.2 ^{o}C, and dramatically higher at hyperthermic values 38–42.5 ^{o}C (Ga, Mamoon, Schlapfer & Tobias, 1972). Brain hyperthermia may lead to the disruption to the BBB resulting in serious consequences for health. The BBB may break down following brain heating allowing enough concentrations of blood-borne neurotoxins such as urea to enter the brain (Habash, Bansal, Krewski & Alhafid, 2007).

The temperature threshold to produce progressive thermal injury to the metabolically active brain cells, BBB, and the vascular endothelium appears to be between 39 and 40 ^{o}C (Bechtold & Brown, 2003; Kiyatkin & Sharma, 2009; Sharma & Hoopes, 2003). Concerns regarding hazards of EM radiation of high RF, several studies indicated that EM fields influence the physiology of the human CNS. Resulting effects of EM exposure which have been reported in the scientific literature include memory loss, learning impairment, headaches and fatigue, sleep disorders and neurodegenerative conditions (Habash et al., 2007).

Interaction of Biological Tissue with Radiofrequency

Interaction of radiofrequency fields with biological tissue can involve either electric or magnetic fields. The interaction mechanisms have been considered thermal and non-thermal, but it has not been established that any of these could result in adverse health effects at radiations levels below guidelines (Challis, 2005). The energy of photons of RF fields is unable to disrupt the weakest chemical bonds and to create free radicals. It is in contrast with ionizing radiation (Pattanaik, 2012). RF fields can interact with biological systems by exerting forces on charges in tissues. These forces act in the presence of random thermal agitation. The absorbed power in tissues generate heat and increase the local temperature and hence affect the biological system (Habash et al., 2007).

An additional heat load on the body due to exposure to RF energy can also elicit effects due to thermoregulatory responses. The basal metabolic rate in human is about one watt per kilogram of the body mass (Browning, Baker, Herron & Kram, 2006; Browning & Kram, 2005). Addition of heat by an RF field at levels comparable to or above the metabolic rate in human can produce significant physiological effects (Foster, 2000; Pattanaik, 2012).

The human body is affected by two mechanisms during RF exposure at different frequencies. These are:

I.   Heating which may lead to serious burning.

II.   Induce electric and magnetic currents that can affect the normal current of heart or CNS.

Therefore the biological effects of RF can be categorized into thermal effects and non-thermal effects (Lak, 2012; Siqueira, Ornetta & Skvarca, 2000).

23

Non-Thermal Effects

The non-thermal effects of RF radiation exposure are becoming important measures of biological interaction with EM fields. It responses of RF can be less noticeable and are often more difficult to explain than thermal effects of RF. These responses are related to the disturbances in the tissue not caused by heating (Bolen, 1994; Siqueira et al., 2000). Non-thermal disruptions have been observed to occur at power density levels that are much lower than SAR levels necessary to induce thermal effects, causing stress and trauma to biological systems. EM fields can interact with the bioelectrical functions of the irradiated human tissue (Dwyer & Leeper, 1978a; 1978b)**.** Research conducted in the Soviet Union and Eastern Europe in 1980 placed a great emphasis on non-thermal effects of biological exposure to RF radiation. They contend that EM interactions with the bioelectrical and biochemical functions of the body constitute a more serious health risk than effects from thermal heating.

Dielectric Properties of a Biological Tissues

The dielectric properties of biological tissues are a measure of the interaction of EMR with its constituents at the cellular and molecular level (Foster & Schwan, 1995). The EM field in biological tissues depends on the spatial distribution and size of the dielectric properties of tissues. The optimum parameter of the dielectric shield greatly depends on the operating frequencies. An accurate knowledge of in-vivo dielectric properties of the tissues and organs in the body is crucial. The dielectric properties of various human tissues help to accurately determine the absorbed power and its spatial distribution during the application of biomedical devices that uses EM

radiation for evaluation of potential hazards to humans (Foster & Schwan, 1995; Gabriel, Lau & Gabriel, 1996; Wessapan, Srisawatdhisukul & Rattanadecho, 2012). The understanding of dielectric properties of biological tissues is based on experimental data forming part of a well-established classical theory of bioelectrical phenomena (Foster & Schwan, 1989). It is high frequency and temperature dependent (Davarcioglu, 2011).

The biological effects that an electric field with a frequency below 1-10 MHz causes to a cell are likely due to interaction mechanisms occurring in the cell membrane. For frequencies above 1-10 MHz, the effects are likely due to interaction mechanisms occurring in the intracellular compartment (Zhang, Yarema & Xu, 2017). Electrical conductivity and permittivity are necessary in calculation of RF power deposition (Collins & Smith, 2001). These vary with the type of body tissue and also depend on the frequency of the applied field.

Electric fields external to the body induce a surface charge on the body and this results in induced currents in the body. The distribution of the power deposition due to the induced current depends on exposure conditions, size and shape of the body and body's position in the field. Therefore, credible database of dielectric properties of tissue is vital (Davarcioglu, 2011; Meredith, 1998). The dielectric properties such as dielectric constant and conductivity of tissues are water content dependent and are determined by the dominant and varies depending on the temperature (Foster & Schwan, 1989; Vander-Vorst, Rosen & Kotsuka, 2006).

In the literature, data on specific conductivity and relative permittivity only at frequencies above 100 Hz exist. For most tissues, data below 100 Hz are very scarce or do not exist at all. Between 100 Hz and 100 kHz, most

tissues, with the exception of the anisotropic tissues, show almost no frequency-dependence (Inoue, Pethig, Al-Ameen, Burt & Price, 1988).

Thermal Effects

The human body tissues have permittivity, conductivity, and permeability dielectric property where EM fields can be absorbed by human tissues and induce conduction and displacement currents. Thermal mechanisms arise from the deposition of power in the biological systems. The duration of exposure can influence the rate of cooling of the tissue by blood flow and this can lead to temperature increase which depends on SAR (Pattanaik, 2012; Qian, El-Sharkawy, Bottomley, & Edelstein, 2013). The heating is two types: dielectric heating occurs at relatively low frequencies from several kHz to MHz and induction heating occurs at a higher frequency from RF to microwaves (Flugstad et al., 2004; Lak, 2012).

At frequencies above 0.1 MHz, heating effects predominate and this has a major consequence for MRI (MHRA, 2015). The RF field distribution is not uniform (Kangarlu, Shellock & Chakeres, 2003). Inhomogeneity increases with increasing field strength and depends on the physical dimensions and geometry of the human body and coil design (Bolen, 1994). Absorption of energy from RF fields used in MRI results in the increased oscillation of water molecules and protein throughout the irradiated tissue area, as a result, generates heat (Bolen, 1994). If this occurs in human tissue, a compensatory dilation of blood vessels results in an increase in blood flow and the removal of the excess heat. The heat dissipated mainly through the skin as compared to heat experience from sunlight which is one of the most familiar forms of non-ionizing radiation (Habash et al., 2007).

The local heating effects during MRI in tissue can become significant and even can cause damage (Bolen, 1994; Luechinger et al., 2004). These include a variety of biological changes and at sufficient heating, tissue damage can occur (Pattanaik, 2012). The configuration of exposure source, dielectric properties of human tissue, age of the patients undergoing MRI, exposure environment, field strength of the RF, scan duration, geometry and size of tissue to be imaged, orientation and field polarization are some of the many factors that influence the interaction between EM fields and human tissues (Johnson & Guy, 1972). The increment of temperature during exposure to RF depends on the intensity of field strength, duration of exposure, the specific area of the body exposed and the efficiency of heat elimination (Habash, 2007; Lai, 2005). The human eye is relatively a small and very complex optical organ of the human head (Karunarathna & Dayawansa, 2006). Temperature changes can affect the eye tissues in several ways (Gokul, Gurung & Adhikary, 2013). The lens of the eyes has no blood flow and therefore takes time to disperse thermal energy. Clinical studies indicate that exposure to radiofrequency and microwave radiation causes physiological damage to the eye that can result in loss of sight (Bolen, 1994; Gokul et al., 2013).

The degree of RF tissue absorption that contribute to the undesired side effect, thus temperature rise in the human body during MRI, depends on thickness of skin and subcutaneous tissue, RF coil configuration, the pulse sequence that is being used, the body composition and orientation (Athey, 1992; Chen & Steckner, 2017; Liu, 2012; Nguyen, Brown, Chang, Krycia & Mirotznik, 2003). Heat regulation in the human body is characterized by conduction, convection, radiation, as well as blood perfusion, metabolism and

27

evaporation (Gokul et al., 2013; Werner, 1977). The human body's thermoregulatory mechanism tends to ensure temperature balance in most cases. High RF levels can lead to tissue damage and other adverse health effects. These occur when the rate of energy absorption exceeds the rate of energy dissipation and the body is not able to cancel the high temperature of tissues by the normal biological activity of the body, such as the blood flow and sweating (Karunarathna & Dayawansa, 2006; Michaelson, 1982). Some researchers have shown that the biological mechanism, such as BBB, Deoxyribonucleic Acid (DNA) strand breakage, cancer, brain tumor, buzzing in the ears may occur (Habash et al., 2007).

Thick and fatty (more water content) tissues allow EM waves to penetrate into them more than thin tissues. When the absorbed energy in the human body is converted to heat, thermal effects occur. Also when the human body is exposed to an electromagnetic source, the body temperature of exposed tissue rises from its normal value and biological effect can occur (Hand & Haar, 1981). It is noticeable that by increasing in frequency of RF fields, the SAR and the heating are increased too (Nguyen et al., 2003; 2004).

Non-Ionizing Radiation Dosimetry

Electromagnetic modelling is being used to accurately measure or calculate the induced current density, SAR, as well as temperature distributions in human tissue exposed to EM fields to address safety challenges in MRI devices in our society (Chen & Steckner, 2017; Van Leeuwen et al., 1999). At EM radiation of frequencies below approximately 100 kHz, many biological effects are quantified in terms of the current density in tissue and this parameter is most often used as a dosimetric quantity (Nepa,

28

2012). At higher frequencies of radiation, many but not all interactions are due to the rate of energy deposition per unit mass. SAR is used to monitor the heating of patients during MRI (Angelone, Ahveninen, Belliveau & Bonmassar, 2010; Kesari, Siddiqui, Meena, Verma & Kumar, 2013).

Dosimetry, either theoretical or experimental, is based on modelling of the human body, which presents obvious differences between individuals (Chou, et al., 1996; Vecchia, 2005). The variations are related to the size and shape of the body, the distribution of biological tissues and the dielectric characteristics of each tissue (Goel, 2014; Nepa, 2012; Obahiagbon & Isabona, 2015; Qaddi & Srifi, 2016). The temperature measurement at imaging location with high-quality thermometry is needed to ensure safety during MRI imaging (Shellock, Gordon & Schaefer, 1986). Measurement of temperature in patients especially in paediatrics with quality thermometer provides the quantitative information needed to develop prognostic parameters that will aid research in planning and dosimetry at location imaged (Cork, Vaughan & Humphrey, 1983; Shinozaki, Deane & Perkins, 1988).

Measurements or estimates of SAR (W/Kg) are not trivial, particularly in human subjects. The absorption of RF energy causes biological reactions to occur in the tissue of the human body (Bolen, 1994; Van Leeuwen et al., 1999). The SAR that is produced during MRI procedure is a complex function of numerous variables including the static magnetic field of the MRI system, the type of RF pulse used, the Repetition Time (TE) and Echo Time (TE), the volume of tissue contained within the coil, the configuration of the anatomical region exposed, the orientation of the body to the field vectors and the

parameters selected by the MRI operator (Nguyen et al., 2004), as well as the ambient air temperature and humidity (Elder & Cahill, 1984).

Temperature measurement methods in an organism are generally classified as invasive or non-invasive. Non-invasive methods for temperature measurement without inserting the sensor into the human body are desirable. However, technologies for measuring temperature accurately by non-invasive methods have not been well established (Childs, Vail, Protheroe, King & Dark, 2005; Moran & Mendal, 2002).

Effect of Radiofrequency on Biological Tissue

The coupling of RF energy into biological systems may be quantified by the induced electric and magnetic fields, power deposition, energy absorption, and the distribution and penetration into biological tissues. (Aggarwal & Gupta, 2011; Chou, et al., 1996; Cullity & Graham, 2011; Valberg, Van Deventer & Repacholi, 2007). SAR (W/kg) is a quantity used to measure the rate at which RF energy is absorbed in a human body. The undisputed health effects that can occur with exposure to RF above 100 kHz energy includes heating of the human body and electro stimulation (RF shocks and burns) (Branch, 2009; Mahrour et al., 2005).

The outcome of thermal effects of whole-body exposure to a given field strength could have outcomes far different for partial body or localized exposure at the same strength (Code, 1999). It has been known for many years that exposure to very high levels of RF radiation can be harmful due to the ability of RF energy to heat biological tissue rapidly, the principle by which microwave ovens cook food (Sánchez-Hernández, 2009; SCENIHR, 2007). Tissue damage in humans could occur during exposure to high RF levels

30

because of the body's inability to cope with or dissipate the excessive heat generated (Karunarathna & Dayawana, 2005; Karunarathna & Dayawansa, 2006).

Thermal Dose

The energy of the RF of EM fields absorbed in tissues results in temperature rise as a result of friction between rapid moving molecules leading to critical biological effect. Various scientific researches on biological effect and health hazard of RF EM fields are on-going (Ahlbom et al., 2004; Kundi, 2005; Organization, 2010). Research studies conducted have indicated that exposure to RF radiation may produce various physiological effects since the majority of the RF power transmitted for imaging is transformed into heat within the patient's tissue as a result of resistive losses (Habash et al., 2007; Schenck, 2000; Shellock, 2000a, 2000b). Therefore, EM dosimetry in MRI has become important as it is one of the EM devices (Chou, et al., 1996; Durney, 1980).

During MRI, patients are exposed to an EM frequency which deposits energy and as a result, temperature increase within patients is impossible to be avoided (Ahlbom et al., 2004; Formica & Silvestri, 2004; Kundi, 2005; Oh et al., 2010; Shellock, Schaefer & Kanal, 1994). Limited published data indicate that human brain temperature falls in the range of 37.4 ^{o}C -37.8 ^{o}C, although the human brain is only 2 % of the body mass which accounts for 20 % of basal metabolism (Arens & Zhang, 2006; Narebski, 1985). The core temperature in the human brain is a very important parameter which if not regulated could lead to brain damage (Dery et al., 2013). According to the United State Food and Drug Administration (USFDA) (2016) guidelines limit,

the core temperature of the head must not be greater than 38 $^{\circ}$C and it should not increase more than 1 $^{\circ}$C and a maximum temperature elevation of less than 1.0 °C is regulated by the Food and Drug Administration (FDA) (2009), government safety guidelines for patients during MRI procedures (Ibrahiem, Dale, Tabbara & Wiart, 2005; ICNIRP, 2009; Shellock & Kanal, 1996; Zaremba, 2000; Zaremba & Phillips, 2002).

The ability to measure and quantify human body temperature accurately is crucial as far as research in thermoregulation is the concern (Houdas & Ring, 2013; Lim, Byrne & Lee, 2008; Lin, Bernardi, Pisa & Cavagnaro, 2008). Core temperature is one of the most important indicators at clinical settings to study thermoregulatory in humans, which describes the maintenance of the body temperature within a prescribed range under conditions in which the thermal load on the human body may vary (Keim, Guisto & Sullivan Jr, 2002; Shibasaki, Wilson & Crandall, 2006). The tolerance levels of exposure for individual patients and volunteers depends to a considerable extent on their individual physiological responses and condition of health, especially their thermoregulatory condition which may be very different from those of a typical healthy individual (MHRA, 2015). The increase in tissue temperature caused by exposure to RF energy during MRI procedure depends on multiple physiological, physical, and environmental factors (Kenny & Jay, 2013). These include the status of the patient's thermoregulatory system, the presence of an underlying health condition, the duration of exposure, the rate at which energy is deposited and the ambient conditions within the MRI system (Shellock & Crues, 2004).

Patients with certain medical disorders or under medication may be at some risk when scanning above the advised levels of exposure. In particular, patients with the compromised thermoregulatory function may be particularly susceptible to RF heating; such patients may well include those with cardiac and circulatory problems, fever, those with impaired renal function, those taking certain drugs such as vasodilators and diuretics and those with implants and certain cancers (MHRA, 2015). In addition, neonates, infants, pregnant women and the elderly are likely to be considered compromised in this respect (MHRA, 2015). Although the primary cause of tissue heating during MR procedures is attributed solely to RF radiation (Sperber, Oldenbourg & Dransfeld, 1984), various reports have suggested that exposure to the powerful static magnetic fields used for MRI procedures may also cause temperature changes.

The thermoregulatory and other physiological changes that occur in response to exposure to RF radiation are dependent on the amount of energy that is absorbed (Gordon, 1992; Shellock & Crues, 2004). The prevailing ambient conditions surrounding patients within the MRI scanner and the room temperature, humidity and airflow will affect the rate of cooling of the individual and should also be taken into account. It is therefore important to have an in-depth understanding of the effects of fluctuating fields on the nervous and muscular systems together with that of the SAR (MHRA, 2015). In humans, thermal loads come from alterations in ambient conditions and from changes in heat production within the human body. The law of conservation of energy forms the basis for the study of autonomic thermoregulation. In the steady state, a rate of energy absorption from the RF

33

field is balanced by heat lost to the environment in other to minimise the storage of heat (Bligh & Johnson, 1973; Kenny & Jay, 2013; Matikka, 2010; Werner, 1994). Metabolism is normally the only internal source of heat, although internal heating can result from magnetic resonance gradient coils (Lin et al., 2008; Nguyen et al., 2004). The brain and major organs in the trunk are the most metabolically active tissues and generate more metabolic heat than muscle at rest. The distribution of heat within these compartments is fast compared with rates at which heat content normally changes. As a result, temperatures at various sites within the core compartments rarely differ by more than a few tenths of a degree centigrade (Sessler & Todd, 2000).

Numerical Dosimetry

Computational modelling has received significant attention in the research community over the past few decades due to its pronounced contribution. This helps in better understanding of the nature, as well as in the development of advanced technologies. Today, a number of numerical simulation methods of penetrating EM fields are used to predict temperature deposition in biological tissue subjects to RF exposure (Kunz & Luebbers, 1993).

Calculation of Temperature in Tissue

The challenges in measuring temperature increase in-vivo during MRI has led to an increase in the use of numerical methods to precisely predict temperature distribution (Gajšek, D'Andrea, Mason, Ziriax & Walters, 2013). In many cases it is advantageous to predict the temperature change from RF energy during MRI in order to assure, depending on the particular MRI field strength and imaging protocols, the desired temperature distribution

(Carluccio, Erricolo, Oh & Collins, 2013) or that no tissues will be heated excessively (Wang, Lin, Vaughan & Collins, 2008).

The Finite-Difference Time-Domain (FDTD) method is generally used for analyzing SAR distribution in human bodies exposed to EM fields (Kunz & Luebbers, 1993). The FDTD method enables the simulation of temporal changes from initial conditions to a transitional period and finally to the steady state, by employing finite differences as approximations for spatial and temporal derivatives that appear in Maxwell's equations. This approach enables EM field analysis for the lossy dielectric medium of the human body (Hand, 2008). Currently, it is a major challenge to accurately predict the heating pattern, or SAR distribution in the subject during MRI, although exposure to increased temperature over time is more easily correlated with potential damage to tissue. Due to complexities and time requirements for calculating temperature, a spatially-averaged SAR value, often averaged over 10 g regions is used much more commonly in safety evaluations (Carluccio et al., 2013). The relationship between temperature and the applied energy distribution is often described with the PBHE (Pennes, 1948).

Measurement of the Brain Temperature Variation

Although magnetic resonance imaging is considerably safer than an x-ray or radio-isotopes techniques (ICNIRP, 2004), temperature measurement in patients undergoing MRI is of clinical relevance since the majority of the applied RF above 100 kHz of EM waves during MRI is converted to heat through resistive tissue losses. Severe deviations from the normal physiological temperature present a serious risk to the human body (Nguyen et al., 2004; NRPB, 2004).

The MRI environment requires a cool ambient temperature for proper magnet function which predisposes patients to heat loss in other to avoid the risk of hyperthermia. Conversely, the MRI scanner generates RF radiation, which is absorbed by the patient and warming of the body caused by RF radiation is likely during routine patients MRI (Machata et al., 2009). The type of thermometer to consistently measure temperature distribution in living tissue during MRI is still the primary problem although temperature measurement of patients during MRI is essential (Xiong, Yu, Shao, Zhu & Wu, 2006). The heat dissipation in patients which allows maintenance of thermal homeostasis during MRI depends on factors including patient's thermoregulatory system and ambient conditions within the MR room (Dwyer & Leeper, 1978a; 1978b). The testis and eye of human have reduced capabilities for heat dissipation and may be injured by elevated temperatures. Therefore, the sites where testis and eyes are found are critical organ system to RF. Therefore, potential harmful effect to these organs during MRI is excessive (MHRA, 2015).

The temperature level is compared with the upper limit at which painful sensations or damage occurs, which is approximately 43-45 °C (Hardy, Wolff & Goodell, 1967). Maintaining human body core temperature between 36.5 to 38.5 °C depends on the sound functioning of the body. As core temperature increases or decreases from these values, malfunctioning of the human body occurs. Thus the greater the discrepancy the greater the malfunctioning (Mendt et al., 2017; Moran & Mendal, 2002) as shown in Figure.
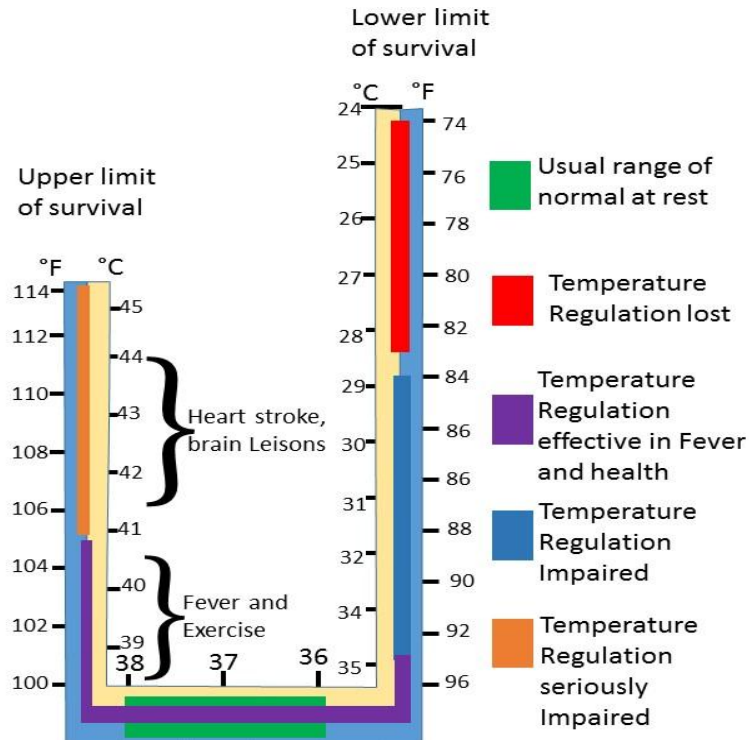
Figure 3: Temperature Limits of Survival.

Source: (Dräger, 2014).

Body core temperature above 41.5 °C, in the range of upper limit of survival or below 33.5 °C in the range of lower limit survival causes a fast decline in the proper functioning of the body, which may result in injury and eventually death (Hensel, 1981a, 1981b). The ability to sense and regulate human body temperature is a key feature of human survival. A deviation of ± 3.5 °C from the resting temperature of 37 °C can result in physiological impairments and fatality (Moran & Mendal, 2002). Brain hyperthermia occurs when brain temperature value exceeds 41 °C (Cabanac & Brinnel, 1987; Kiyatkin, 2004) because the human body's core temperature is stable under normal conditions. Deviation from normal body temperature is an excellent indicator of a body in an abnormal condition (Lessard, Wong & Schmidt, 1988). A rise of 1 °C is generally acceptable to a normal healthy person

(MHRA, 2015). The actual temperature rise at any time will depend on the balance between the energy absorbed and the energy transferred from the region of the body concerned. The ambient temperature, air flow, clothing and humidity all play a major role in the rate of dissipation. The lower the ambient temperature and the lower the humidity, the greater the heat transfer (Werner, 1994).

With regard to localized heating, it seems reasonable to assume that adverse effects will be avoided with a reasonable certainty if temperatures in localized regions of the head are less than 38 °C (ICNIRP, 2004). The skin, the subcutaneous tissue and the fat in subcutaneous tissue are the human body's heat insulators. Thus, the skin acts as an effective radiator system, and the flow of blood to the skin is an effective mechanism for transferring heat from the human body core to the skin (Lessard et al., 1988). Fat is the most efficient heat insulator since it conducts about one third as much heat as the other insulators. The insulator system beneath the skin is an effective means for maintaining internal temperature, while the temperature of skin approaches the environmental temperature (Cena & lark, 1981a; 1981b; Richards, 2013). Therefore damage to tissue during MRI may be caused by exposure to high levels of RF energy because the human body is not equipped to dissipate the excessive amounts of heat generated. Possible injuries include skin burns, deep burns, heat exhaustion and heat stroke may occur (Zamanian & Hardiman, 2005). Due to the different EM properties of the body tissues the EM power absorption is not uniformly decreasing function of depth in an organ (Van Leeuwen et al., 1999).

Currently, invasive thermometry provides extremely limited information about thermal dose distributions in the human body as a clinical problem, rather non-invasive thermometry helps to visualize full 3-D temperature distributions permitting easier and better understanding of inhomogeneous thermal dose distributions (Kok et al., 2015; Masters, 1980). The forehead fever scan is one of the non-invasive thermometers that measures human body temperature from the surface skin of the forehead. It consists of plastic encased thermo-phototropic substances and changes colour over a specific short range. This thermometer quickly estimates human body temperature and provides a better estimation of oral temperature than axillary (Masters, 1980). The forehead skin temperature which can be measured by thermistors and Liquid Crystal Thermometers (LCT) estimate human body core temperature (Moran & Mendal, 2002). Approximately two degrees must be added to the measured skin temperature in order to estimate core temperature (Dräger, 2014; Liu, Chang & Chang, 2004; Pompei & Pompei, 2004).

Normal core temperature is considered to be the temperature of the brain, heart and lungs. The sites that have been commonly used are oral, rectal, axillary, tympanic, oesophageal and forehead of human. Although the most accurate human body temperature is measured at the hypothalamus, a site not accessible by any practical means (Knies, 2003). The correlation between skin and core temperature has in at least one case data indicated to be poor (Brull, Cunningham, Connelly, O'Connor & Silverman, 1993; Lacoumenta & Hall, 1984) others, however, reported the measurement to be reliable (Allen, Horrow & Rosenberg, 1990; Lees et al., 1978). The difficulty

with many of these studies is that they were based on simple linear correlation, a frequently inadequate technique (Bland & Altman, 1986). According to Piasecka, Strąk & Maciejewska (2017), comparative data analysis of heating surface temperature distributions from both Infrared thermography (IRT) and liquid crystal thermography (LCTG) which are non-invasive techniques showed similar values in temperature distributions. They concluded that there is the goodness of fit between the temperature measured with IRT and that recorded by means of LCTG. The measurement of forehead temperature is an excellent point of reference for recognizing raised human body temperature. The forehead temperature measured by plastic encased thermo-phototropic substances that change colour over a specific short range estimates human body temperature better than axillary temperature (Masters, 1980).

In consideration of the temperature monitoring during brain MRI, with regard to which device to estimate brain temperature, MRI non-magnetic skin LCT is safe to be used (Liu, 2012). LCT can detect temperature changes as small as 0.3 °C (54 °F). A strip of LCT is placed on the human body surface to monitor body temperature changes. Relative temperature is indicated by a colour change. This method of measuring temperature is used primarily to monitor temperature change instead of actually measuring core body temperature. Commercially available LCT strips can measure temperatures within the range of 34.3 °C to 40.0 °C (94.1 °F to 104 °F) (Lessard et al., 1988).

Temperature Measurement during Magnetic Resonance Imaging

According to Shellock (1988), the MRI protocol used conventional RF pulse sequences, as follows: spin echo, sagittal plane, TR = 600, TE = 25,

40

acquisition matrix = 128 x 256, slice thickness = 10 mm, average number of slices = 20, average imaging time = 2:40 minutes; spin echo, axial plane, TR = 2000, TE = 30 and 60, acquisition matrix = 256 x 256, slice thickness = 5 mm, average number of slices = 40, average imaging time = 8:40 minutes.

Temperature changes as a result of tissue heating caused by exposure to RF radiation during MRI protocols by high field strength MRI of the brain is a primary safety concern. A 1.5 T superconducting magnet operating at 64 MHz for proton imaging, statistically indicated significant increase in temperatures of the forehead of patients undergoing MRI of the brain using infrared thermometer (Shellock, 1988; Shellock & Crues, 1988).

The temperature change in the brain of patients undergoing brain MRI examination of field strengths 0.3 T and 1.5 T using MRI protocols were investigated using digital clinical thermometer. The digital clinical thermometer was calibrated to measure temperatures in a range of 36 ^{o}C to 40 ^{o}C with a resolution of 0.1 ^{o}C. This thermometer was used to insert the right external auditory canal of patients to measure patients brain temperatures experimentally before and immediately after brain MRI (Dery et al., 2013). A combined weight and height scale was also used to measure patient weight and height. Patient's age, weight, height, gender, Body Mass Index (BMI) and total scan duration were also measured and recorded. Although, the temperature changes of the pre- and post-scan tympanic temperatures were all within guidance levels set by ICNIRP, (2009) for core temperatures. Patients' temperature change did rise by more than 1.0 ^{o}C. The brain temperature change of the patients measured was not greater than 38 ^{o}C (Dery et al., 2013).

According to Dery et al., (2013) SAR value at each of the protocols was monitored since SAR of MRI scanner depends upon the type of sequence pulse, the TR, TE and the type of transmitter RF coil used. The SAR value for all protocols was compared with the standard of 3.2 W/kg for head MRI in an average time of 10 minutes set by the USFDA, (2016). They clearly stated that any variation can be attributed to operator's manipulation of the Number of Signals Averaged (NSA) during the scan and in effect the acquisition time. Because lower scan time resulted in high SAR value in some cases in 1.5 T compared with 0.3 T during scanning protocols investigated (Dery et al., 2013). According to Dery et al., 2013 as MRI field strength increases, so do the RF energy deposition in the patient. This permit higher resolution and faster scanning resulting in temperature increase as safety concerns.

Due to the complex inhomogeneous nature of the human head, Nguyen et al., (2004) used a finite-difference numerical method to solve a PBHE to model temperature distribution and simulates the temperature variation as a function of RF exposure and SAR. In their study heat losses due to respiration, radiation, and evaporation were not considered. Convective cooling between the skin and the air was neglected. Only conductive cooling was considered. Moreover, heat losses due to more complicated thermal regulatory responses such as perspiration and increased local blood flow rates were also not included. The assumptions made by Nguyen et al., (2004) include the following;

1. The tissue properties are isotropic within a tissue type and constant with temperature and time.

2. The arterial blood temperature and the initial temperature for all tissues are equal to 37 ^{o}C.

3. The density and specific heat of the blood are constant. Since the tissue density and the specific heat are not a function of time.

Chapter Summary

Absorption of energy from RF fields above 100 kHz used in MRI induced current. This leads to power dissipation within the human body tissues, and in turn will lead to accumulation of energy with time and a rise in human body temperature. Hence, heating effects predominate and this is the major consequence for MRI.

Brain cells are exceptionally sensitive to thermal damage. Despite the differences in brain dimensions and in some of the anatomical structures amongst patients, normothermic values of brain cell is in the range of 34.2–38 ^{o}C, slightly higher 2–4 fold at hypothermic values 32.2–34.2 ^{o}C, and dramatically higher at hyperthermic values 38–42.5 ^{o}C. The ability to sense and regulate body temperature is a key feature for patients' survival in MRI environment. A deviation of $\pm$ 3.5 °C from the resting temperature ranging from 36 to 37.5 °C can result in physiological impairments and fatality especially in paediatrics.

Various scientific researches on biological effect and health hazard of RF EM fields are on-going; therefore, RF EM field dosimetry in MRI has become important as it is one of the EM devices although MRI is considerably safer than an x-ray or radio-isotopes techniques. The number of paediatrics and adults patients undergoing MRI as a diagnostic technique has increased dramatically in Ghana with few publications available on clinical experience

with MRI from Ghana. This, however, may be as a result of lack of technologies for measuring patients' temperature in MRI despite the fact that temperature increase within patients is impossible to be avoided. The challenges in measuring temperature increase in-vivo during MRI have led to the use of numerical methods to precisely predict brain temperature distribution and experimentally measure patients' temperature as a validation which may presents obvious differences between individuals. Therefore, the numerical method of the study assumes temperature distributions along the three dimensions of homogeneous size independent (head) brain in the study

CHAPTER THREE

MATERIALS AND METHODS

Introduction

This chapter describes the materials and methods of the research. The methods of the study constitute numerical determination and experimental measurement of temperature variation in patients. The numerical model of the study comprises physical model of the brain (head) before, during and after MRI scan. A mathematical model, simulation, and prediction of brain temperature are also carried out. Patients' brain temperature in MRI scan was experimentally measured to validate the numerical method. MRI facilities of field strength above 100 kHz were used. Diagnostic Centre Limited MRI facility and 37 Military Hospital MRI facilities are shown in Figure 27 and 28 respectively, (Appendix A), both in Accra-Ghana were used for measurements.

Instruments used for Temperature Measurement

The contact devices used in the study were clinical mercury thermometer, liquid crystal thermometer strip and the non-contact device used was an infrared thermometer. These calibrated thermometers are shown in Appendix B (Figure 29).

Clinical Mercury Thermometer

This is non-invasive contact thermometer placed under the arm to measure core temperature of the body. The clinical thermometer used in this study was calibrated on 16th of February, 2016 at the temperature laboratory of the Ghana Standards Authority (GSA), Accra-Ghana. The calibrated thermometer ranges from 36 ^{o}C to 40 ^{o}C with a resolution of 0.1 ^{o}C, as shown

in Table 1 under ambient conditions of a temperature 25 ± 5 ^{o}C and relative humidity 55 ± 20 %.

Table 1: Calibration Results of the Clinical Thermometer.

Mean Reference Reading ^{o}C	Mean Equipment under test Reading ^{o}C	Deviation ^{o}C	Uncertainty K
36.1	36	-0.1	0.1
37.1	37	-0.1	0.1
38.1	38	-0.1	0.1
39.1	39	-0.1	0.1
40.1	40	-0.1	0.1

Source: Ghana Standard Authority (GSA), (2016).

Liquid Crystal Thermometer Strip

Liquid crystal thermometer strip used consists of plastic encased thermo-phototropic substances that change colour over a specific short range of temperature. It is used to measure forehead temperature which quickly estimates body temperature. The LCT used was calibrated on 16th of February, 2016 at the temperature laboratory of the GSA, Accra-Ghana. The calibrated LCT ranges 33 ^{o}C to 41 ^{o}C with the precision of 1.0 ^{o}C. The correct temperature measurement of LCT was read after it was placed in the centre of patient's forehead and green colour, which signifies forehead temperature, appeared.

Infrared Thermometer

The infrared thermometer used in this study has multiple uses and operates in a room of temperature ranging from 10 ^{o}C to 40 ^{o}C. It consists of ABS plastics, temperature sensor, infrared temperature measuring element,

microcomputer controlled circuit, liquid crystal display, backlight, and buzzer. It is used to take body temperature ranges from 32 ^{o}C to 42.2 ^{o}C by detecting the infrared heat given off by the forehead. It also measures the brain temperature ranges from 0 ^{o}C to 100 ^{o}C by detecting the infrared heat given off by the eardrum.

The methods used in this study determined temperature change before brain MRI, real-time brain temperature changes during brain MRI and temperature changes immediately after MRI of the brain.

Experimental Method

This section describes the experimental methods used to validate the numerical calculations of the study. Imaging protocols and baseline temperature were assessed using Eddy Current Correction (ECC) phantom before patients MRI scan, as shown in Figure 30 (Appendix C). Patients' (paediatrics and adults) temperatures were measured and recorded as shown in Tables 5, 6 and 7 (Appendix D) to validate the numerical results obtained.

Phantom Measurement

Real-time temperature measurement of the phantoms was carried out at MRI centres at 37 Military Hospital and Diagnostic Centre Limited using LCT. This was done to evaluate the imaging protocols and the baseline temperature at each centre before patients' examinations as shown in Appendix C. The ambient temperatures of the MRI suites were measured. MRI quality assurance procedures were applied to these two clinical MRI scanners as daily routine throughout the ten months data collection (September 2016-June, 2017) of the study.

47

The American College of Radiology MRI guide for phantom set-up was used for ECC phantom set-up at the centre of the RF coils. Axial, coronal, and sagittal images with a slice thickness of 5 mm and an inter-slice gap of 5 mm were acquired in each of the scans. A conventional spin echo sequence was used for the T1-weighted imaging (TR/TE = 500/20 ms). Dual echo images were obtained from the spin echo scan (TR/TE = 2000/20 ms, for the first echo, and 2000/80 ms for the second echo). In-plane resolution was set to be 1×1 mm. Following the ACR guidance, SNR, signal standard, helium level, RF scale, uniformity, geometric accuracy, slice thickness accuracy, slice position accuracy, signal intensity, and percentage signal ghosting were quantitatively measured.

One of the most important safety aspects of using MRI scanner for imaging is patients' temperature monitoring during the application of RF-power and, hence, the SAR. In the study, the energy deposition during MRI of patients was monitored and strategically controlled. SAR was obtained through the intrinsic computer software on the MRI scanner. The SAR value for each patient was calculated based on the specific protocol chosen. This is as a result of the software registered by the manufacturers of the MRI systems used in the study. This made use of the patient weight, height, density of the volume being scanned, the protocol chosen; scan time, number of slices chosen, NSA and number of acquisition. The operating mode of the MRI systems operated within normal (Level 0) operating mode.

Forehead and Tympanic Temperature Measurement

This work covered one hundred and fourteen (114) volunteer patients who underwent brain scanned using 1.5 T MRI at 37 Military Hospital and 0.3

48

T at Diagnostic Centre Limited both found in Accra, Ghana. Forehead and tympanic temperatures of the patients were measured. On the day of the MRI, patients were made to fill out a screening form. The type of examination, sex and age were recorded. Combined height and weight scales were used for patients above one year and five months old. Informed consent of the patients and/ or their legal representatives was received after the study protocol was approved by the ethics board of University of Cape Coast Review Board (UCCIRB) with ethical clearance – ID NO: (UCCIRB/CHAS/2016/01).

The study protocol had the clear aim to measure patients' temperature before, during, and immediately after brain MRI. Measurements were collected in every single patient with temperature in a range of 36-37.5 ^{o}C referred for brain MRI of field strength above 100 kHz in a non-random order. Out of one hundred and fourteen (114) patients, fifty (50) adult patients aged from 32 to 68 years, weighed from 50 to 113 kg (BMI ranges from 22.16 to 44.16 kg. m-^{2}) undergoing brain MRI of operating frequencies above 100 kHz (0.3 T and 1.5 T) brain temperatures were measured. A calibrated LCT strip with 1.0 ^{o}C precision and a range of 33 ^{o}C to 41 ^{o}C was used to measure forehead temperature of patients' before, during and immediately after brain MRI examination. A calibrated IRT (accuracy 0.1 ^{o}C) was used to measure pre-and-post scan tympanic temperatures of patients by inserting into the right ear canal of the patients. The total scan duration of the adults was in a range of 22 to 32 minutes. The remaining sixty-four (64) of the one hundred and fourteen (114) patients are paediatrics (aged 7 months to 16 years). Pre-and-post scan tympanic temperatures of the paediatrics were measured with the

49

IRT. This was done by inserting into the right ear canal of the patients the probe of the IRT.

The magnetic resonance imaging sequences did last 3-6 minutes during image acquisition. The MRI examinations of the paediatrics lasted within 15-50 minutes. All paediatrics patients who had sedation or anesthesia received continuous monitoring and support during examination time. In some cases, a contrast agent (dye) was given intravenously to improve the quality of the images. On completion of the scan, the earplugs were removed and patients were brought out of the magnet room. The post-scan temperature was then measured immediately at the end of each period and results were recorded on a data sheet (Appendix D).

The ambient temperature of the MRI suite was measured after MRI scan. The scanned parameters and SAR were recorded from the control console of the MRI machine as the patients undergo the examination. Sweating of patients during MRI scan was evaluated qualitatively where D was assigned when no moisture was detected, S when some moisture was detected, and an HS when distinct beads of sweat are visible.

Numerical Methodology

A 3-D PBHE was modelled to evaluate the effects of RF radiation exposure in the human head and also determining the induced internal EM field as well as its spatial distribution in brain MRI operating above 100 kHz. The modelled equation was numerically used to determine temperature variations in patients undergoing brain MRI

Theoretical Analysis: Thermal Model

The Penne's bio-heat equation (1948) model provides suitable temperature distribution in the whole body, an organ and tumour. This help in studying the heat rise in biological tissue in which heat exchange mechanism such as thermal conduction, convection, perfusion of blood, regional heat source and metabolic heat generation in tissue are taken into account (Dery et al., 2013; Durkee Jr & Antich, 1991a, 1991b; Pennes, 1948). Because the analysis of a heterogeneous model for a human is a difficult theoretical task (Elwasife & Almassri, 2017), this study homogenously analyzed the head model predicting temperature distribution in brain MRI.

Temperature increase analysis of the EM field of RF power deposition in the human head model is calculated using an explicit method based on FDTD and Finite Difference Method (FDM). FDTD and FDM are applied to solve PBHE to determine temperature changes in the human tissue during brain MRI.

In this study, central difference scheme of FDTD and FDM are employed to discretize the heat equation and assume time is dependent on FDTD and time independent in FDM. Programming language (Matlab version R2017A) was used to write algorithms. The algorithms simulate the results obtained to demonstrate the induced EM field and its spatial distribution in brain MRI as well as the thermo-mechanical interaction of the biological tissue.

A physical model of the research shown in Figure 4 depicts temperature distribution in the brain (head) before, during and after exposure to EM radiation of RF from MRI scan. Thermal properties of tissue: thermal

51

conductivity, specific heat capacity and density have been measured by various groups and reported in the literature (Prakash, 2010). Thermal properties of the biological tissues in the human head model taken to be constant are shown in Table 2. The energy-balance equation for the physical model of the homogeneous head is summarized as:

$$\mathbf{S} = \mathbf{ARF} \pm \partial \mathbf{Q}_m \pm \partial \mathbf{W}_b \pm H_{lost} \tag{4}$$

Where $\mathbf{S}$ is the rate of storage of energy in the head, $\mathbf{ARF}$ is rate of heat entering through the bounding surface of the head, $\partial \mathbf{Q}_m$ is the rate of change of metabolic energy generated in the head, $\partial \mathbf{W}_b$ is the rate of change of energy transported by bloodstream in the head, and H_{lost} is the total heat lost due to the environment.

Before Head MRI   After Head MRI   During Head MRI
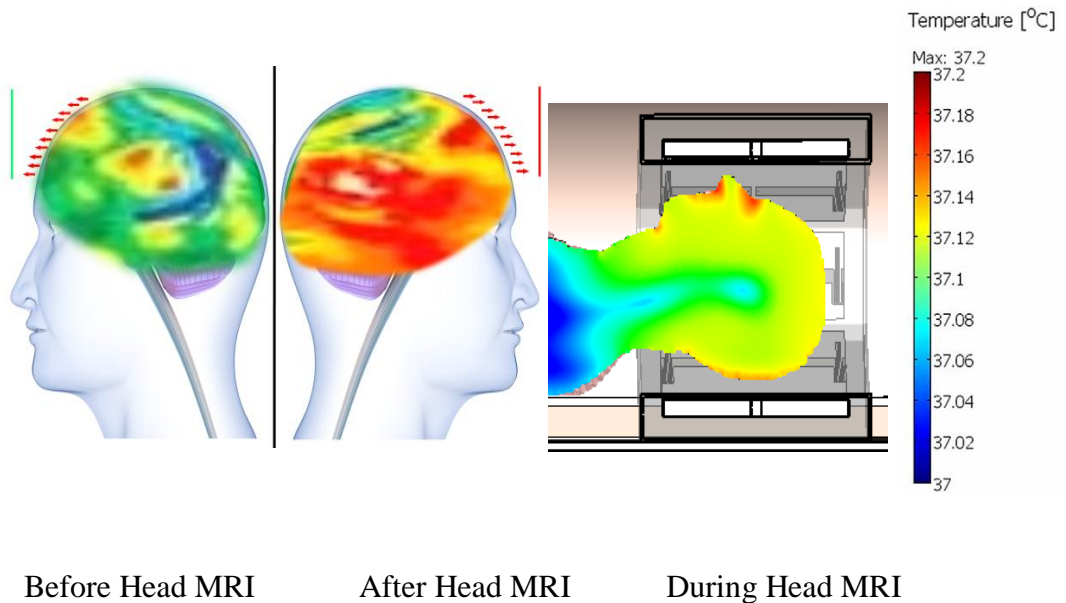
Figure 4: Physical Model of Homogeneous Head Temperature in 3D.

Source: (Wessapan et al., 2012).

52

Table 2: Thermal Properties for the Biological Tissues Contained in the

Human Head Model

Tissue	Head tissue density, ρ (kg/m^3)	Specific capacity of head tissues, C (Jkg^{-1} ^{o}C^{-1})	Thermal conductivity of head tissues, K (Wm^{-1} ^{o}C^{-1})	Energy generated in the head tissues, Q_m (W/m^3)
Bone	1,080.0	2,110.0	0.7	26.1
Cerebrospinal Fluid	1,007.0	3,800.0	0.5	0.0
Gray Matter	1,035.5	3,680.0	0.6	15,575.0
White Matter	1,027.4	3,600.0	0.5	5.192.0
Muscle	1,041.0	3,720.0	0.5	687.0
Skin	1,100.0	3,150.0	0.3	1,100.0

Source: Collins et al., 2004.

The 3-Dimensional Bio-Heat Modelling of Human Thermal System

The evolution and the distribution of the temperature inside the living tissues are governed by the heat-exchange such as the heat conduction, the blood flow, and the metabolic heat. They depend also on the contribution of external sources such as the power deposited by RF sources (Ibrahiem et al., 2005; Ozen, Helhel, & Bilgin, 2011). The partial differential equation of PBHE of Equation (5) is demonstrated in the energy balanced in Equation (4) and this is expressed in terms of SAR and heat exchange which is shown in the media with uniform material properties in Equations (6) and (7), respectfully.

53

$$\rho_t C_t \frac{\partial T}{\partial t} = Q_r + \nabla.(k_t \nabla T) + \rho_{bl} V_b C_{pbl}(T_{art} - T) + Q_m \qquad (5)$$

$$\rho_t C_{Pt} \frac{\partial T}{\partial t} = \rho_t SAR + \nabla.(k_t \nabla T) + \rho_{bl} V_b C_{pbl}(T_{art} - T) + Q_m \qquad (6)$$

$$\rho_{(x,y,z)} c_{p(x,y,z)} \frac{\partial T_{(x,y,z)}}{\partial t} = \rho SAR + \nabla.(k \nabla T) +$$
$$\rho_{bl} V_b C_{pbl}(T_{art} - T_{(x,y,z)}) - (h_{R(x,y,z)} + h_{C(x,y,z)} + h_{E(x,y,z)}) \qquad (7)$$

From Equation 5, $\rho_t C_t \frac{\partial T}{\partial t}$, is thermal energy storage in the tissue, where ρ_t and C_t are the tissue density (kgm$^{-3)}$) and the specific heat capacity of the tissue (J kg^{-1}°C^{-1}) respectfully. $\frac{\partial T}{\partial t}$ is the rate of temperature rise and Q_r, is the external heating source. $\nabla.(k_t \nabla T)$ is the heat conduction through tissue where k_t is the tissue conductivity (Wm^{-1}°C^{-1}), $\rho_{bl} V_b C_{pbl}$ Mass flow rate of blood per unit volume of tissue where ρ_{bl}, V_b, and C_{pbl} are the blood density (kgm^{-3}), volumetric rate of blood (m^3 s) and specific heat capacity of blood (J kg^{-1}°C^{-1}) respectfully. T_{art} (°C) arterial temperature and T (°C) is the local tissue temperature. Q_m is Metabolic heat generation (W\m^3).

SAR as a result of MRI scanner, is subsituted in Equation 5 to modify PBHE as shown in Equation 6. Hence, $\rho_t SAR$ (W/m^3), is the rate of energy deposited per unit volume of the tissue in brain MRI. The $(h_{R(x,y,z)} + h_{C(x,y,z)} + h_{E(x,y,z)})$ is the total heat lost due to the environment as a result of heat radiation $(h_{R(x,y,z)})$, heat convection $(h_{C(x,y,z)})$, and heat evaporation $(h_{E(x,y,z)})$ as shown in the 3-D modified PBHE in Equation 7.

Metabolic Heat Generation

The model accounts for the metabolic heat generation of the head tissues. The metabolic heat is assumed to be generated uniformly by metabolic and chemical reactions but the rate of metabolic heat generation of an individual head tissues are not equal. The total amount of heat generated in the head is given by:

$$Q_m = \int Q_{m(x,y,z)} dv \tag{8}$$

The gray matter has the highest metabolic heat generation amount of 15,575 W/m^3. In contrast, cerebrospinal fluid has no ability to produce heat. Therefore, cerebrospinal fluid metabolic heat generation value is zero. The skin has the second largest metabolic heat generation of 1,100 W/m^3. Each head layer metabolic heat generation is shown in Table 2

The Role of Blood in Heat Transfer

An assumption is made based on Fick's principle that blood enters capillaries at the temperature of arterial blood, T_{art}, where heat exchanges occur to bring the temperature to that of the surrounding tissue, T. Hence, total energy exchange between blood and tissue is given as

$$E_H = \int \rho_{bl} \times V_b \times Cp_{bl} \times (T_{art} - T) \tag{9}$$

where ρ_{bl} and Cp_{bl} are the density and specific heat capacity of the blood respectively. Both properties can be taken as constant. $\rho_{bl} \times V_b \times Cp_{bl}$ is the mass flow rate of blood which is a function of location.

Another assumption is that no heat storage occurs in the bloodstream when the heat exchange occurs between the capillary bed and the tissue. However, over short periods and severe environments, heat stored in the

tissue, is likely to be important in man for periods of an hour (Cena & Clark, 1981a; 1981b). In sum, under transient conditions, part of the heat energy generated or transferred to the control volume of tissue may go to alter the amount stored inside it. Thus, the rate of change in storage of thermal energy is given by Equation (10)

$$E_H = \frac{\partial}{\partial t} \int \rho c_p T dv \qquad (10)$$

Heat Exchange with Environment

When the temperature of the body surface is lower than that of the body interior heat flow inside the human body occurs. The blood supply to the skin is the main determinant of heat transport to the skin. Heat loss occurs by the physical processes of radiation, convection, evaporation and conduction Radiation (h_R) and convection (h_C) are the most significant sources accounting for approximately 60% of heat loss. The blood vessels heat transfer is due to convection and the core body tissues transfer of heat in subcutaneous blood vessels which emit infrared rays from the skin surface to lose heat is by radiation (Yildirim, 2005).

Radiation

. The radiation heat loss from the skin accounts for hyperthermia tissue at the model-air interface which is expressed as;

$$h_R = \varepsilon \times \sigma \times A_{eff} \left((T_{skin} + 273)^4 - (T_{air} + 273)^4 \right) \qquad (11)$$

where ε is the emissivity which is approximately equal to the absorptivity of human skin which is 0.97. Stefan-Boltzmann Constant σ is 5.67051×10^{-8} W/ (m^2.K^4) and A_{eff} the effective area radiated heat (m^2). T_{skin} is the temperature of the skin (^oC); T_{air}, the ambient air temperature (Yildirim, 2005).

Convection

The equation for characterizing convective (h_C) heat losses in the blood vessels is shown in Equation 12.

$$h_C = h_C \times A_{eff} (T_{skin} - T_{air})$$ (12)

where h_C, convective heat transfer coefficient, is estimated from the Nusselt number, Nu as shown in Equation (13)

$$\mathbf{Nu} = \frac{h_c \times D_h}{K_a}$$ (13)

In the model, Nusselt correlation is used to calculate the Nusselt number. According to Yildirim, (2005), the Nusselt number for free convection from a human body is given in Equation (14)

$$\text{Nu} = 0.63 Gr^{0.25} \Pr^{0.25}$$ (14)

Where $\Pr$ is Prandel number of the air at a given temperature and Gr is the Grashof number which is expressed in Equation (15) (Cena & Clark, 1981a; 1981b).

$$Gr = \frac{g \times \beta \times (T_{skin} - T_{air}) \times L^3}{V^3{}_a}$$ (15)

where

$$\beta = \frac{1}{T_f}$$ (16)

and

$$T_f = \frac{T_{skin} + T_{air}}{2}$$ (17)

In Equation (15), g is the acceleration due to gravity (9.8 m/s^2), V is the kinematic viscosity of the air (m^2 s), L is the length of the head (m), T_f in

Equation (17) is the film temperature where T_{skin} is the surface temperature of the body and T_{air} is the temperature of surroundings.

Evaporation

The human body depends on evaporation (h_C) for heat dissipation when the environmental temperature is warmer than the skin or when convection and radiation are insufficient. Evaporation is the next major source accounting for about 22% of heat loss. In order to calculate the diffusional heat loss, Inouye's correlation is used (Yildirim, 2005). This correlation gives the diffusional heat loss per unit area in Equation (18)

$$h_E = \frac{4148}{3600} \times (0.35) \times A_{eff} \left(p_{skin-}p_{air} \right) \tag{18}$$

where p_{skin} is the vapor pressure of sweat at skin temperature and p_{air} is the partial pressure of water vapor in the ambient air, calculated from Equation (19) and (20) in millimeters of mercury.

$$p_{skin} = 1.92T_{skin} - 25.3 \qquad \text{(mmHg)} \tag{19}$$

$$p_{air} = p_{v} \times (\%RH) \qquad \text{(mmHg)} \tag{20}$$

Heat Conduction

Conduction (h_C) is the loss of molecular kinetic energy in the form of heat from the skin to the surroundings. Conduction contributes roughly 15% of heat loss from the skin to the surrounding. The conductive heat transfer between the tissue and surrounding tissue, obeys the Fourier's Law of Conduction shown in Equation (21)

$$E_{H(x,y,z,t)} = -K_{h} \nabla T(x, y, z, t) \tag{21}$$

where the temperature gradient is a vector normal to the isothermal surface, the heat flux vector $E_{H(x,y,z,t)}$ represents heat flow per unit time, per unit area of the isothermal surface in the direction of the decreasing temperature and K_h is referred as the thermal conductivity of mammalian tissue which is dependent upon tissue temperature and location.

Since the heat flux vector $E_{H(x,y,z,t)}$ points in the direction of decreasing temperature, the minus sign is included in Equation (21) to make heat flow a positive quantity. The divergence of the temperature, T, in the coordinate system, $E_{H(x,y,z,t)}$ is given Equation (22)

$$\nabla T = i \frac{\partial T}{\partial x} + j \frac{\partial T}{\partial y} + k \frac{\partial T}{\partial z}, \tag{22}$$

where i, j, k are the unit direction vectors along the x, y, z-directions, respectively. The total conductive heat C_T, through the control surface of a tissue is given in Equation (23)

$$C_T = -\int E_H . fdA, \tag{23}$$

where A is the surface area of the volume element V, f is the outward-drawn normal unit vector to the surface element dA, E_H is the heat flux vector at dA. The divergence theorem is used to convert the surface integral to volume integral.

$$-\int E_H . fdA = \int \nabla . E_{H(x,y,z,t)} dv \tag{24}$$

After integrating the Equation (24) on over control volume of the tissue element, the rate of heat $E_{H(x,y,z,t)}$ entering through the bounding surface of V is obtained. The derivative of $\nabla E_{H(x,y,z,t)}$ is given in equation

59

(25). The divergence of the heat flux vector E_H in coordinate system (x, y, z) is given by

$$\nabla E_H (x, y, z) = \frac{1}{x}\frac{\partial}{\partial x}(xE_x) + \frac{1}{y}\frac{\partial}{\partial y}(E_y) + \frac{1}{z}\frac{\partial}{\partial z}(E_z) \tag{25}$$

Applying the Equation (23) to the three components of the heat flux vector in the (x, y, z) directions, the Equations (26), (27) and (28) are obtained. The three components of the heat flux vector, thus, Equations (26), (27) and (28) are substituted into Equation (25) to obtain (29).

$$E_{Hx} = -k\frac{\partial T}{\partial x} \tag{26}$$

$$E_{Hy} = -k\frac{1}{y}\frac{\partial T}{\partial y} \tag{27}$$

$$E_{Hz} = -k\frac{\partial T}{\partial z} \tag{28}$$

$$\nabla E_H (x, y, z) = \frac{1}{x}\frac{\partial}{\partial x}(-k.x\frac{\partial T}{\partial x}) + \frac{1}{x}\frac{\partial}{\partial y}(-k\frac{1}{x}\frac{\partial T}{\partial y}) + \frac{\partial}{\partial z}(-k\frac{\partial T}{\partial z}) \tag{29}$$

Therefore, using divergence theorem, the rate of heat E_H entering through the surface integral is converted to volume integral by substituting $\nabla E_H (x, y, z, t)$ into the Equation (24).

The Specific Absorption Rate

The specific absorption rate is linked to the electric field strength through the relationship $SAR = \sigma\frac{|E^2|}{2\rho}$, where σ, is the conductivity in (S/m), E is the electric field in V/m and ρ is density of tissue in kg/m^3. The study analyzes the rise of temperature associated with the exposure to MRI RF emissions. The rise of temperature is small. Therefore, it is also

60

assumed that the electromagnetic dielectric and thermal properties of the tissues are not modified by such a small increase of temperature. The maximum rise in temperature (∂T_{max}) caused by the EM energy deposited was obtained from the difference between the temperature for the exposed model to RF emissions ($SAR \neq 0$) and that of the unexposed model ($SAR = 0$) (with the phantom set in head coil inside MRI scanner yet to be scanned) (Malik et al., 2015).

Passive System Equation

With the help of the first law of thermodynamics, the volumetric bio-heat equation is obtained and this requires that the rate of heat gain minus rate of heat loss is equal to the rate of heat stored in the tissue. The substitution of Equations (7), (8), (9), and (24) into Equation (4) yields

$$-\int_v \nabla.E_{H(x,y,z,t)}dv + \int_v Q_{m(x,y,z)}dv + \int_v \rho_{bl} \times V_{bl} \times Cp_{bl} \times (T_{art} - T)dv - \frac{\partial}{\partial t}\int_v \rho c_p Tdv = 0$$

$$(30)$$

$$\int -\nabla.E_{H(x,y,z,t)}dv + Q_{m(x,y,z)}dv + \rho_{bl} \times V_{bl} \times Cp_{bl} \times (T_{art} - T)dv - \rho c_p \frac{\partial T(x,y,z,t)}{\partial t}dv = 0$$

$$(31)$$

Equation (31) is derived for an arbitrarily small volume element (v) within the in-vivo tissue, hence the volume (v) is chosen so small as to remove the integral to obtain Equation (32)

$$\rho c_p \frac{\partial T(x,y,z,t)}{\partial t} = -\nabla E_{H(x,y,z,t)} + Q_{m(x,y,z)}$$
$$+\rho_{bl} \times w_{bl} \times Cp_{bl} \times (T_{art} - T) \qquad (32)$$

Equation (29) was substituted into Equation (32) to achieve bio-heat Equation (33). The Equation (33) expresses the fact that; at any time, the sum

61

of the heat transfer through the three directions of a sphere, the heat produced by it and the heat transported by blood, is equal to the rate of temperature variation $\frac{\partial T}{\partial t}$, at any point. Therefore,

$$\rho_t c_t \frac{\partial T(x,y,z,t)}{\partial t} = \left(\frac{1}{x} \frac{\partial}{\partial x} \left(k_t \frac{\partial T}{\partial x} \right) + \frac{1}{x^2} \frac{\partial}{\partial y} \left(k_t \frac{\partial T}{\partial y} \right) + \frac{\partial}{\partial z} \left(k_t \frac{\partial T}{\partial z} \right) \right)$$
$$+ Q_{m(x,y,z)} + \left(\rho_{bl} \times V_{bl} \times C\rho_{bl} \times (T_{art} - T) \right) \tag{33}$$

Equation (33) is obtained after using equation (29). Equation (33) (bio-heat equation) describes the heat dissipation in a homogenous, infinite tissue volume.

According to Equation (33), from left to right, the term on the left is the storage of heat within the tissue. (ρ_t (kg/m^3) is the density of the tissue, c_t (J/kg K) is the specific heat of the tissue, t is the time in seconds). The second term is the heat conduction term, which shows the heat flow from warmer to a colder tissue region in radial, tangential, and axial directions. (k_t is the tissue conductivity (W.m^{-1}.K^{-1}), T is the tissue temperature (K)). The third term, Q_m (W/m^3), is heat produced by metabolism, and the last term is the rate of energy transported by bloodstream (T_{art} is the arterial temperature and $\rho_{bl}, V_{bl}, C_{bl}$ denote the density of blood (kg/m^3), volumetric flow rate (m^3 s) and specific heat of the blood (J/kg K), respectively).

In order to find out the temperature distribution of the overall body, the bio-heat Equation (33) is solved in the radial, tangential and axial directions by using the finite difference technique. At the outer surface of the human body, heat is removed by a linear combination of convection, radiation, and sweat evaporation. Thus, for head, the total heat loss due to the

environment is calculated by the sum of the radiation heat loss, convection heat loss, and evaporation heat loss as shown in Equation (34)

$$Heat_{loss} = \varepsilon \times \sigma \times A_{eff}\left((T_{skin}+273)^4 - (T_{air}+273)^4\right) + h_c \times A_{eff}(T_{skin}-T_{air})$$
$$+ \frac{4148}{3600} \times (0.35) \times A_{eff}\left(p_{skin-}p_{air}\right) \tag{34}$$

Therefore, Equation (29) is substituted into the bio-heat Equation (5) to generate Equation (35)

$$\rho c_p \frac{\partial T(x,y,z,t)}{\partial t} = \frac{1}{x}\frac{\partial}{\partial x}\left(kx\frac{\partial T}{\partial x}\right) + \frac{1}{x^2}\frac{\partial}{\partial y}\left(k\frac{\partial T}{\partial y}\right) + \frac{\partial}{\partial z}\left(k\frac{\partial T}{\partial z}\right)$$
$$+ \rho SAR + Q_{m(x,y,z)} + \left[\rho_{bl} \times w_{bl} \times C\rho_{bl} \times (T_{art}-T)\right] - Heat_{loss} \tag{35}$$

Solution Technique

To achieve the main aim of the study, a partial derivative form of 3-D modelled of PBHE (35) is solved. The finite-difference technique is used to solve the bio-heat equation by using the explicit method. A spherical geometry is selected in order to reproduce a head- like model. The radius of the sphere is 100 mm to reproduce the average head size. The spherical model is divided into small 3-D tissue elements as shown in Figure 5 depicting the impact direction in numerical simulations.
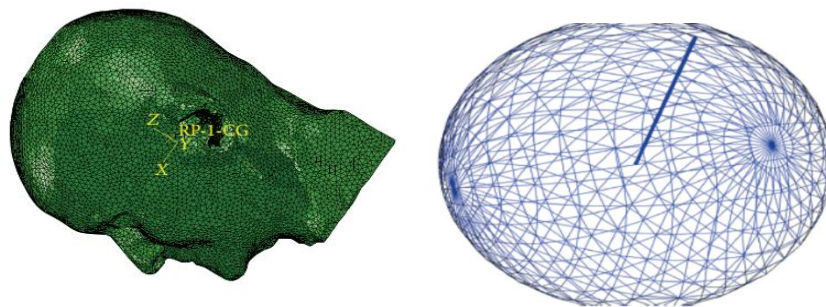
Figure 5: Illustration of the Impact Direction in Numerical Simulations.

Source: (Yang et al., 2014).

63

The modelled bio-heat Equation (25) was changed into finite difference form in order to calculate the temperature of nodes. The coordinate, (x, y, z) in Figure 6 of point B at a node in a sphere coordinate system represents (r, ϕ, z). The subscripts (i, j, k) are used to designate the (r, ϕ, z) locations of discrete nodal points.
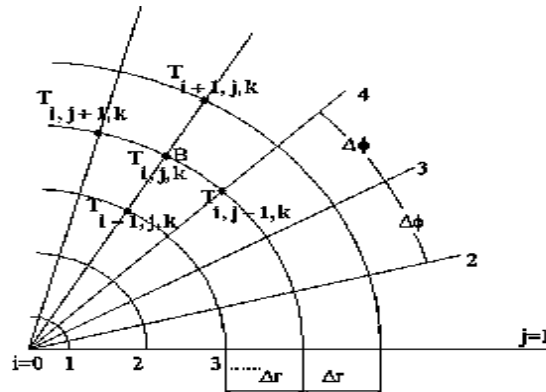
Figure 6: A (r, ϕ, z) Network in the Spherical Coordinate System.

Source: (Yildirim, 2005).

Finite Difference Time Domain (FDTM)

The explicit method is derived through a differential approach by the discretization of the modelled PBHE on an orthogonal grid for a uniform spacing by applying a finite difference scheme. With this approach, at the location ($i\delta x$, $j\delta y$, $k\delta z$), the temperature at time step $f + 1$ is estimated using the tissues characteristics shown in Table 2 and discretized in time and the integer f is used where $t = f\Delta t$. The finite difference approximation to the time derivatives in the bio-heat equation is expressed as an approximation of time derivatives (Yildirim, 2005).

The time grid, $0 = t_0 < t_1 < ... < t_{f-2} < t_{f-1} < t_f < ... < t_f < \infty$ with a constant step $\Delta t = t_f - t_{f-1}$ is introduced using Lagrange interpolations. For the points

64

$(t_{f-2}, T_{f-2}), (t_{f-1}, T_{f-1}) \, \& \, (t_f, T_f)$ where,

$T_{f-2} = T(x, y, z, t_{f-2}), \quad T_{f-1} = T(x, y, z, t_{f-1}), \quad T_f = T(x, y, z, t_f)$ are obtain and

expressed as in Equation (36).

$$t \in [t_{f-2}, t_f]: T(x, y, z, t) = T_{f-2} \frac{(t-t_{f-1})(t-t_f)}{(t_{f-2}-t_{f-1})(t_{f-2}-t_f)} + T_{f-1} \frac{(t-t_{f-2})(t-t_f)}{(t_{f-1}-t_{f-2})(t_{f-1}-t_f)} + T_f \frac{(t-t_{f-2})(t-t_{f-1})}{(t_f-t_{f-2})(t_f-t_{f-1})}$$

$$= T_{f-2} \frac{(t-t_{f-1})(t-t_f)}{2(\Delta t)^2} - T_{f-1} \frac{(t-t_{f-2})(t-t_f)}{(\Delta t)^2} + T_f \frac{(t-t_{f-2})(t-t_{f-1})}{2(\Delta t)^2} \qquad (36)$$

On the basis of Equation (36) the time derivative is obtained as Equations (37)

and (38):

$$t \in [t_{f-2}, t_f]: \frac{\partial T(x, y, z, t)}{\partial t} = T_{f-2} \frac{2t - t_f - t_{f-1}}{2(\Delta t)^2} - T_{f-1} \frac{2t - t_f - t_{f-2}}{(\Delta t)^2} + T_f \frac{2t - t_{f-1} - t_{f-2}}{2(\Delta t)^2}$$

$$\qquad (37)$$

and then,

$$\left. \frac{\partial T(x, y, z, t)}{\partial t} \right|_{t=t_f} = \frac{T_{f-2} - 4T_{f-1} + 3T_f}{2\Delta t} \qquad (38)$$

The 3-D problem is oriented in a cartesian coordinate system (x, y, z) to

generates Equation (39).

$$\nabla^2 T(x, y, z) = \frac{\partial^2 T(x, y, z, t)}{\partial x^2} + \frac{\partial^2 T(x, y, z, t)}{\partial y^2} + \frac{\partial^2 T(x, y, z, t)}{\partial z^2} \qquad (39)$$

Applying the central difference scheme for Equation (37) with respect to the

geometrical co-ordinates to constant mesh step, h, can be taken into account in

Equation (37) to generate Equation (40)

$$\left(\frac{\partial^2 T}{\partial x^2} + \frac{\partial^2 T}{\partial y^2} + \frac{\partial^2 T}{\partial z^2} \right) = \frac{T_{i-1,j,k} - 2T_{i,j,k} + T_{i+1,j,k}}{h^2} + \frac{T_{i,j-1,k} - 2T_{i,j,k} + T_{i,j+1,k}}{h^2}$$

$$+ \frac{T_{i,j,k-1} - 2T_{i,j,k} + T_{i,j,k+1}}{h^2} \qquad (40)$$

where $T_{i,j,k} = T(x_i, y_j, z_k, t), T_{i-1,j,k} = T(x_{i-1}, y_j, z_k, t)$,

Using the explicit scheme of FDTD, Equation (33) is approximated as Equation (41)

$$\rho c_p \frac{{T_{i,j,k}}^{n+1} - {T_{i,j,k}}^{n}}{\Delta t} = \frac{T_{i-1,j,k} - 2T_{i,j,k} + T_{i+1,j,k}}{h^2} + \frac{T_{i,j-1,k} - 2T_{i,j,k} + T_{i,j+1,k}}{h^2}$$

$$+ \frac{T_{i,j,k-1} - 2T_{i,j,k} + T_{i,j,k+1}}{h^2} + \rho SAR + Q_{m(x,y,z)}$$

$$+ \left[\rho_{bl} \times w_{bl} \times C\rho_{bl} \times (T_{art} - T) \right] - Heat_{loss} \tag{41}$$

$$\rho c_p \frac{{T_{i,j,k}}^{f+1} - {T_{i,j,k}}^{f}}{\Delta t} = \frac{1}{h^2}\left(T_{i-1,j,k}^{f-1} + T_{i+1,j,k}^{f-1} + T_{i,j-1,k}^{f-1} + T_{i,j+1,k}^{f-1} + T_{i,j,k-1}^{f-1} + T_{i,j,k+1}^{f-1} - 6T_{i,j,k}^{f-1} \right)$$

$$+ \rho SAR + Q_{m(x,y,z)} + \left[\rho_{bl} \times w_{bl} \times C\rho_{bl} \times (T_{art} - T) \right] - Heat_{loss} \tag{42}$$

Equation (35) generates a system of linear equations as shown in Equation (42)

Finite Difference Method (FDM)

Applying the central difference scheme of Equation (35) with respect to the geometrical co-ordinates to constant mesh step h is also expressed as Equation (40). Using the explicit scheme of FDM Equation (35) is approximated as shown in Equation 41.

$$T_{i,j,k} = \frac{1}{h^2}\left(T_{i-1,j,k}^{f-1} + T_{i+1,j,k}^{f-1} + T_{i,j-1,k}^{f-1} + T_{i,j+1,k}^{f-1} + T_{i,j,k-1}^{f-1} + T_{i,j,k+1}^{f-1} - 6T_{i,j,k}^{f-1} \right) + \rho SAR$$

$$+ \frac{1}{k}\left(Q_{m(x,y,z)} + \left[\rho_{bl} \times w_{bl} \times C\rho_{bl} \times (T_{art} - T) \right] \right) - Heat_{loss} \tag{43}$$

Equation (29) generates a system of linear Equations as shown in Equation (44)

$$T_{i,j,k} = \frac{1}{h^2}\left(\begin{array}{l} T_{i-1,j,k}^{f-1} + T_{i+1,j,k}^{f-1} + T_{i,j-1,k}^{f-1} + T_{i,j+1,k}^{f-1} + T_{i,j,k-1}^{f-1} + T_{i,j,k+1}^{f-1} - \dfrac{\rho c_p}{2k\Delta xyz}T_{i,j,k}^{(f-2)} \\ + \dfrac{\rho_{bl} \times w_{bl} \times C\rho_{bl} \times (T_{art} - T)}{k} \end{array} \right) + \rho SAR + Q_{m(x,y,z)}$$

$$+ \left\{ -\frac{w_{bl} \times C\rho_{bl}}{k} - \frac{6}{h^2} \right\} T_{i,j,k}^{(f-1)} - Heat_{loss} \tag{44}$$

Boundary Conditions

With the finite difference time domain, the rise in temperature at a time is the difference between the temperature calculated for the model exposed to the RF source, $T((i,j,k,t),(SAR\neq 0))$ and $T(i,j,k,t),(SAR=0))$, is the temperature for the unexposed model. The main assumption of this model is that blood enters the brain with the body temperature and leaves it with brain temperature. For the transient head temperature distribution, the air temperature with time-varying moving inside the spherical head and the heat dissipated by the time-dependent convection, $k\dfrac{\partial T}{\partial A}=h(t)(T-T_{art})$ where T_{en} is environmental temperature and h is the heat transfer coefficient. $T(A)=T_o(A),$ when $t=0$.

Table 3: The Boundary Conditions of Bio-Heat Equation.

Number	Boundary Condition (BC)	Finite Difference form of BC	Fictitious Temperature
BC1	$(x,y,z)\in\Gamma:T(x,y,z,t)=T_{art}(x,y,z)=37^oC$	$T_{i,j,k}\big|_{t=0}=37^oC$	$T_{art_{(x,y,z)}}=T_{i,j,k}$
BC2	$t=0:T(x,y,z,t)=T_0,\dfrac{\partial T(x,y,z,t)}{\partial t}\bigg|_{t=0}=0$	$\dfrac{T_{i,j,k}^{\,f+1}-T_{i,j,k}^{\,f}}{\Delta t}\bigg|_{t=0}=0$	$T_{i,j,k}^{\,f+1}=T_{i,j,k}^{\,f}$
BC3	$k\dfrac{\partial T}{\partial(x,y,z)}=h(t)(T-T_{art})$	$T(i,j,k)=T_o(,j,k)$, $t=0$	

Using the boundary condition of the modified PBHE in Table 3, the resultant linear Equations (42) and (44) were solved with a programming

67

language (Matlab version, R2017A). The algorithms for the solved equations shown in Appendix E were stimulated to demonstrate the thermo-mechanical interaction of the biological tissue in the brain.

Polynomial Fitting

The relation between experimental temperature before scan (TBS) and temperature after scan (TAS) of patients was calculated using poly-fitting:

$p(x) = -x^3 + 0.0042x^2 - 0.16x - 1.92$ for temperature prediction. With the help of Excel patients TAS was predicted.

Chapter Summary

In the study, the SAR value which based on the scan time, number of slices chosen, NSA and number of acquisition was monitored and strategically controlled. One hundred and fourteen (114) volunteer patients underwent brain scanned of MRI of field strength 1.5 T MRI at 37 Military Hospital and 0.3 T at Diagnostic Centre Limited both found in Accra, Ghana. Forehead and tympanic temperatures of the patients were measured after the study protocol was approved by the ethics board of University of Cape Coast Review Board (UCCIRB) with ethical clearance – ID NO: (UCCIRB/CHAS/2016/01).

The Penne's bio-heat equation (1948) was modelled to provide a suitable numerical homogenously model of temperature distribution in the human brain where heat exchange mechanism such as thermal conduction, convection, perfusion of blood, regional heat source and metabolic heat generation in tissue were taken into account. Explicit method of FDTD and FDM were applied to solve modified PBHE to determine temperature changes in the human tissue during brain MRI with the help of Matlab. With the help of thermal properties for the biological tissues contained in the human head

model and the appropriate boundary conditions used, the modified PBHE was stimulated to demonstrate the thermo-mechanical interaction of the biological tissues in the brain.

CHAPTER FOUR

RESULTS AND DISCUSSION

Introduction

The study modified PBHE to numerically estimate the brain temperature of patients during MRI. The modified Penne's equation was solved in three dimensions, and the algorithms of the solved equation for the temperature simulation were obtained with the help of Matlab. The numerical results were compared with the experimental results.

In this section, the results from the theoretical model and experimental data are presented and discussed.

Steady State Temperature Distribution in Three Dimensions

The results of the numerical simulation obtained are as follows:

The code of Equation (44) is shown in Appendix E where $T\left[(i,j,k),(SAR=0,t=0)\right]$ depicts the evolution and the distribution of the temperature inside the head shown in Figure 7.
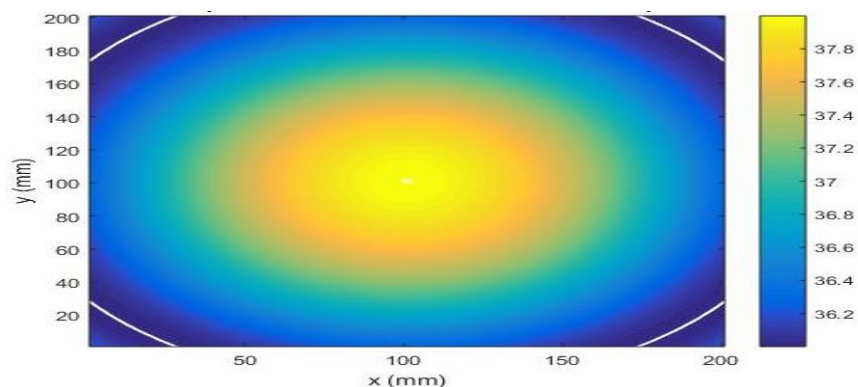
Figure 7: Brain Temperature Distribution before EMR Exposure.

The code of Equation (44) shown in Appendix E where $T\left[(i,j,k),(SAR=3.2,t=0)\right]$ depicts the distribution of the temperature

70

inside the head as a result of the power deposited by RF of frequencies above 100 kHz sources shown in Figure 8.
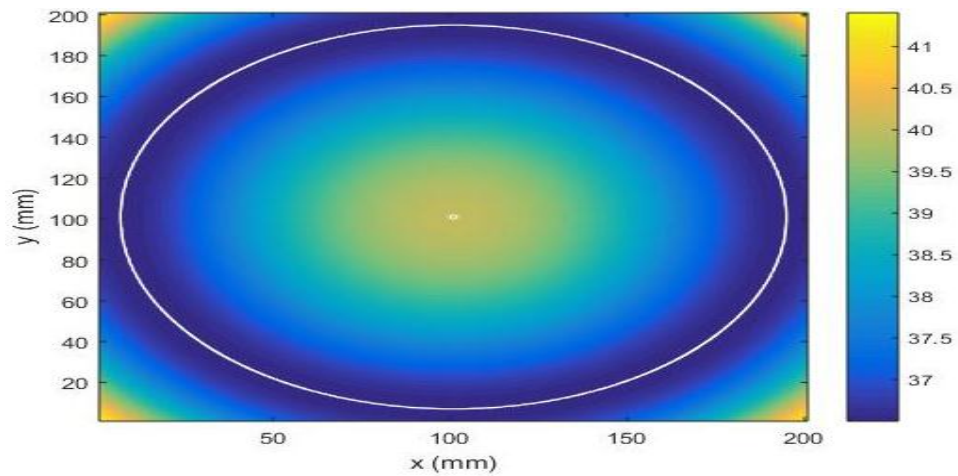
Figure 8: Brain Temperature Distribution after EMR Exposure.

Figure 7 depicts the temperature distribution of human head (brain) before the EMR exposure in three dimensions. The temperature values of the simulated temperature distributions of the patients before undergoing MRI in Figure 7 shows that skin surface maintains a lower temperature in comparison with the temperature inside the brain of the patient which is one of the site of the core temperature of human. Thus, the temperature values of the skin are within the range of 36.2 ^{o}C to 36.8 ^{o}C which falls within the normal human body temperature readings. The temperature distribution inside the brain is in the range of 36.9 ^{o}C to 37.8 ^{o}C. This indicates normal temperature range and moderate fever. Thus, high-temperature distributions occur inside the brain. The results show that brain temperature is cooler at peripheral areas of the head and warmer approaching the core of the brain which confirms with a study carried out by Zhu et al., (2006) and a reviewed article by Mcilvoy, (2004) (Mcilvoy, 2004; Zhu, et al., 2006).

71

In addition, the epidural space temperatures from the theoretical calculation shown in Figure 7 before MRI is in the range of 36.9 ^{o}C to 37.4 ^{o}C and the lateral ventricle is in the range of 37.5 ^{o}C to 37.8 ^{o}C by a gradient of 0.1- 0.3 ^{o}C. Therefore, according to Mellergard 1994, 1995, Mellergard and Norstrom 1990, 1991, and in this study, the temperature within brain varies by depth and temperature measured in epidural space is lower than temperatures measured in lateral ventricle (Mellergård, 1994, 1995; Mellergard & Nordström, 1990; Mellergård & Nordström, 1991).

Figure 8 shows the brain temperature profile of the various temperature distributions after MRI of field strength above 100 kHz. It indicates the head temperature after patients received a RF pulse of EMR during brain MRI. The temperature values of the simulated temperature distributions after brain MRI showed that skin surface after MRI recorded temperatures in the range of 40.0 ^{o}C to 41.0 ^{o}C and the temperatures at the centre of the patients' brain is in the range of 38.0 ^{o}C to 39.5 ^{o}C.

By comparing the theoretical models of brain temperature distribution before and after EMR exposure, the temperatures recorded confirmed literature reviewed (Habash et al., 2007; Lak, 2012; MHRA, 2015); that, there is absorption of energy from RF fields during MRI by tissues resulting in excessive temperature elevation at the skin surface of patients which suggests that the ohmic heating of tissue is greatest at the surface and minimal at the centre of the patient's brain, and this agrees with Proceedings of the International Conference on Non-Ionizing Radiation (ICNIRP) (2004) at UNITEN (ICNIRP, 2004).

Transient State Temperature Distribution in Three Dimensions

The results of the numerical simulation obtained from the written code of Equation (43) shown in Appendix E where,

$$(x, y, z) \in \Gamma : T(x, y, z, t)\big|_{t \neq 0} = T_{art}(x, y, z) = 37^{o}C \quad \text{and} \quad T\big[(i, j, k, t), (SAR = 3.2)\big] \text{ is}$$

shown in Figures 9 and 10.
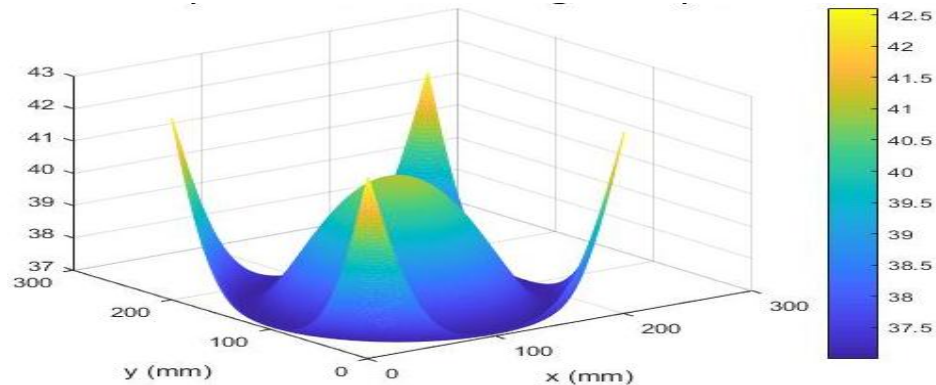
Figure 9: 3-D Brain Temperature during Brain MRI.

The thermal simulation of EM RF of frequency above 100 kHz based on FDTD method depicting temperature changes caused by RF absorption during brain MRI using 3-D modified PBHE is illustrated in Figure 9. The peaks temperature changes caused by EM RF absorption in Figure 9 is illustrated in 2-D shown in Figure 10 as the hot spots during MRI scan.
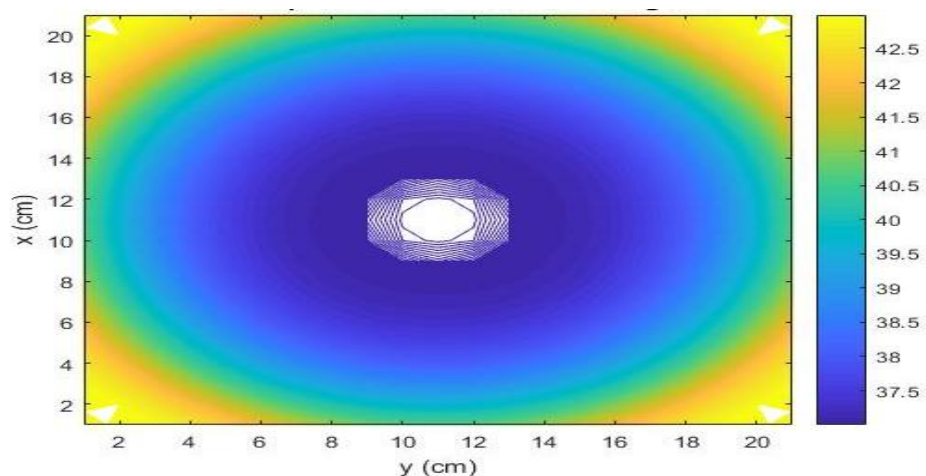
Figure 10: 2-D Head Temperature during Brain MRI.

73
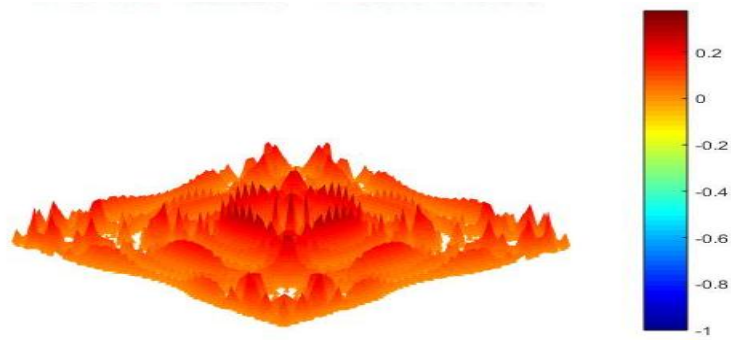
Figure 11: Head Temperature during Brain MRI, t = 20.62 seconds.

The simulated results of the numerical calculation shown in Figure 11 depicts the transient temperature profiles of the in-vivo brain tissue temperature from the code of Equation (42) shown in Appendix E where,

$$\left(x, y, z\right) \in \Gamma : T\left(x, y, z, t\right)\big|_{t=20.62 \text{sec.}} = T_{art}\left(x, y, z\right) \neq 37^{o}C \text{ and } T\left[\left(i, j, k, t\right), \left(SAR = 3.2\right)\right].$$
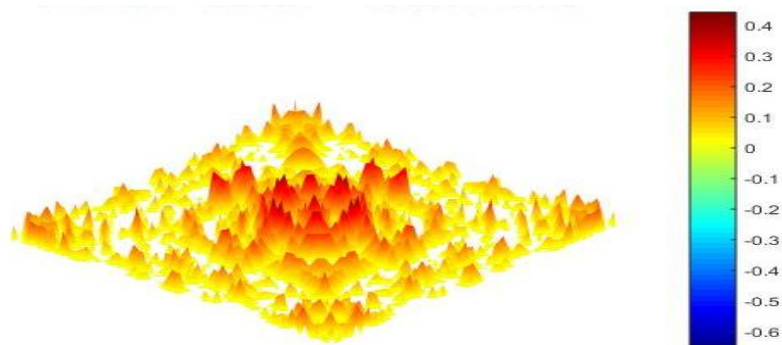
Figure 12: Head Temperature during Brain MRI, t = 30.92 seconds.

The simulated results of the numerical calculation shown in Figure 12 depicts the transient temperature profiles of the in-vivo brain tissue temperature from the code of Equation (42) shown in Appendix E where,

$$\left(x, y, z\right) \in \Gamma : T\left(x, y, z, t\right)\big|_{t=30.92 \text{sec.}} = T_{art}\left(x, y, z\right) \neq 37^{o}C \text{ and } T\left[\left(i, j, k, t\right), \left(SAR = 3.2\right)\right].$$
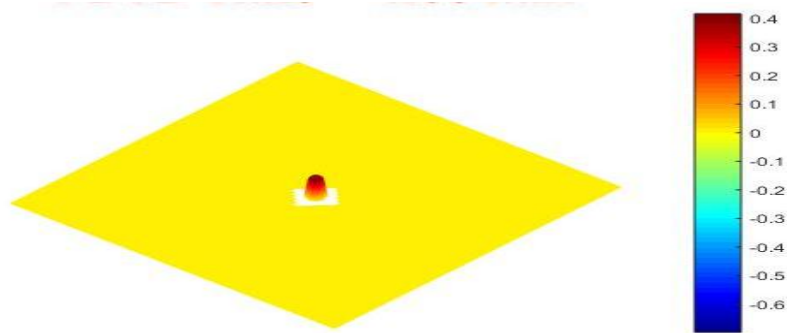
Figure 13: Head Temperature during Brain MRI, t = 1.03 minutes.

The simulated results of the numerical calculation shown in Figure 13 depicts the transient temperature profiles of the in-vivo brain tissue temperature from the code of Equation (42) shown in Appendix E where,

$$(x,y,z)\in\Gamma : T(x,y,z,t)\big|_{t=1.03\min.} = T_{art}(x,y,z)\neq 37^{o}C \text{ and } T\big[(i,j,k,t),(SAR=3.2)\big].$$
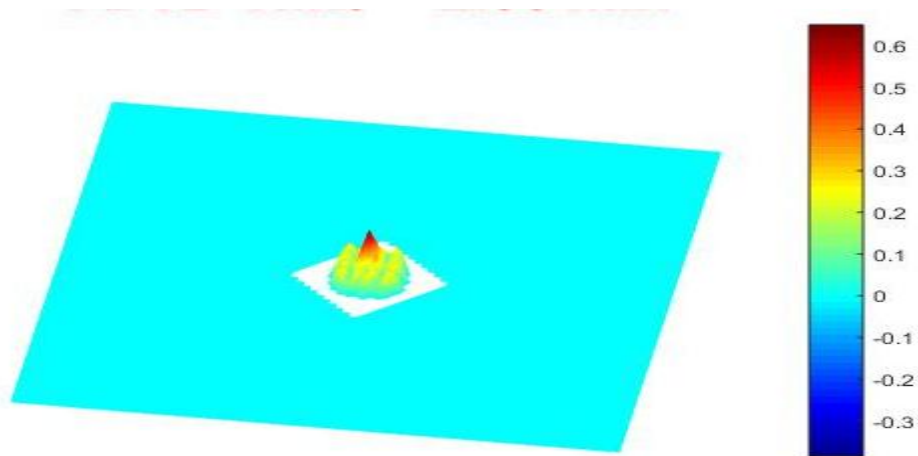
Figure 14: Head Temperature during Brain MRI, t = 2.06 minutes.

The simulated results of the numerical calculation shown in Figure 14 depicts the transient temperature profiles of the in-vivo brain tissue temperature from the code of Equation (42) shown in Appendix E where,

$$\left(x,y,z\right) \in \Gamma : T\left(x,y,z,t\right)\Big|_{t=2.06\,\text{min.}} = T_{art}\left(x,y,z\right) \neq 37^{o}C \ \text{ and } \ T\left[\left(i,j,k,t\right),\left(SAR=3.2\right)\right].$$
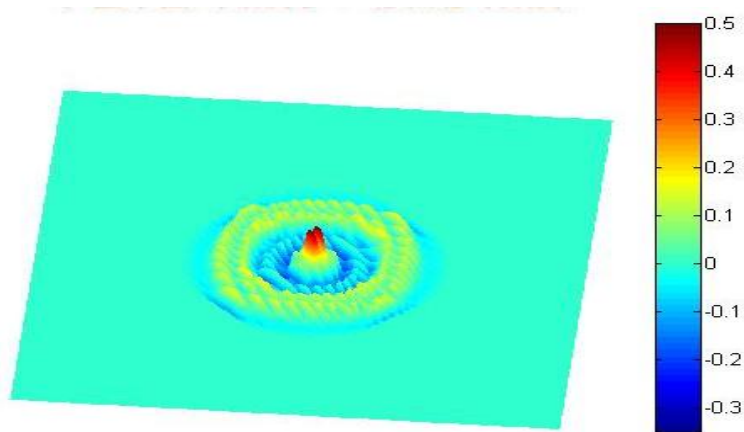
Figure 15: Head Temperature during Brain MRI, t = 5.15 minutes.

The simulated results of the numerical calculation shown in Figure 15 depicts the transient temperature profiles of the in-vivo brain tissue temperature from the code of Equation (42) shown in Appendix E where,

$$\left(x,y,z\right) \in \Gamma : T\left(x,y,z,t\right)\Big|_{t=5.15\,\text{min.}} = T_{art}\left(x,y,z\right) \neq 37^{o}C \ \text{ and } \ T\left[\left(i,j,k,t\right),\left(SAR=3.2\right)\right]$$

Discussion

The 3-D and 2-D simulation of Figure 9 and 10 respectively depict volumetric energy deposition due to RF absorption during MRI scan. The RF fields emitted during MRI penetrate the exposed biological tissues and produce heat as shown in Figure 9. The simulated results of this study include contributions of patient and environmental parameters as well as contributions from radiation, convection, and evaporation. The results indicate anticipating thermal effect during head MRI.

This thermal effect can cause hyperthermia and damage biological tissues. The minimum temperature during MRI from the simulated results is 0.5 °C higher than the baseline physiological temperature which is 37.5 °C, and this confirms with the limited published data of the human brain

76

temperature (Narebski, 1985). The maximum temperature is recorded as 42.5 $^{\circ}$C at the skin. This maximum temperature recorded is approximately in the temperature upper limit at which painful sensations or damage occur (Hardy et al., 1967). Due to the different thermal properties of the tissues and the organs of the head, Figure 9 depicts that RF of the EMR of MRI which leads to tissue heating is the highest in the skin, low in the skull, but higher again in the brain, and this agrees with Leeuwen et al., (Van Leeuwen et al., 1999) work.

From the results obatined by Nguyen et al., (2004) and this study, it is not surprising that the maximum SAR of RF causing the hyperthermia recorded from the simulated results during head MRI is within the skin. This indicates 'hot spot' sites since the magnitude of electric field from the RF transmitter to the tissue during MRI scan increases dramatically as one approaches the transmitter coil. The result also agrees with Zamanian & Hardiman (2005), that there is a low penetration of RF EM energy at the skin surface which leads to high absorption of RF energy. This accounts for the hot spots of the skin region and can lead to burning effects. The simulated results showed that during brain MRI, abnormal high brain temperature will be recorded. The present work clearly shows that the hyperthermia recorded may affect the body's regulatory mechanism.

The simulated results of this study (stated it here) indicate that the average temperature during brain MRI of frequency above 100 kHz exceeds the FDA recommended value of 38 $^{\circ}$C stated in the FDA Guidance for MRI system safety and patient exposures (Ibrahiem et al., 2005; Ng, 2003; ICNIRP, 2009; Zaremba & Phillips, 2002; FDA, 2009; Zaremba, 2000).

Figures 11, 12, 13, 14 and 15 show head temperature change during brain MRI. The maximum head tissue temperature of the brain exposed to RF energy at frequencies above 100 kHz recorded at a time $t = 20.62\,\text{sec}$ is 0.2 $^{\circ}$C and $t = 30.92\,\text{sec}$ is 0.4 $^{\circ}$C, as shown in Figures 11 and 12, respectively. Figures 13 and 14 depict anticipated head temperature distribution in the head during MRI at scan duration of 1.03 minutes and 2.06 minutes, respectively. The highest temperature measured during the scan duration of 1.03 minutes and 2.06 minutes are 0.4 $^{\circ}$C and 0.6 $^{\circ}$C, respectively. The head temperature distribution is clearly seen in Figure 15 which depicts anticipated head temperature distribution during brain MRI in 5.15 minutes.

The results shown in Figures 11 to Figure 15 depict the temperature profiles of the in-vivo brain tissue temperature model and agrees with the results obtained that there is energy deposition in patients exposed to electromagnetic frequency and as a result, temperature increase within patients is impossible to be avoided, and the brain temperature variations during brain MRI increase as scan duration increases (Ahlbom et al., 2004; Formica & Silvestri, 2004; Kundi, 2005).

Experimental Validation Results

The pre-scan and post-scan tympanic temperatures of sixty-four (64) children aged between 7 months and 16 years measured with the IRT show the highest temperature change of 1.5 $^{\circ}$C for frequencies above 100 kHz (0.3 T and 1.5 T) as shown in Figures 16, 17 and 18.

Intermittent Tympanic Temperature Measurement
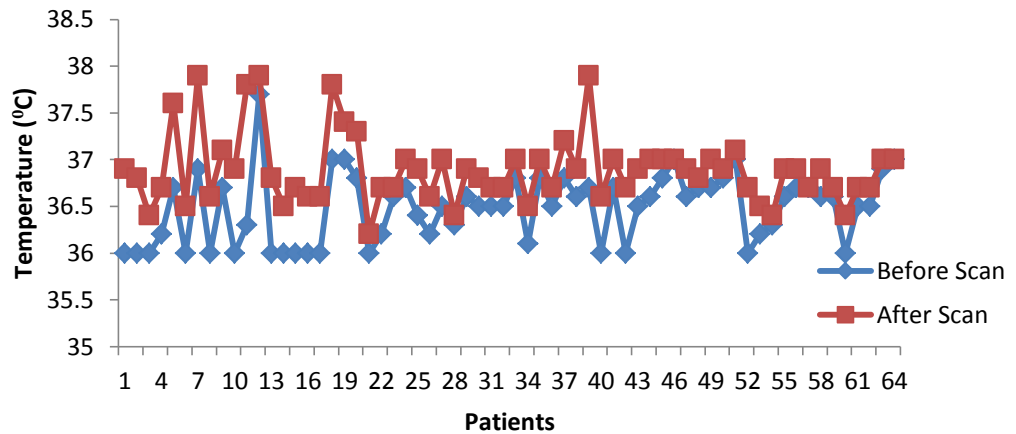
Figure 16: Experimental Analysis of Patients' Temperature before and after MRI Scan.

Figure 16 shows the temperature recorded before and after MRI scan of the sixty-four paediatric patients (aged 7 months to 16 years). These patients underwent brain MRI of RF above 100 kHz. The field strength of the MRI is 0.3 T and 1.5 T.
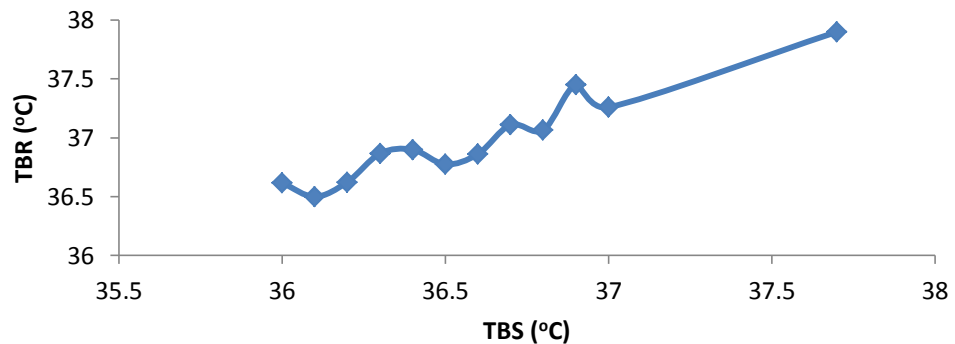
Figure 17: Experimental Analysis of Patients' Temperature increase after MRI.

Figure 17 depicts the pre-scan tympanic temperatures against the post-scan tympanic temperatures from the experimental temperature measurement.

79
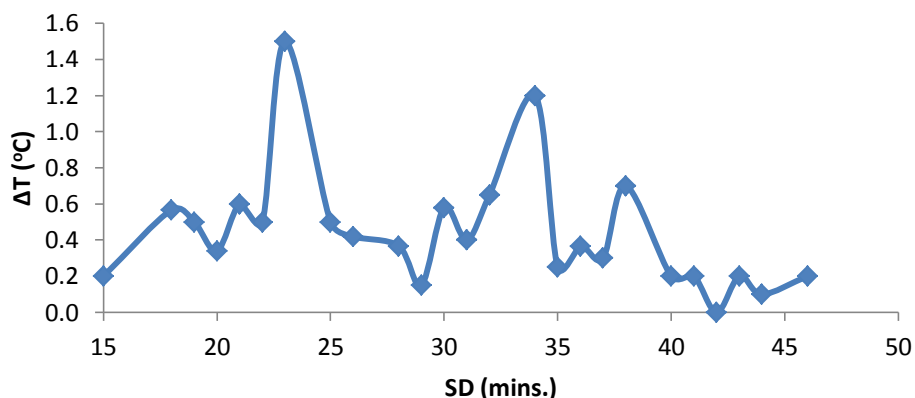
Figure 18: Experimental Analysis of Patients' Temperature Change with
Scan Duration.

Figure 18, depicts patients temperature change with scan duration where the highest change in temperature recorded was 1.5 ^{o}C at scan duration of 23 minutes.

Paediatric Patients Temperature Variations

The sixty-four paediatric patients (Figure 16) underwent MRI of field strength 0.3 T and 1.5 T. The temperature values measured before and after MRI of the patients are in the range of 36 ^{o}C to 38 ^{o}C. The pre-scan temperature measured is in the range of 36 ^{o}C to 37 ^{o}C, while the post-scan temperatures are 36.2 ^{o}C and 37.9 ^{o}C. Despite the ambient temperature of the MRI suite being maintained at 20 to 24 ^{o}C, the recorded SAR was 3.2 W/kg and no active warming device was used during MRI, the experimental results confirm Formica & Silvestri (2004), Shellock et al., (1994) and Machata et al., (2009) and the studies that patients' temperature increases during MRI scan (Formica & Silvestri, 2004; Machata et al., 2009; Shellock et al., 1994).

By comparing the experimental results of this study to validate the theoretical results despite the difference in the magnitude of the temperature

80

values in both theoretical and experimental results, there is temperature increase as patients are exposed to EMR. The theoretical simulated lowest and highest temperature measured during MRI was 37.0 ^{o}C and 41.0 ^{o}C, respectively which were higher than the experimental lowest and highest temperature measured as 36.2 ^{o}C and 37.9 ^{o}C, respectively. This may be as a result of the body's thermoregulatory mechanism which tends to ensure temperature balance by cancelling the high temperature of tissues by the normal biological activity of the body.

The graph of temperatures before scan against the temperatures after scan shown in Figure 17 is the experimental results of the study. It shows that patients with pre-scan tympanic temperatures below 37 ^{o}C recorded post-scan tympanic temperatures not above 37.5 ^{o}C, whilst patients whose pre-scan tympanic temperatures were at 37 ^{o}C and above recorded post-scan tympanic temperatures between 37.5 ^{o}C and 38.0 ^{o}C.

The tympanic temperature recorded in this study after brain MRI scan was between 36 ^{o}C to 38 ^{o}C and this falls within normal body temperature with scan duration less than one hour. The values of the pre-scan tympanic and post-scan tympanic were all within guidance levels (Ibrahiem et al., 2005; ICNIRP, 2009), of which there was no rise in body temperature (not more than 1.0 ^{o}C). The recorded head temperature values are not greater than 38.0 ^{o}C which confirms Dery et al, (2013). The highest increase in temperature change was 1.5 ^{o}C as shown in Figure 17 of the experimental results which depict the temperature change in patients after brain MRI scan and scan duration. The pre and post-scan temperatures resulted in temperature change of 1.5 ^{o}C was 36.3 ^{o}C and 37.8 ^{o}C, respectively of a patient sedated with midazolam. This

1.5 ^{o}C temperature change recorded may not pose any potential health hazard to the patients since the post-scan tympanic temperature is well below the recommended guidance levels set by International Electro-technical Commission (IEC) (2010).

Though the increase in temperature change confirms the results of Machata et al., (2009), that children undergoing MRI under sedation are at risk of hyperthermia (Machata et al., 2009). The change in temperature of the children who underwent MRI scan does not depend on the scan duration. In Figure 18, the highest change in temperature was 1.5 ^{o}C at scan duration of 23 minutes of a patient and temperature of 0.0 ^{o}C was recorded at the end of 43 minutes scan of patients. These changes could be as a result of differences in patients' physiological conditions.

Non-Invasive Continuous Forehead Temperature Measurement

Continuous real-time brain temperature was recorded using liquid crystal thermometers within head coil and infrared thermometer during MRI of fifty (50) patients aged from 32 to 68 years who underwent brain MRI of RF above 100 kHz (0.3 T and 1.5 T).
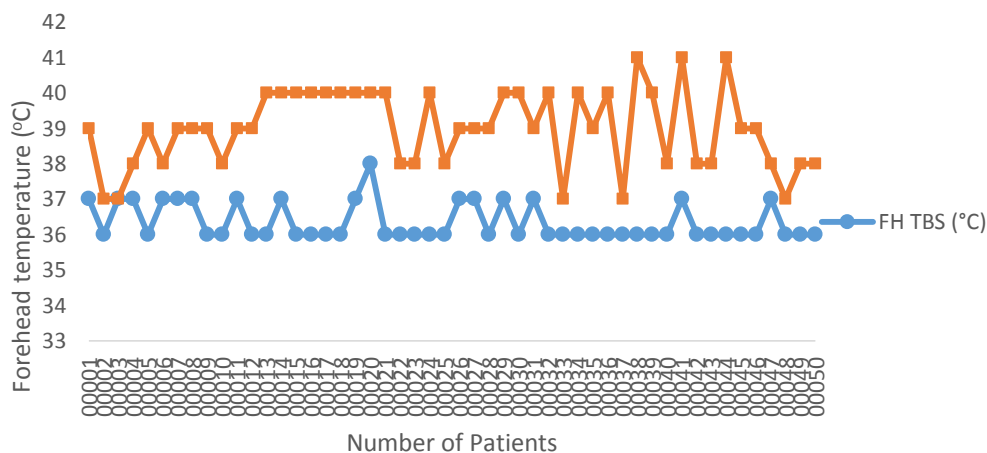
Figure 19: Experimental Analysis of Patients' Forehead Temperature before and during Brain MRI Scan.

82

Figure 19 shows forehead temperatures recorded before and during MRI scan of the fifty (50) patients aged from 32 to 68 years who underwent brain MRI of RF above 100 kHz.
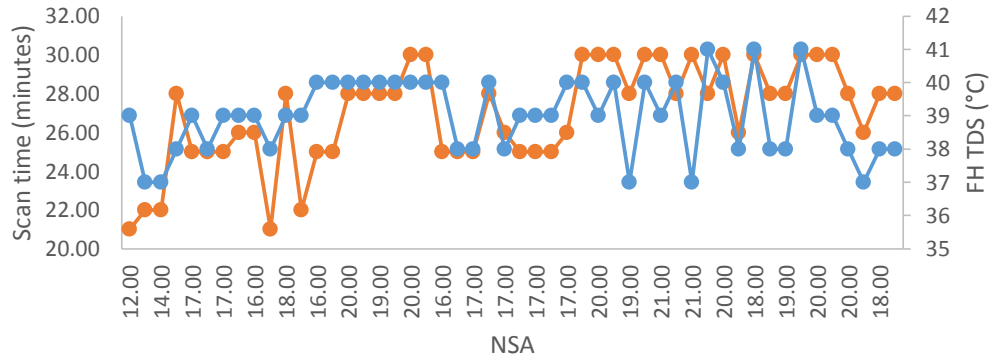
Figure 20: Experimental Analysis of Patients' Forehead Temperature during Brain MRI Scan with Scan Time and NSA.

Figure 20 depicts patients' forehead temperature with the corresponding scan duration and NSA, and the recorded SAR value was 3.2 W/kg with no active warming device being used.
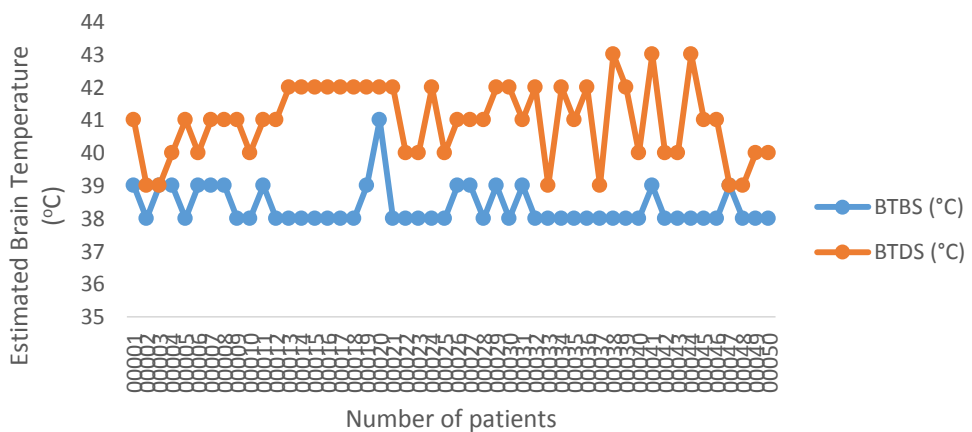
Figure 21: Estimated Patients' Brain Temperature before and during Brain MRI Scan.

Figure 21 estimates brain temperature during brain MRI which resulted from the forehead skin temperature Figure (19) and addition of two degrees (41 ^{o}C +2 ^{o}C).
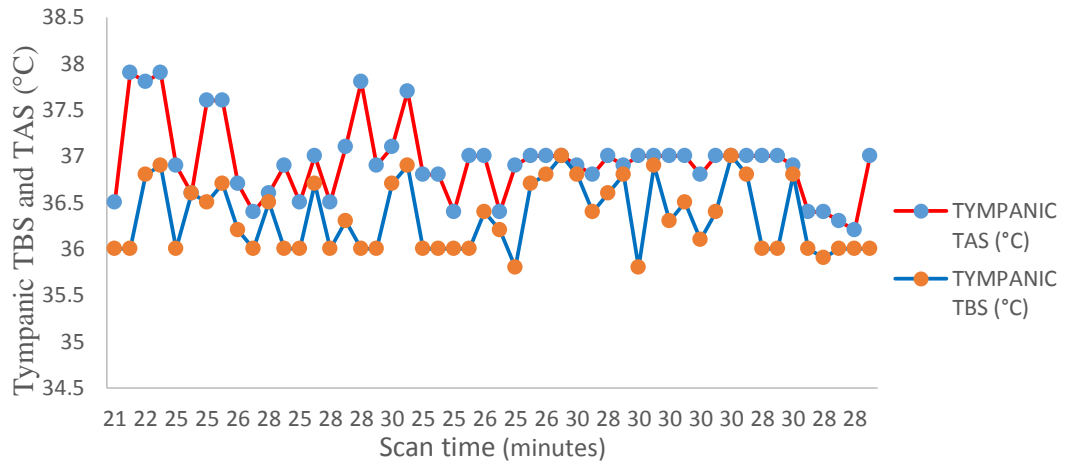
Figure 22: Experimental Analysis of Patients' Tympanic Temperature before and after Brain MRI Scan of Field Strength 0.3 T and 1.5 T.

Figure 22 shows intermittent measurement of brain temperature during brain MRI with an infra-red thermometer by measuring the right tympanic temperature before scan (TBS) and after the scan (TAS)
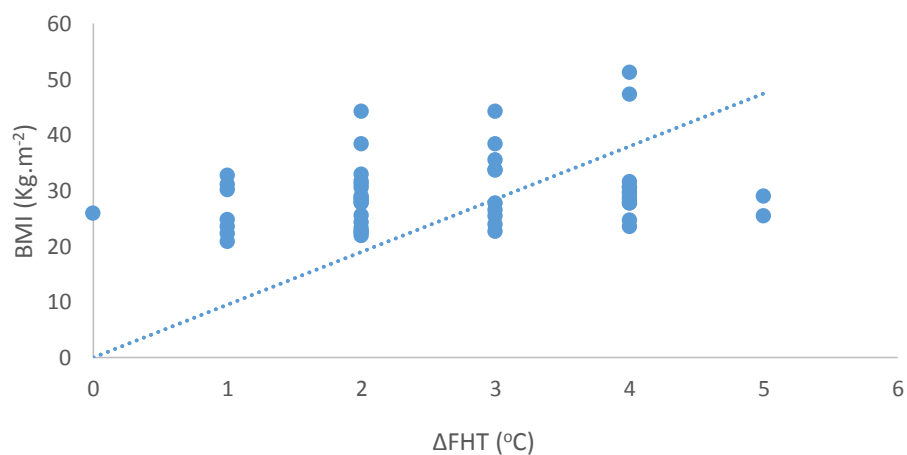
Figure 23: Experimental Analysis of Patients' Forehead Temperature Change during Brain MRI scan.

84

Figure 23 shows the relationship between forehead temperature change and BMI of patients
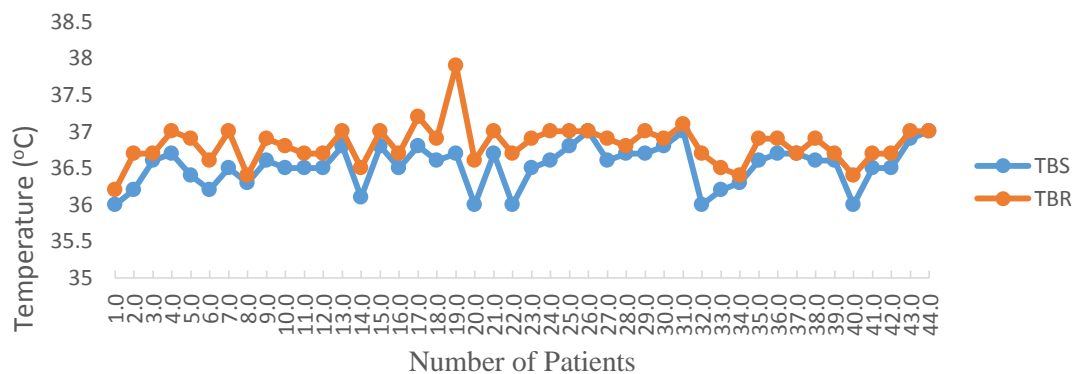
Figure 24: Experimental Analysis of Patients' temperature change before and after Brain MRI scan at a field strength of 0.3 T.

Figure 24 depicts forty-four (44) patients temperatures recorded during MRI of the static magnetic field strength 0.3 T.
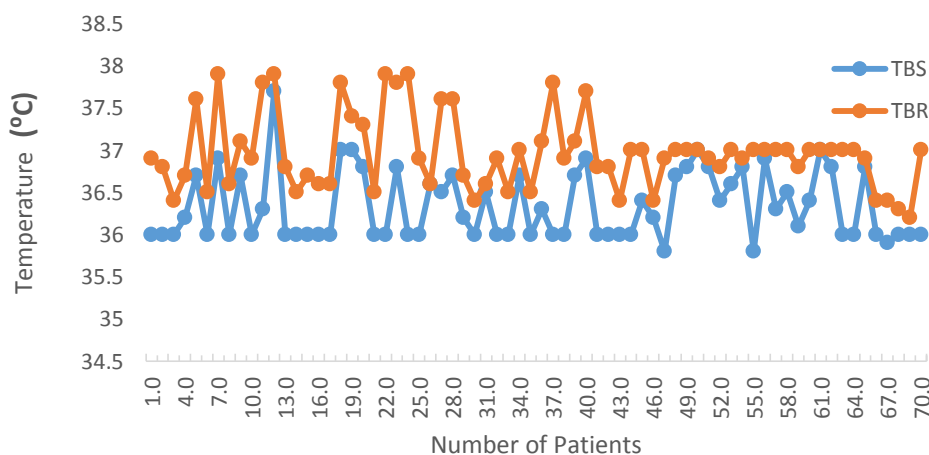
Figure 25: Experimental Analysis of Patients' Temperature change before and after Brain MRI Scan at a Field Strength of 1.5 T.

Figure 25 depicts seventy (70) patients who underwent brain MRI of the static magnetic field strength of 1.5 T.

85

Prediction of Patients Temperature after Magnetic Resonance Imaging
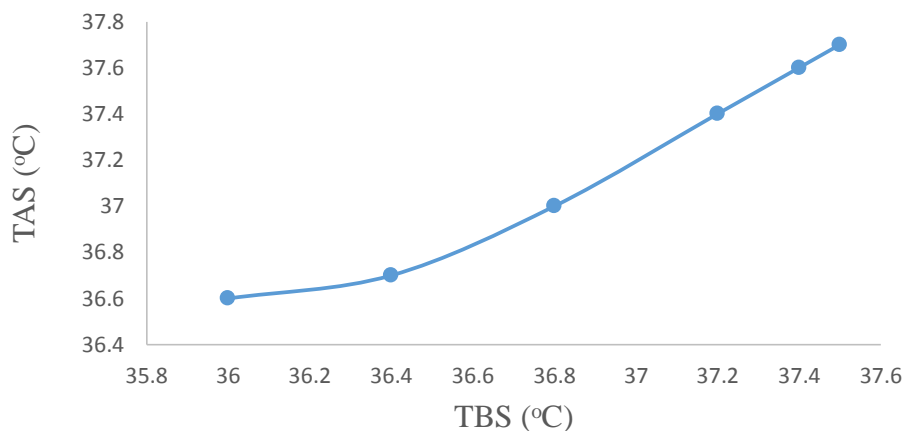
Figure 26: Prediction of Patients' Temperature after Brain MRI Scan.

Figure 26 predicts patients' temperature after scan when patients' temperature is in the range of 36 ^{o}C-37.5 ^{o}C before brain MRI.

Temperature Rise

The fifty (50) patients (Figure 19) aged from 32 to 68 years who underwent brain MRI of RF above 100 kHz field strength of MRI are 1.5 T and 0.3 T. The temperature values measures before and during brain MRI of patients with LCT are in the range of 36 ^{o}C - 41 ^{o}C. The pre-scan forehead temperatures are in the range of 36 ^{o}C - 38 ^{o}C, while the forehead temperature during MRI recorded is in the range of 37 ^{o}C to 41 ^{o}C. The highest temperature recorded during brain MRI is 41 ^{o}C at scan duration of 30 minutes at NSA of 20 shown in Figure 20. In spite of keeping the ambient temperature of the MRI suite from 20 to 24 ^{o}C, and the recorded SAR value was 3.2 W/kg with no active warming device being used. The average pre-scan forehead temperatures of patients who recorded 41 ^{o}C during forehead scan were 36.3 ^{o}C with a temperature change of 4.7 ^{o}C.

86

By comparing the theoretical results with the experimental results, the actual measured temperature of the strip of the LCT placed on the forehead during MRI (Figure 19) monitored skin temperature trend instead of actual measuring brain temperature. This accounts for the difference in the magnitude of the temperature values in both the numerical and experimental results as shown in Figures 9, 10 and 19.

The highest estimated brain temperature during brain MRI of the study (Figure 21) is 43 ^{o}C, which resulted from the highest forehead skin temperature (Figure 19) and addition of two degrees (41 ^{o}C +2 ^{o}C). The highest value of the estimated brain temperature is 0.5 ^{o}C higher than the highest simulated brain temperatures during brain MRI. This highest estimated temperature value is a deviation of $\pm$ 3.5°C from the resting temperature of 37 °C depicting brain hyperthermia since the temperature value is above 40 ^{o}C – 41 ^{o}C (Kiyatkin, 2004) and this may be as a result of the pathological condition of the patients who underwent the brain MRI.

The intermittent measurement of brain temperature before scan (TBS) is in the range of 36 ^{o}C to 37 ^{o}C and TAS is in the range of 36.2 ^{o}C to 37.9 ^{o}C (Figure 22). The experimental results of TBS and TAS indicate that there is an increase in brain temperature after brain MRI despite the fact that the recorded post-scan temperatures were all within guidance levels since the rise in temperature is not more than 1.0 ^{o}C (Ng, 2003). Thus, the study, therefore, predicts that there is excessive elevation of patients' brain temperature which could exceed the guidance level.

Figure 23 shows the relationship between forehead temperature change and BMI of patients investigated. The BMI has been classified as

underweight, normal range, overweight and obese in a range <18.50 Kg/m^2, 18.50-24.9 Kg/m^2, ≥25.00 Kg/m^2 and ≥30.00 Kg/m^2, respectively, which are age independent (Brown et al., 2000; Flegal, Carroll, Ogden & Johnson, 2002; Gallagher et al., 2000; Organization, 2000). The highest obese recorded was 51.11Kg/m^2 with pre-and-post scan forehead temperature of 36.0 ^{o}C and 40.0 ^{o}C, respectively, with a temperature change of 4.0 ^{o}C. The patients with the highest average temperature change of 4.7 ^{o}C during brain MRI scan have an average BMI from 27.1 to 29.1 Kg/m^2. Figure 23 illustrates a linear relationship, since BMI of patients' increases by approximately the same rate as the forehead temperature changes by one unit. The study confirms the results of Zamanian & Hardiman (2005) that BMI correlates with the rise in body temperature during MRI since thick and fatty (more water content) tissues allow EM waves to penetrate more than in thin tissues. Therefore, the estimated brain temperature in the study assumes to be the same as the core temperature which agrees with the study conducted by Childs et al., (2005).

Figures 24 and 25 depict temperatures recorded during MRI of patients of field strength 0.3 T and 1.5 T. Out of forty-four (44) patients who underwent brain MRI of the static magnetic field strength of 0.3 T (Figure 24), approximately 93 % of the patients' brain temperature measured after the brain MRI was below 37 ^{o}C while approximately 7 % of the patients' brain temperature measured after the brain MRI recorded above 37 ^{o}C. At the highest temperature recorded after brain MRI of the static magnetic field strength of 0.3 T was 37.9 ^{o}C. The patient who recorded the highest brain temperature change of 1.2 ^{o}C had a temperature of 36.7 ^{o}C before brain MRI.

Also, seventy (70) patients underwent brain MRI of the static magnetic field strength of 1.5 T (Figure 25). Approximately, 24% of patients' brain temperatures measured after brain MRI were above 37 ^{o}C, while 76% of the patients recorded below 37 ^{o}C. The highest temperature recorded after brain MRI of the static magnetic field strength of 1.5 T was 37.9 ^{o}C. Patients who recorded the highest brain temperature after brain MRI, recorded brain temperature of 36 ^{o}C before brain MRI. The brain temperature change of the patient was 1.9 ^{o}C.

Figure 26 is the result of fitting polynomial predicting temperature of patients after scan. This result has shown that patients' temperature increases after MRI scan. Statistically, the experimental study depicts significant head tissues heating which may have no serious physiologic consequence. The study agrees with Shellock (2000a; 2000b) research conducted that RF power of EM field of MRI induce heat within patients' tissues due to resistive losses and the thermogenic qualities of the EM field. The differences in the brain temperature changes are as a result of the different RF from the clinical MRI systems used (0.3 Tesla and 1.5 Tesla). The SAR value recorded from both MRI systems during patient's scan was 3.2 W/kg.

Table 4: Qualitative Evaluation of Adult Patient's sweat during MRI

Number of Patients	BMI (Kg/m^2) range	Temperature values During MRI (^{o}C)	Sweat
5	21.4 to 27.4	37.0	D
12	18.9 to 30.9	38.0	D
14	19.4 to 33.4	39.0	S
16	19.9 to 37 9	40.0	HS
3	22.7 to 26.7	41.0	HS

MRI is a non-invasive and considered painless. Both adults and children experience anxiety during the MRI examination. Sweating of fifty (50) adult patients during MRI scan was evaluated qualitatively where D was assigned when no moisture was detected, S is when some moisture was detected, and HS is when distinct beads of sweat was visible (Table 4). Five (5) patients and twelve (12) patients with average BMI of ranging from 21.4 to 27.4 Kg/m^2 and 18.9 to 30.9 Kg/m^2, respectively, recorded 37 ^{o}C and 38 ^{o}C as temperature value during MRI recorded no moisture. Fourteen (14) patients of BMI ranging from 19.4 to 33.4 Kg/m^2 with 39 ^{o}C during MRI recorded moisture while sixteen (16) patients of 40 ^{o}C recorded as temperature during MRI and three (3) patients of 41 ^{o}C, recorded as temperature during MRI have BMI ranging from 19.9 to 37 9 Kg/m^2 and 22.7 to 26.7 Kg/m^2, respectively, in both cases recorded distinct beads of sweat.

From Table 4, the result shows that patients become warm due to the interaction of the radio waves with the body, therefore it is normal for patients with larger body frame which may results in overweight and obese to sweat. This study agrees with the literature reviewed by Oh et al., (2010), that it is important to accurately characterize the heating of tissues due to the RF energy applied during MRI and the results of the study has shown that there is a great variations in the experiences of patients undergoing MRI examinations and that care of patients in MRI environment needs to be individualized.

Chapter Summary

This study numerically estimate temperature profiles in different regions of the human head during brain MRI. A theoretical model, based on modified PBHE equation with appropriate boundary conditions, has been

developed to examine the transient and steady states of brain temperature at hyperthermic condition during brain MRI. The numerical computation was carried out using MATLAB as a tool. Various parameters which include physiological and numerical values have been used to formulate the model. The numerical results were compared with the experimental results of the study.

CHAPTER FIVE

SUMMARY, CONCLUSIONS AND RECOMMENDATIONS

Overview

This study modelled Penne's bio-heat equation and used MATLAB programming language to predict in-vivo power deposition in brain tissues before, during and after brain MRI of RF above 100 kHz. Patients who were referred for (head) brains MRI at field strength of 0.3 T (12.77 MHz) and the 1.5 T (63.86 MHz) head temperatures were measured experimentally. The results of the study showed excessive temperature elevation at the skin surface of the patients due to the ohmic heating during MRI of RF above 100 kHz.

Summary

This study has developed a numerical dosimetry to estimate brain temperature increase during MRI. Experimental thermal dosimetry was carried out to complement the theoretical dosimetry. Finite-difference technique was used to solve the modelled 3-D PBHE to find out temperature distribution of head (brain) of patients during brain MRI. The modelled equation was discretized using the central-difference scheme to homogenously predict temperature distribution during brain MRI in transient and steady states. Experimental studies and clinical observations were conducted at the MRI facilities of field strength 0.3 T and 1.5 T to provide additional validation of the numerical model.

Conclusions

With the appropriate boundary conditions, the modified PBHE has been used to predict temperature increase in both steady-state and transient state in-vivo brain temperature profile in MRI. The steady-state theoretical

model predicts that there is excessive elevation of temperature during MRI with the highest temperature recorded on the forehead during MRI and temperature does drop in patients after the MRI examinations. This change in temperature does not correlate with duration of the MRI scan. The transient numerical study of RF exposure of the study suggests that the majority of RF pulses used in MRI for the excitation of the nuclei are transformed into heat within the patient's tissues. The lowest temperature during MRI from the transient simulated results was 37.5 °C and the highest temperature was 42.5 °C during brain scan of duration less than sixty minutes. The transient temperature profiles of the in-vivo brain tissue of different thermal properties revealed that brain temperature variations during brain MRI increases as scan duration increases.

The experimental results validate the theoretical results. The highest estimated brain temperature during brain MRI of the study is 43 °C, and it depicts brain hyperthermia since the temperature value is above 41 °C. This may be as a result of the strength of the MRI, the scan duration and the pathological condition of the patients who underwent the brain MRI. The results of regression analysis of the experimental data showed a positive correlation between BMI and patients temperature change in brain MRI. Though the intermittent measured pre-and-post scan temperatures were all within guidance levels, the study predicts that there is the excessive elevation of patient's brain temperature which depends on scan duration in brain MRI, and this exceeds the guidance level. This might contribute to the causes of profuse localize sweating of some patients during MRI in the acceptable ambient MRI environment.

93

The study has published empirical data that the increase in patient's temperature during MRI depends significantly on the strength of the magnet, and scan duration. It has also provided empirical evidence establishing a positive correlation between BMI and temperature increase in patients in brain MRI.

Recommendations

The following are recommendations made to ensure the safety of patients undergoing brain MRI scan.

Health professionals

The experimental data obtained demonstrated that the elevation of patient's temperature during MRI scan depends on the RF power and BMI. Thus, the higher the RF power deposition the greater the increase in temperature. As the MRI field strength is increased to provide higher contrast in MRI, MRI examiners are encouraged to consider the risk associated with sudden increase in temperature which could pose a threat to patients' health, especially those with an impaired thermoregulation system which may include paediatrics, the elderly and patients with high BMI. Therefore, MRI professionals are recommended to input the actual patients' variables (age, height and weight).

It is also recommended that continuous temperature monitoring in MRI scan should be the most paramount, particularly if the scan durations are prolonged.

Medical implant industry

Temperature distributions during MRI do not correlate well with SAR limit. Therefore, the density, specific heat capacity and the thermal

94

conductivity of all the artificial (prosthesis) devices that replace a missing body should be provided. This may go a long way to accurately predict temperature distribution in MRI to ensure that a patient is not excessively heated by the RF magnetic fields used to create the magnetic resonance signal.

Suggestion for Further Research Work

At high-field MRI, physicists concern is the safety of patients receiving high power RF pulses and the potential for tissue heating or burns effects. MRI is becoming an increasingly common form of examination for both adults and children. Therefore, this work could be done by considering the head as a heterogeneous organ as well as size dependant. It is also possible to design electro-scan thermometer with the help of polynomial fitting equation developed to predict patients temperature before MRI scan.

95

REFERENCES

Adair, E. R., & Black, D. R. (2003). Thermoregulatory responses to RF energy absorption. *Bioelectromagnetics, 24*(S6).

Aggarwal, A., & Gupta, A. (2011). *Effect of electromagnetic radiations on humans: A study*. In *Students' Technology Symposium (TechSym), 2011 IEEE* (pp. 75-80). IEEE.

Ahlbom, A., Green, A., Kheifets, L., Savitz, D., & Swerdlow, A. (2004). Epidemiology of health effects of radiofrequency exposure. *Environmental Health Perspectives, 112*(17), 1741.

Allen, G. C., Horrow, J. C., & Rosenberg, H. (1990). Does forehead liquid crystal temperature accurately reflect "core" temperature? *Canadian Journal of Anaesthesia, 37*(6), 659.

Alsop, D. C., Connick, T. J., & Mizsei, G. (1998). A spiral volume coil for improved RF field homogeneity at high static magnetic field strength. *Magnetic Resonance in Medicine, 40*(1), 49-54.

Angelone, L. M., Ahveninen, J., Belliveau, J. W., & Bonmassar, G. (2010). Analysis of the role of lead resistivity in specific absorption rate for deep brain stimulator leads at 3 T MRI. *IEEE Transactions on Medical Imaging, 29*(4), 1029-1038.

Arens, E. A., & Zhang, H. (2006). The skin's role in human thermoregulation and comfort. *Center for the Built Environment*. Berkeley, USA: California Digital Library

Athey, T. (1992). Current FDA guidance for MR patient exposure and considerations for the future. *Annals of the New York Academy of Sciences, 649*(1), 242-257.

Barentsz J. O., Debruyne F. M. J., Ruijs S. H. J. (1990) General Principles of MRI. In: *Magnetic Resonance Imaging of Carcinoma of the Urinary Bladder*. Series in Radiology, vol 21. Springer, Dordrecht

Barnes, F. S., & Greenebaum, B. (2006). *Biological and medical aspects of electromagnetic fields*: CRC press. New York.

Bechtold, D. A., & Brown, I. R. (2003). Induction of Hsp27 and Hsp32 stress proteins and vimentin in glial cells of the rat hippocampus following hyperthermia. *Neurochemical Research, 28*(8), 1163-1173.

Bitar, R., Leung, G., Perng, R., Tadros, S., Moody, A. R., Sarrazin, J., & Nelson, A. (2006). MR pulse sequences: what every radiologist wants to know but is afraid to ask. *Radiographics, 26*(2), 513-537.

Bland, J M., & Altman, D. G. (1986). Statistical methods for assessing agreement between two methods of clinical measurement. *The lancet, 327*(8476), 307-310.

Bligh, J., & Johnson, K. G. (1973). Glossary of terms for thermal physiology. *Journal of Applied Physiology, 35*(6), 941-961.

Blink, E. J. (2004). mri: Physics. Polytechnic University, Brooklyn, NY 11201.

Bolen, S. M. (1994). *Radiofrequency/Microwave Radiation Biological Effects and Safety Standards: A Review* (No. RL-TR-94-53). ROME LAB ROME NY.

Bourland, J. D., Nyenhuis, J. A., Noe, W. A., Schaefer, J. D., Foster, K. S., & Geddes, L. A. (1996). *Motor and sensory strength-duration curves for MRI gradient fields.* Paper presented at the Proceedings of the Society of Magnetic Resonance 4th Annual Meeting, New York.

Branch, C. S. (2009). Limits of human exposure to radiofrequency electro-magnetic energy in the frequency range from 3 kHz to 300 GHz. *safe code, 6*.

Brown, C. D., Higgins, M., Donato, K. A., Rohde, F. C., Garrison, R., Obarzanek, E., & Horan, M. (2000). Body mass index and the prevalence of hypertension and dyslipidemia. *Obesity, 8*(9), 605-619.

Brown, R. W., Haacke, E M., Cheng, Y. C. N., Thompson, M. R., & Venkatesan, R. (2014). *Magnetic resonance imaging: physical principles and sequence design*: John Wiley & Sons. Cleveland, Ohio, USA

Browning, R. C., Baker, E. A., Herron, J. A., & Kram, R. (2006). Effects of obesity and sex on the energetic cost and preferred speed of walking. *Journal of Applied Physiology, 100*(2), 390-398.

Browning, R. C., & Kram, R. (2005). Energetic cost and preferred speed of walking in obese vs. normal weight women. *Obesity, 13*(5), 891-899.

Brück, K. (1989). Thermal balance and the regulation of body temperature *Human physiology* (pp. 624-644): Springer.

Brull, S. J., Cunningham, A. J., Connelly, N. R., O'Connor, T. Z., & Silverman, D. G. (1993). Liquid crystal skin thermometry: an accurate reflection of core temperature? *Canadian Journal of Anesthesia/Journal canadien d'anesthésie, 40*(4), 375-381.

Bryan, Y. F., Templeton, TP W., Nick, T. G., Szafran, M., & Tung, A. (2006). Brain magnetic resonance imaging increases core body temperature in sedated children. *Anesthesia & Analgesia, 102*(6), 1674-1679.

Buchli, R., Saner, M., Meier, D., Boskamp, E. B., & Boesiger, P. (1989). Increased RF power absorption in MR imaging due to RF coupling between body coil and surface coil. *Magnetic Resonance in Medicine, 9*(1), 105-112.

Buonocore, M. H., & Maddock, R. J. (2015). Magnetic resonance spectroscopy of the brain: a review of physical principles and technical methods. *Reviews in the Neurosciences, 26*(6), 609-632.

Bushberg, J. T., & Boone, J. M. (2011). *The Essential Physics of Medical Imaging*: New York London, Lippincott Williams & Wilkins.

Bushong, S. C., & Clarke, G. (2014). *Magnetic resonance imaging: physical and biological principles*: USA, Elsevier Health Sciences.

Cabanac, M., & Brinnel, H. (1987). The pathology of human temperature regulation: Thermiatrics. *Cellular and Molecular Life Sciences, 43*(1), 19-27.

Callaghan, P. T. (1993). *Principles of nuclear magnetic resonance microscopy*: Oxford, Oxford University Press.

Carluccio, G., Erricolo, D., Oh, S., & Collins, C. M. (2013). An approach to rapid calculation of temperature change in tissue using spatial filters to approximate effects of thermal conduction. *IEEE Transactions on Biomedical Engineering, 60*(6), 1735-1741.

Cena, K., & Clark, J. A. (1981a). Physics, physiology and psychology. *Studies in Environmental Science, 10*, 271-283.

Cena, K., & Clark, J. A. (1981b). *Bioengineering, thermal physiology and comfort* (Vol. 10): New York, Elsevier Scientific Publishing Company.

Challis, L. J. (2005). Mechanisms for interaction between RF fields and biological tissue. *Bioelectromagnetics, 26*(S7).

Chang, I. A., & Nguyen, U. D. (2004). Thermal modeling of lesion growth with radiofrequency ablation devices. *Biomedical Engineering Online, 3*(1), 27.

Chen, X., & Steckner, M. (2017). Electromagnetic computation and modeling in MRI. *Medical Physics*, *44*(3), 1186-1203.

Childs, C., Vail, A., Protheroe, R., King, A. T., & Dark, P. M. (2005). Differences between brain and rectal temperatures during routine critical care of patients with severe traumatic brain injury. *Anaesthesia, 60*(8), 759-765.

Chou, C. K., Bässen, H., Osepchuk, J., Balzano, G., Petersen, R., Meitz, M., & Heynick, L. (1996). Radio frequency electromagnetic exposure. *Journal of Bioelectromagnetics, 17*, 195-208.

Code Safety. (1999). Limits of Human Exposure to Radiofrequency Electromagnetic Fields in the Frequency Range from 3 kHz to 300 GHz. *Environmental Health Directorate, Health Protection Branch, Health Canada, Canada*.

Collins, C. M., Liu, W., Wang, J., Gruetter, R., Vaughan, J. T., Ugurbil, K., & Smith, M. B. (2004). Temperature and SAR calculations for a human head within volume and surface coils at 64 and 300 MHz. *Journal of Magnetic Resonance Imaging, 19*(5), 650-656.

Collins, C. M., & Smith, M. B. (2001). Signal-to-noise ratio and absorbed power as functions of main magnetic field strength, and definition of "90°" RF pulse for the head in the birdcage coil. *Magnetic Resonance in Medicine, 45*(4), 684-691.

Cork, R. C., Vaughan, R. W., & Humphrey, L. S. (1983). Precision and accuracy of intraoperative temperature monitoring. *Anesthesia & Analgesia, 62*(2), 211-214.

Crow, W. N. (2000). Projectile Cylinder Accidents Resulting from the Presence of Ferromagnetic Nitrous Oxide or Oxygen Tanks in the MR Suite.

Cullity, B. D., & Graham, C. D. (2011). *Introduction to magnetic materials*: John Wiley & Sons, INC., Hoboken, New Jersey.

Dale, B. M., Brown, M. A., & Semelka, R. C. (2015). Principles of magnetic resonance imaging 2. *MRI Basic Principles and Applications*, 39-64.

Davarcioglu, B. (2011). The dielectric properties of human body tissues at electromagnetic wave frequencies. *Int. J. Sci. and Adv. Technol, 1*(5), 12-19.

De Graaf, R. A. (2013). *In vivo NMR spectroscopy: principles and techniques*. John Wiley & Sons INC., England.

Dechent, J. F., Buljubasich, L., Schreiber, L. M., Spiess, H. W., & Münnemann, K. (2012). Proton magnetic resonance imaging with para-hydrogen induced polarization. *Physical Chemistry Chemical Physics, 14*(7), 2346-2352.

Demers, P., Findlay, R., Foster, K., Bryan K., Moulder, J., Nicol, A. M., & Stam, R. (2014). *A Review of Safety Code 6 (2013): Health Canada's Safety Limits for Exposure to Radiofrequency Fields.* Paper presented at the Royal Society of Canada.

Dempsey, M. F., Condon, B., & Hadley, D. M. (2001). Investigation of the factors responsible for burns during MRI. *Journal of Magnetic Resonance Imaging, 13*(4), 627-631.

Dery, T. B., Darko, E. O., Amoako, J. K., & Kyere, A. K. (2013). An Iterative Method for the Determination of Temperature Distribution in Patients Undergoing Brain Magnetic Resonance Imaging (MRI) Examinations. *International Journal of Science and Technology, 3*(3).

Dixon, R. L., & Ekstrand, K. E. (1982). The physics of proton NMR. *Medical Physics, 9*(6), 807-818.

Dräger. (2014). The significance of core temperature-Pathophysiology and measurement methods. Retrieved from www.draeger.com website:

Durkee Jr, J. W., & Antich, P. P. (1991a). Characterization of bioheat transport using an exact solution of the cylindrical geometry, multi-region, time-dependent bioheat equation. *Physics in Medicine and Biology, 36*(10), 1377.

Durkee Jr, J. W., & Antich, P. P. (1991b). Exact solutions to the multi-region time-dependent bioheat equation with transient heat sources and boundary conditions. *Physics in Medicine and Biology, 36*(3), 345.

Durney, C. H. (1980). Electromagnetic dosimetry for models of humans and animals: A review of theoretical and numerical techniques. *Proceedings of the IEEE, 68*(1), 33-40.

Dwyer, M. J., & Leeper, D. B. (1978a). *A Current Literature Report on the Carcinogenic Properties of Ionizing and Non-: Ionizing Radiation*.

Dwyer, M. J., & Leeper, D. B. (1978b). Carcinogenic properties of ionizing and non-ionizing radiation. *Microwaves and Radiofrequencies, 2*, 1-28.

Elder, J. A., & Cahill, D. F. (1984). *Biological effects of radiofrequency radiation*: Health Effects Research Laboratory, Office of Research and Development, US Environmental Protection Agency.

Elwasife, K.Y., & Almassri, M. R. (2017). Numerical Study The Dielectric Properties And Specific Absorption Rate Of Nerve Human Tissue At Different Frequencies. *Boson Journal of Modern Physics, 4*(1), 269-278.

Food and Drug Administration (FDA), (2009). Primer on Medical Device Interactions with Magnetic Resonance Imaging System, Retrieved from:http://www.fda.gov/MedicalDevices/DeviceRegulationandGuidance/Guidance Documents/ cm107721.htm, Retrieved on: (29/12/2017) at 10:46 pm;

Faruque, M. R. I., Islam, M. T., & Misran, N. (2010). Effect of human head shapes for mobile phone exposure on electromagnetic absorption. *Informacije MIDEM, 40*(3), 232-237.

Fields, R. E. (1997). Evaluating compliance with FCC guidelines for human exposure to radiofrequency electromagnetic fields. *OET bulletin*, *65*, 10.

Finelli, D. A., Rezai, A. R., Ruggieri, P. M., Tkach, J. A., Nyenhuis, J. A., Hrdlicka, G., & Shellock, F. G. (2002). MR imaging-related heating of

deep brain stimulation electrodes: in vitro study. *American Journal of Neuroradiology, 23*(10), 1795-1802.

Flegal, K. M., Carroll, M. D., Ogden, C. L., & Johnson, C. L. (2002). Prevalence and trends in obesity among US adults, 1999-2000. *Jama, 288*(14), 1723-1727.

Flugstad, B. A., Ling, Q., Kolbe, E. R., Wells, J. H., Zhao, Y., & Park, J. W. (2004). Variable frequency automated capacitive radiofrequency (RF) dielectric heating system*: U.S. Patent No. 6,784,405*. Washington, DC: U.S. Patent and Trademark Office.

Földes, Z. (2016). The effects of synchronous music on patients undergoing magnetic resonance imaging. Master's Thesis of University of Jyväskylä   Retrieved from: https://uh-ir.tdl.org/uh-ir/handle/10657/1 Retrieved on 22/04/2017.

Formica, D., & Silvestri, S. (2004). Biological effects of exposure to magnetic resonance imaging: an overview. *Biomedical Engineering Online, 3*(1), 11.

Foster, K. R. (2000). Thermal and nonthermal mechanisms of interaction of radio-frequency energy with biological systems. *IEEE Transactions on Plasma Science, 28*(1), 15-23.

Foster, K. R., & Schwan, H. P. (1995). Dielectric properties of tissues. *Handbook of Biological Effects of Electromagnetic Fields, 2*, 25-102.

Foster, K. R., & Schwan, H. P. (1989). Dielectric properties of tissues and biological materials: a critical review, ö CRC Crit. *Rev. Biomed. Eng, 17*, 25-104.

Ga, B. H., Mamoon, A. M., Schlapfer, W. T., & Tobias, C. A. (1972). Effects of temperature on spontaneous bioelectric activity of cultured nerve cells. *Brain Research, 40*(2), 527-533.

Gabriel, S., Lau, R. W., & Gabriel, C. (1996). The dielectric properties of biological tissues: II. Measurements in the frequency range 10 Hz to 20 GHz. *Physics in Medicine and Biology, 41*(11), 2251.

Gajšek, P., D'Andrea, J. .A, Mason, P. A., Ziriax, J.M., & Walters, T. J. (2013). 3.2 Mathematical Modeling Using Experimental and Theoretical Methods in Evaluating Specific Absorption Rates (SAR). *Biological Effects of Electromagnetic Fields: Mechanisms, Modeling, Biological Effects, Therapeutic Effects, International Standards, Exposure Criteria*: New York, Springer-Verleg Berlin Heiderberg

Gallagher, D., Heymsfield, S. B., Heo, M., Jebb, S. A., Murgatroyd, P. R., & Sakamoto, Y. (2000). Healthy percentage body fat ranges: an approach for developing guidelines based on body mass index. *The American journal of clinical nutrition, 72*(3), 694-701.

Goel, A. (2014). Evaluating the Effect of Distance on Specific Absorption Rate Values inside a Human Head Model. *International Journal of Innovation and Scientific Research, 12*(1), 186-189

Gokul, K. C., Gurung, D. B., & Adhikary, P. R. (2013). FEM approach for transient heat transfer in human eye. *Applied Mathematics, 4*(10), 30.

Gordon, C. J. (1992). Local and global thermoregulatory responses to MRI fields. *Annals of the New York Academy of Sciences, 649*(1), 273-284.

Ghana Standard Authority (GSA), (2016). Clinical Thermometer. *Scientific Metrology.* Gulf St. Accra, Ghana

Habash, R. (2007). *Bioeffects and therapeutic applications of electromagnetic energy*: CRC press, London.

Habash, R. W. Y., Bansal, R., Krewski, D., & Alhafid, H. T. (2007). Thermal therapy, Part IV: electromagnetic and thermal dosimetry. *Critical Reviews in Biomedical Engineering, 35*(1-2).

Hand, J. W. (2008). Modelling the interaction of electromagnetic fields (10 MHz–10 GHz) with the human body: methods and applications. *Physics in Medicine and Biology, 53*(16), R243.

Hand, J. W., & Haar, G. (1981). Heating techniques in hyperthermia. *The British Journal of Radiology, 54*(642), 443-466.

Hansson-Mild, K., Alanko, T., Decat, G., Falsaperla, R., Gryz, K., Hietanen, M., & Sandström, M. (2009). Exposure of workers to electromagnetic fields. A review of open questions on exposure assessment techniques. *International Journal of Occupational Safety and Ergonomics, 15*(1), 3-33.

Hardy, J. D., Wolff, H. G., & Goodell, H. (1967). Pain sensations and reactions. Williams and Wilkins, 1952: reprinted by Hafner Publishing Co, New York.

Hartwig, V., Giovannetti, G., Vanello, N., Lombardi, M., Landini, L., & Simi, S. (2009). Biological effects and safety in magnetic resonance imaging: a review. *International Journal of Environmental Research and Public Health, 6*(6), 1778-1798.

Hendee, W. R., & Morgan, C. J. (1984). Magnetic resonance imaging Part Physical principles. *Western Journal of Medicine, 141*(4), 491.

Hensel, H. (1981a). Temperature sensation in man. *Thermoreception and temperature regulation. Monogr Physiol Soc*(38), 18-32.

Hensel, H. (1981b). Thermal comfort in man. *Thermoreception and Temperature Regulation.* Academic Press, London.

Heymsfield, S. (2005). *Human body composition* (Vol. 918): Canada, Human kinetics.

Hilschenz, I., Körber, R., Hans-Jürgen, S., Fedele, T., Hans-Helge, A., Cassará, A. M., & Burghoff, M.(2013). Magnetic resonance imaging at frequencies below 1 kHz. *Magnetic Resonance Imaging, 31*(2), 171-177.

Hitchcock, R. T., & Patterson, R. M. (1995). *Radio-frequency and ELF electromagnetic energies: A handbook for health professionals*: John Wiley & Sons, INC., Canada.

Houdas, Y., & Ring, E. F. J. (2013). *Human body temperature: its measurement and regulation*: Bath, England, Springer Science & Business Media LLC.

Hu, X., & Norris, D. G. (2004). Advances in high-field magnetic resonance imaging. *Annu. Rev. Biomed. Eng., 6*, 157-184.

Ibrahiem, A., Dale, C., Tabbara, W., & Wiart, J. (2005). Analysis of the temperature increase linked to the power induced by RF source. *Progress In Electromagnetics Research, 52*, 23-46.

International Commission on Non-Ionizing Radiation Protection (ICNIRP). (2004). Medical magnetic resonance (MR) procedures: protection of patients. *Health Physics, 87*(2), 197-216.

International Commission on Non-Ionizing Radiation Protection (ICNIRP), (2009). Amendment to the ICNIRP "Statement on medical magnetic resonance (MR) procedures: protection of patients". *Health Physics, 97*(3), 259-261.

International Electro-technical Commission (IEC). (2010). Medical electrical equipment - particular requirements for the safety of magnetic resonance equipment for medical diagnosis. *Regulating Medicine and Medical Devices, 2*(33).

Inglis, B., Buckenmaier, K., SanGiorgio, P., Pedersen, A. F., Nichols, M. A., & Clarke, J. (2013). MRI of the human brain at 130 microtesla. *Proceedings of the National Academy of Sciences, 110*(48), 19194-19201.

Inoue, T., Pethig, R., Al-Ameen, T. A. K., Burt, J. P. H, & Price, J. A. R. (1988). Dielectrophoretic behaviour of Micrococcus lysodeikticus and its protoplast. *Journal of Electrostatics, 21*(2-3), 215-223.

Jagannathan, N. R. (1999). Magnetic resonance imaging: bioeffects and safety concerns. *Indian Journal of Biochem Biophys, 36*(5), 341-7.

Jamieson, I. A. (2014). Changing perspectives–improving lives. *Presentation given at the EESC Electromagnetic Hypersensitivity Public Hearing. European Economic and Social Committee, Brussels, 4th November*.

Johnson, C. C., & Guy, A. W. (1972). Nonionizing electromagnetic wave effects in biological materials and systems. *Proceedings of the IEEE, 60*(6), 692-718.

Kanal, E., Barkovich, A J., Bell, C., Borgstede, J. P., Bradley Jr, W. G., Froelich, J. W., & Kuhni-Kaminski, E.. (2007). ACR guidance

document for safe MR practices: 2007. *American Journal of Roentgenology, 188*(6), 1447-1474.

Kangarlu, A., Shellock, F. G., & Chakeres, D. W. (2003). 8.0-Tesla human MR system: Temperature changes associated with radiofrequency-induced heating of a head phantom. *Journal of Magnetic Resonance Imaging, 17*(2), 220-226.

Karunarathna, M. A. A., & Dayawana, I. J. (2005). Human exposure to RF radiation in Sri Lanka. *Sri Lankan Journal of Physics, 6*.

Karunarathna, M. A. A., & Dayawansa, L. J. (2006). Energy absorption by the human body from RF and microwave emissions in Sri Lanka. *Sri Lankan Journal of Physics, 7*.

Kauffman, G. (2014). Nobel prize for MRI imaging denied to Raymond V. Damadian a decade ago. *Chemical Educator, 19*, 73-90.

Keengwe, I. N., Hegde, S., Dearlove, O., Wilson, B., Yates, R. W., & Sharples, A. (1999). Structured sedation programme for magnetic resonance imaging examination in children. *Anaesthesia, 54*(11), 1069-1072.

Keim, S. M., Guisto, J. A, & Sullivan Jr, J. B. (2002). Environmental thermal stress. *Annals of Agricultural and Environmental Medicine, 9*(1), 1-15.

Kenny, G. P., & Jay, O. (2013). Thermometry, calorimetry, and mean body temperature during heat stress. *Compr Physiol*, *3*(4), 1689-719.

Kesari, K. K., Siddiqui, M., Meena, R., Verma, H. N., & Kumar, S. (2013). Cell phone radiation exposure on brain and associated biological systems: NISCAIR-CSIR, India.

Kirkham, A. P. S., Emberton, M., & Allen, C. (2006). How good is MRI at detecting and characterising cancer within the prostate? *European urology, 50*(6), 1163-1175.

Kiyatkin, E. A. (2004). Brain hyperthermia during physiological and pathological conditions: causes, mechanisms, and functional implications. *Current Neurovascular Research, 1*(1), 77-90.

Kiyatkin, E. A., & Sharma, H. S. (2009). Permeability of the blood–brain barrier depends on brain temperature. *Neuroscience, 161*(3), 926-939.

Knies, R. C. (2003). Temperature measurement in acute care: The who, what, where, when, why, and How. Retrieved from: *http://enw.org/Research Thermometry. htm,* Retrieved on 25/08/16

Kok, H. P., Wust, P., Stauffer, P. R., Bardati, F., Van Rhoon, G. C., & Crezee, J. (2015). Current state of the art of regional hyperthermia treatment planning: a review. *Radiation Oncology (London, England), 10*.

Kundi, M. (2005). Epidemiology of health effects of radiofrequency exposure. *Environmental Health Perspectives, 113*(3), A151.

Kunz, K. S., & Luebbers, R. J. (1993). *The finite difference time domain method for electromagnetics*: CRC press, New York.

Kuperman, V. (2000). *Magnetic Resonance Imaging: Physical Principles and Applications*: Academic Press, Boston.

Lacoumenta, S., & Hall, G. M. (1984). Liquid crystal thermometry during anaesthesia. *Anaesthesia, 39*(1), 54-56.

Lai, H. (2005). Biological effects of radiofrequency electromagnetic field. *Encyclopedia of Biomaterials and Biomedical Engineering, 10*, 1-8.

110

Lak, A. (2012). Human health effects from radiofrequency and microwave fields. *Journal of Basic and Applied Scientific Research, 2*(12), 12302-12305.

Laurence, A. S. (2000). Sedation, safety and MRI. *The British Journal of Radiology, 73*(870), 575-577.

Lees, D. E., Schuette, W., Bull, J. M., Whang-peng, J., Atkinson, E. R., & Macnamara, T. E. (1978). An evaluation of liquid-crystal thermometry as a screening device for intraoperative hyperthermia. *Anesthesia & Analgesia, 57*(6), 669-674.

Lessard, C. S., Wong, W. C., & Schmidt, G. F. (1988). Temperature measurement and monitoring devices: Texas A and M Univ College Station Bioengineering Program. Retrieved from : http://www.dtic.mil/dtic/tr/fulltext/u2/a201643.pdf   Retrieved   on 19/092017

Levine, G. N., Gomes, A. S., Arai, A. E., Bluemke, D. A., Flamm, S. D., Kanal, E., & Wilke, N. (2007). Safety of magnetic resonance imaging in patients with cardiovascular devices. *Circulation, 116*(24), 2878-2891.

Levitt, M. H. (2001). *Spin Dynamics: Basics of Nuclear Magnetic Resonance*, 196. John Wiley & Sons, Southampton.

Lim, C. L., Byrne, C., & Lee, J. K. W. (2008). Human thermoregulation and measurement of body temperature in exercise and clinical settings. *Annals Academy of Medicine Singapore, 37*(4), 347.

Lin, J. C., Bernardi, P., Pisa, S., & Cavagnaro, M. (2008). SAR and temperature: simulations and comparison to regulatory limits for MRI, *J. Magn. Resonance.*

Liu, C. C., Chang, R. E., & Chang, W. C. (2004). Limitations of forehead infrared body temperature detection for fever screening for severe acute respiratory syndrome. *Infection Control & Hospital Epidemiology, 25*(12), 1109-1111.

Liu, Y. (2012). *Numerical and Experimental Study of MRI RF Signal Interactions with Various Medical Devices* .

Liu, Y. (2012). *Numerical and experimental study of MRI RF signal interactions with various medical devices* (Doctoral dissertation). Retrieved from: http://hdl.handle.net/10657/830   Retrieved on 16/03/2016

Lu, H., Nagae-Poetscher, L. M., Golay, X., Lin, D., Pomper, M., & van Z., P. (2005). Routine clinical brain MRI sequences for use at 3.0 tesla. *Journal of Magnetic Resonance Imaging, 22*(1), 13-22.

Lucas, A. J., Hawkes, R. C., Ansorge, R. E., Williams, G. B., Nutt, R. E., Clark, J. C., & Carpenter, T A. (2006). Development of a combined microPET-MR system. *Technology in cancer research & treatment, 5*(4), 337-341.

Luechinger, R., Zeijlemaker, V. A., Pedersen, E. M., Mortensen, P., Falk, E., Duru, F., & Boesiger, P. (2004). In vivo heating of pacemaker leads during magnetic resonance imaging. *European Heart Journal, 26*(4), 376-383.

Macchia, R. J., Termine, J. E., & Buchen, C. D. (2007). Magnetic Resonance Imaging and the Controversy of the 2003 Nobel Prize in Physiology or Medicine. *The Journal of Urology, 178*(3), 783-785.

Machata, A. M., Willschke, H., Kabon, B., Prayer, D., & Marhofer, P. (2009). Effect of brain magnetic resonance imaging on body core temperature in sedated infants and children. *British Journal of Anaesthesia, 102*(3), 385-389.

Macovski, A., & Conolly, S. (1993). Novel approaches to low-cost MRI. *Magnetic Resonance in Medicine, 30*(2), 221-230.

Mahrour, N., Pologea-Moraru, R., Moisescu, M. G., Orlowski, S., Levêque, P., & Mir, L. M. (2005). In vitro increase of the fluid-phase endocytosis induced by pulsed radiofrequency electromagnetic fields: importance of the electric field component. *Biochimica et Biophysica Acta (BBA)-Biomembranes, 1668*(1), 126-137.

Malik, S. J., Beqiri , A., Price, A. N., Teixeira, J. N., Hand, J. W., & Hajnal, J. V. (2015). Specific absorption rate in neonates undergoing magnetic resonance procedures at 1.5T and 3T. *NMR Biomed*, 28: 344–352

Masters, J. E. (1980). Comparison of axillary, oral, and forehead temperature. *Archives of Disease in Childhood, 55*(11), 896.

Matikka, H. (2010). *The effect of metallic implants on the RF energy absorption and temperature changes in head tissues*: University of Eastern Finland.

McCarthy M. J. (1994) *Fundamental Principles of MRI*. In: Magnetic Resonance Imaging in Foods. Springer, Boston, MA

Mcilvoy, L. (2004). Comparison of brain temperature to core temperature: a review of the literature. *Journal of Neuroscience Nursing, 36*(1), 23.

McJury, M., & Frank, G. (2000). Auditory noise associated with MR procedures: a review. *Journal of Magnetic Resonance Imaging, 12*(1), 37-45.

McRobbie, D. W., Moore, E. A., & Graves, M. J. (2017). *MRI from Picture to Proton*: Cambridge university press.

Mellergård, P. (1994). Monitoring of rectal, epidural, and intraventricular temperature in neurosurgical patients *Brain Edema IX* (pp. 485-487): Springer.

Mellergård, P. (1995). Intracerebral temperature in neurosurgical patients: intracerebral temperature gradients and relationships to consciousness level. *Surgical Neurology, 43*(1), 91-95.

Mellergard, P., & Nordström, C. H. (1990). Epidural temperature and possible intracerebral temperature gradients in man. *British Journal of Neurosurgery, 4*(1), 31-38.

Mellergård, P., & Nordström, C. H. (1991). Intracerebral temperature in neurosurgical patients. *Neurosurgery, 28*(5), 709-713.

Mendt, S., Maggioni, M. A., Nordine, M., Steinach, M., Opatz, O., Belavý, D., & Gunga, H. C. (2017). Circadian rhythms in bed rest: Monitoring core body temperature via heat-flux approach is superior to skin surface temperature. *Chronobiology International, 34*(5), 666-676.

Meredith, R. J. (1998). *Engineers' Handbook of Industrial Microwave Heating*: London, United Kindom: The Institution of Electrical Engineers

Medicine and Healthcare Product Regulatory Agency (MHRA). (2015). Safety Guidelines for Magnetic Resonance Imaging Equipment in Clinical Use.

Michaelson, S. M. (1982). Health implications of exposure to radiofrequency/microwave energies. *Occupational and Environmental Medicine, 39*(2), 105-119.

Moran, D. S., & Mendal, L. (2002). Core temperature measurement. *Sports Medicine, 32*(14), 879-885.

Mordy, J. T. (2012). Government procures latest MRI facilities for public hospital Retrieved from: www.ghanaweb.com Retrieved on: (29/08/2016) at 2.30 pm

Moritani, T., Ekholm, S., & Westesson, P. L. A. (2009). *Diffusion-weighted MR imaging of the brain*, London, New York: Springer, Science & Business Media.

Nakada, T. (2007). Clinical application of high and ultra high-field MRI. *Brain and Development, 29*(6), 325-335.

Narebski, J. (1985). Human brain homeothermy during sleep and wakefulness: An experimental and comparative approach. *Ada Neurobiologiae Experimental, 45*, 63-75.

National Radiological Protection Board. (2004) (NRPB). *Advice on Limiting exposure to Electromagnetic Fields (0-300GHz)* Vol. 15 (pp. 2).

Nepa, P. (2012). Electromagnetic Radiations and Biological Interactions. Retrieved 28/01/2016, 2016, from p.nepa@iet.unipi

Ng, K. H. (2003). *Non-ionizing Radiations–Sources, Biological Effects, Emissions and Exposures.* Paper presented at the Proceedings of the international conference on non-ionizing radiation at UNITEN.

Nguyen, U., Brown, S., Chang, I., Krycia, J., & Mirotznik, M. S. (2003). *Numerical Evaluation of Heating in the Human Head Due to Magnetic Resonance Imaging (MRI).* Paper presented at the Medical Imaging 2003.

Nguyen, U. D., Brown, J. S., Chang, I. A., Krycia, J., & Mirotznik, M. S. (2004). Numerical evaluation of heating of the human head due to magnetic resonance imaging. *IEEE Transactions on Biomedical Engineering, 51*(8), 1301-1309.

Obahiagbon, K., & Isabona, J. (2015). Specific Absorbtion Rate and Temperature rise Computation in Human Tissues due to Electromagnetic Field emission from Mobile Phones at 900 MHz and 1800 MHz, Computing. *Information Systems, Development Informatics & Allied Research Journal, 6*(2).

Oh, S., Webb, A. G., Neuberger, T., Park, B., & Collins, C. M. (2010). Experimental and numerical assessment of MRI-induced temperature change and SAR distributions in phantoms and in vivo. *Magnetic Resonance in Medicine, 63*(1), 218-223.

Oshinski, J. N., Delfino, J. G., Sharma, P., Gharib, A. M., & Pettigrew, R. I. (2010). Cardiovascular magnetic resonance at 3.0 T: current state of the art. *Journal of Cardiovascular Magnetic Resonance, 12*(1), 55.

Ozen, S., Helhel, S., & Bilgin, S. (2011). Temperature and burn injury prediction of human skin exposed to microwaves: a model analysis. *Radiation and Environmental Biophysics, 50*(3), 483-489.

Pacetti, S. D. (2003). MRI medical device markers utilizing fluorine-19: *U.S. Patent No. 6,574,497*. Washington, DC: U.S. Patent and Trademark Office.

Pattanaik, S. (2012). Biological effects of RF/MW radiations on human. *Archives of Applied Science Research, 4*(1), 381-387.

Pearson, H. (2003). Magnetic pioneers net Nobel for putting medicine in the picture. *Nature, 425*(6958), 547-548.

Pennes, H. H. (1948). Analysis of tissue and arterial blood temperatures in the resting human forearm. *Journal of Applied Physiology, 1*(2), 93-122.

Piasecka, M., Strąk, K., & Maciejewska, B. (2017). Calculations of flow boiling heat transfer in a minichannel based on Liquid Crystal and Infrared Thermography data. *Heat Transfer Engineering, 38*(3), 332-346.

Plewes, D. B., & Kucharczyk, W. (2012). Physics of MRI: a primer. *Journal of Magnetic Resonance Imaging, 35*(5), 1038-1054.

Pompei, F., & Pompei, M. (2004). Non-invasive Temporal Artery Thermometry: *Physics, Physiology, and Clinical Accuracy*. *in Thermosense XXVI* (Vol. 5405, pp. 61-68). International Society for Optics and Photonics.

Prakash, P. (2010). Theoretical modeling for hepatic microwave ablation. *The Open Biomedical Engineering Journal, 4*, 27.

Qaddi, M. H., & Srifi, M. N. (2016). RF/microwaves biological effects and dielectric properties of human tissues. *Materials Research Proceedings, 1*. Kenitra, Morocco: Material Research Forum LLC.

Qian, D., El-Sharkawy, A. M. M., Bottomley, P. A., & Edelstein, W. A. (2013). An RF dosimeter for independent SAR measurement in MRI scanners. *Medical Physics, 40*(12).

Recoskie, B. J., Scholl, T. J., Zinke-Allmang, M., & Chronik, B. A. (2010). Sensory and motor stimulation thresholds of the ulnar nerve from electric and magnetic field stimuli: implications to gradient coil operation. *Magnetic Resonance in Medicine, 64*(6), 1567-1579.

Repacholi, M. H. (1998). Low-level exposure to radiofrequency electromagnetic fields: Health effects and research needs. *Bioelectromagnetics, 19*(1), 1-19.

Rezai, A. R., Finelli, D., Nyenhuis, J. A., Hrdlicka, G., Tkach, J., Sharan, A., & Shellock, F. G. (2002). Neurostimulation systems for deep brain stimulation: in vitro evaluation of magnetic resonance imaging–related heating at 1.5 tesla. *Journal of Magnetic Resonance Imaging, 15*(3), 241-250.

Richards, S. (2013). *Temperature regulation*. New York: Springer, Science and Business Media.

Riederer, S. J. (2004). MR imaging: its development and the recent Nobel Prize. *Radiology, 231*(3), 628-631.

Romero, J. M., Schaefer, P. W., Grant, P E., Becerra, L., & González, R G. (2002). Diffusion MR imaging of acute ischemic stroke. *Neuroimaging Clinics, 12*(1), 35-53.

Sánchez-Hernández, D. A. (2009). *High Frequency Electromagnetic Dosimetry*: London, Artech House.

Scientific Committee on Emerging and Newly Identified Health Risks (SCENIHR). (2007). Possible effects of Electromagnetic Fields (EMF) on Human Health. Retrieved from : http://ec.europa.eu/health/phrisk/committees/04_scenihr/docs/scenihr o_007.pdf Retrieved on 12/11/ 2015

Schaefer, D. J., Bourland, J. D., & Nyenhuis, J. A. (2000). Review of Patient Safety in Time Varying Gradient Fields. *Journal of Magnetic Resonance Imaging, 12*(1), 20-29.

Schaefer, P. W., Grant, P E., & Gonzalez, R G. (2000). Diffusion-weighted MR imaging of the brain. *Radiology, 217*(2), 331-345.

Schenck, J. F. (2000). Safety of strong, static magnetic fields. *Journal of Magnetic Resonance Imaging, 12*(1), 2-19.

Schwan, H. P., & Piersol, G. M. (1955). The Absorption Of Electromagnetic Energy In Body Tissues: A Review and Critical Analysis. *American Journal of Physical Medicine & Rehabilitation, 34*(3), 425-448.

Sessler, D. I., & Todd, M. M. (2000). Perioperative heat balance. *Anesthesiology: The Journal of the American Society of Anesthesiologists, 92*(2), 578-578.

Sharma, H. S., & Hoopes, P. J. (2003). Hyperthermia induced pathophysiology of the central nervous system. *International Journal of Hyperthermia, 19*(3), 325-354.

Shellock, F. G. (1988). MR imaging of metallic implants and materials: a compilation of the literature. *American Journal of Roentgenology, 151*(4), 811-814.

Shellock, F. G., & Crues, J. V. (1988). Temperature changes caused by MR imaging of the brain with a head coil. *American Journal of Neuroradiology, 9*(2), 287-291.

Shellock, F. G., Gordon, C. J., & Schaefer, D. J. (1986). Thermoregulatory responses to clinical magnetic resonance imaging of the head at 1.5 tesla. Lack of evidence for direct effects on the hypothalamus. *Acta Radiologica. Supplementum, 369*, 512-513.

Shellock, F. G. (1994). Magnetic resonance: bioeffects, safety, and patient management. *New York: Raven, 10*, 101-121.

Shellock, F. G. (2000a). *Magnetic Resonance Procedures: Health Effects and Safety*, New York: Crc Press.

Shellock, F. G. (2000b). Radiofrequency energy-induced heating during MR procedures: a review. *Journal of Magnetic Resonance Imaging, 12*(1), 30-36. .

Shellock, F. G., & Crues, J. V. (2004). MR procedures: biologic effects, safety, and patient care. *Radiology, 232*(3), 635-652.

Shellock, F. G., & Kanal, E. (1996). *Magnetic resonance: Bioeffects, Safety, and Patient Management,* Lippincott: Williams & Wilkins.

Shellock, F. G., Schaefer, D. J., & Kanal, E. (1994). Physiologic responses to an MR imaging procedure performed at a specific absorption rate of 6.0 W/kg. *Radiology, 192*(3), 865-868.

Shibasaki, M., Wilson, T. E., & Crandall, C. G. (2006). Neural control and mechanisms of eccrine sweating during heat stress and exercise. *Journal of Applied Physiology, 100*(5), 1692-1701.

Shinozaki, T., Deane, R., & Perkins, F. M. (1988). Infrared tympanic thermometer: evaluation of a new clinical thermometer. *Critical Care Medicine, 16*(2), 148-150.

Siauve, N., Scorretti, R., Burais, N., Nicolas, L., & Nicolas, A. (2003). Electromagnetic fields and human body: a new challenge for the electromagnetic field computation. *COMPEL-The International Journal for Computation and Mathematics in Electrical and Electronic Engineering, 22*(3), 457-469.

Simon, H. B. (1993). Hyperthermia. *New England Journal of Medicine, 329*(7), 483-487.

Simunic, D., Wach, P., Renhart, W., & Stollberger, R. (1996). Spatial distribution of high-frequency electromagnetic energy in human head during MRI: numerical results and measurements. *IEEE Transactions on Biomedical Engineering, 43*(1), 88.

Siqueira, G., Ornetta, V. C., & Skvarca, J. (2000). Non-Ionizing Electromagnetic Radiation in the Radiofrequency Spectrum and its Effects on Human Health.

Sperber, D., Oldenbourg, R., & Dransfeld, K. (1984). Magnetic field induced temperature change in mice. *Naturwissenschaften, 71*(2), 100-101.

Subaar, C., Amoako, J. K., Darko, E. O., Ansah - Narh, T., & Dery, T. B. (2014). Finite Difference Time Domain Appraoch of Thermal Effect on Peadiatric Patients Undergoing Magnetic Resonance Imaging In

Ghana. . *Research Journal in Engineering and Applied Sciences, 3* (2), 93 - 97.

United State Food and Drug Administration (USFDA), (2016). Submission of Premarket Notifications for Magnetic Resonance Diagnostic Devices, Retrieved from: https://www.fda.gov/regulatory-information/search-fda-guidance documents/submission- premarket-notifications-magnetic-resonance-diagnostic-devices Retrieved on: (18/09/2017) at 09:50 pm;

Valberg, P. A., Van Deventer, T. E., & Repacholi, M. H. (2007). Workgroup report: base stations and wireless networks—radiofrequency (RF) exposures and health consequences. *Environmental Health Perspectives, 115*(3), 416.

Van Leeuwen, G. M., Lagendijk, J. W., Van Leersum, B. J., Zwamborn, A. P. M., Hornsleth, S. N., & Kotte, A. N. (1999). Calculation of change in brain temperatures due to exposure to a mobile phone. *Physics in medicine and biology, 44*(10), 2367.

Vander-Vorst, A., Rosen, A., & Kotsuka, Y. (2006). *RF/microwave interaction with biological tissues* (Vol. 181), Canada.: John Wiley & Sons.

Vecchia, P. (2005). The approach of ICNIRP to protection of children. *Bioelectromagnetics, 26*(S7).

Wang, Z., Lin, J. C., Mao, W., Liu, W., Smith, M. B., & Collins, C. M. (2007). SAR and temperature: simulations and comparison to regulatory limits for MRI. *Journal of Magnetic Resonance Imaging, 26*(2), 437-441.

Wang, Z., Lin, J. C., Vaughan, J. T., & Collins, C. M. (2008). Consideration of physiological response in numerical models of temperature during MRI of the human head. *Journal of Magnetic Resonance Imaging, 28*(5), 1303-1308.

Wang, Z. M., Pierson, R. N., & Heymsfield, S. B. (1992). The five-level model: a new approach to organizing body-composition research. *The American Journal of Clinical Nutrition, 56*(1), 19-28.

Weiss, C. R., Nour, S. G., & Lewin, J. S. (2008). MR-guided biopsy: A review of current techniques and applications. *Journal of Magnetic Resonance Imaging, 27*(2), 311-325.

Werner, J. (1977). Mathematical treatment of structure and function of the human thermoregulatory system. *Biological Cybernetics, 25*(2), 93-101.

Werner, J. (1994). Beneficial and detrimental effects of thermal adaptation *Thermal Balance in Health and Disease* (pp. 141-154), Bochum, Germany: Springer.

Wessapan, T., Srisawatdhisukul, S., & Rattanadecho, P. (2012). Specific absorption rate and temperature distributions in human head subjected to mobile phone radiation at different frequencies. *International Journal of Heat and Mass Transfer, 55*(1), 347-359.

World Health Organization (WHO). (2000). *Obesity: preventing and managing the global epidemic* (No. 894): Geneva, Switzerland: WHO Press.

World Health Organization (WHO). (2010). WHO research agenda for radiofrequency fields. Geneva, Switzerland: WHO Press.

Xiong, L., Yu, J., Shao, D., Zhu, H., & Wu, X. (2006). Noninvasive thermometer for HIFU and its scaling. *Ultrasonics, 44*, e31-e35.

Yang, B., Tse, K. M., Chen, N., Tan, L. B., Zheng, Q. Q., Yang, H. M., & Lee, H. P. (2014). Development of a finite element head model for the study of impact head injury. *BioMed Research International*, *2014*.

Yildirim, E. D. (2005). A mathematical model of the human thermal system. *Izmir Institute of Technology, Urla Izmir Turkey*.

Zamanian, A., & Hardiman, C. (2005). Electromagnetic radiation and human health: A review of sources and effects. *High Frequency Electronics, 4*(3), 16-26.

Zaremba, L. A. (2000). 9 FDA Guidance for Magnetic Resonance System Safety and Patient Exposures: Current Status and Future Considerations. *Magnetic Resonance Procedures: Health Effects and Safety*, 183.

Zaremba, L., & Phillips, R. (2002). *FDA guidelines for magnetic resonance equipment safety*. Paper presented at the MEDICAL PHYSICS.

Zhang, X., Yarema, K., & Xu, A. (2017). *Biological Effects of Static Magnetic Fields*: Singarepore: Springer Nature.

Zhu, M., Ackerman, J. J. H., Sukstanskii, A. L., & Yablonskiy, D. A. (2006). How the body controls brain temperature: the temperature shielding effect of cerebral blood flow. *Journal of Applied Physiology, 101*(5), 1481-1488.

APPENDICES

APPENDIX A

MRI MACHINES

A 0.3 T Permanent Magnet Airis Elite Machine Used at the Diagnostic Centre Limited Manufactured by Hitachi Medical Corporation.

A 1.5 T Superconducting Magnet MR Machine Used at the 37 Military Hospital Manufactured by Philips.

125

APPENDIX B

THE CALIBRATED THERMOMETERS

Contact and Non-contact Thermometers.

APPENDIX C

ECC PHANTOM SET UP

Assessment of Imaging Protocols and Baseline Temperature.

APPENDIX D

DATA SHEET

APPENDIX D-1: PAEDIATRICS DATA FROM MRI OF FIELD STRENGTH OF 1.5 T AT 37 MILITARY HOSPITAL.

HPT	REGION	SEX	AGE	HEIGHT	Weight	BMI	SD	TBS	TAS	TBR	TAR	ΔT(TAS-TBS)
MH001	Brain	Female	1.5	0.6	8.8	24.44	22	36	36	36.9	36.9	0.9
MH002	Brain	Female	0.7	0.35	4	32.65	21	36	36	36.8	36.8	0.8
MH003	Brain	Male	6	1	19	19	21	36	36.1	36.4	36.3	0.4
MH004	Brain	Male	0.7	0.4	5.4	33.75	20	36.2	36	36.7	36.6	0.5
MH005	Brain	Male	14	1.3	35.2	20.83	25	36.7	36.7	37.6	37.5	0.9
MH006	Brain	Female	0.7	0.38	5.1	35.32	26	36	36	36.5	36.5	0.5
MH007	Brain	Female	0.9	0.45	7.9	39.01	18	36.9	36.5	37.9	37.9	1
MH008	Brain	Male	0.8	0.6	8	22.22	19	36	36	36.6	36.6	0.6
MH009	Brain	Male	16	1.59	58.9	23.3	22	36.7	37.1	37.1		0.4
MH010	Brain	Male	4	0.79	20	32.05	32	36	36.2	36.9	36.9	0.9
MH011	Brain	Female	13	1.22	41	27.55	23	36.3	36.8	37.8	37.7	1.5
MH012	Brain	Female	13	1.22	40	26.87	26	37.7	37.8	37.9	37.8	0.2
MH013	Brain	Female	13	1.55	43	17.9	30	36		36.8		0.8
MH014	Brain	Male	4	1.17	25	18.26	26	36	36	36.5	36.3	0.5
MH015	Brain	Male	6	1.19	16.5	11.65	30	36	36	36.7	36.6	0.7
MH016	Brain	Female	14	1.26	49	30.86	28	36		36.6		0.6
MH017	Brain	Male	0.9	0.38	5	34.63	26	36	36.4	36.6	36	0.6
MH018	Brain	Female	15	1.2	52	36.11	30	37	37.4	37.8	37.5	0.8
MH019	Brain	Male	13	1.26	45	28.34	31	37	37.6	37.4	37.4	0.4
MH020	Brain	Male	11	1.11	46	37.33	28	36.8	37.4	37.3	37.1	0.5

APPENDIX D-2: PAEDIATRICS DATA FROM MRI OF FIELD STRENGTH OF 0.3 T AT 37 DIAGNOSTIC CENTRE LIMITED.

HPT	REGION	SEX	AGE	HEIGHT	Weight	BMI	SD	TBS	TAS	TBR	TAR	ΔT
DC001	Brain	Female	12	1.38	77.5	40.7	15	36		36.2		0.2
DC002	Brain	Male	13	1.4	35	17.86	20	36.2		36.7		0.5
DC003	Brain	Male	3	0.98	14	14.58	28	36.6	36.4	36.7	36.6	0.1
DC004	Brain	Male	16	1.78	80	25.25	20	36.7		37		0.3
DC005	Brain	Female	14	1.56	40	16.44	18	36.4		36.9		0.5
DC006	Brain	Female	13	1.35	40	21.95	19	36.2		36.6		0.4
DC007	Brain	Male	13	1.38	39	18.05	36	36.5		37		0.5
DC008	Brain	Female	0.9	1.38	8	14.22	20	36.3	36	36.4	36.2	0.1
DC009	Brain	Male	12	1.42	31.5	15.62	20	36.6		36.9		0.3
DC010	Brain	Female	4	0.99	15	15.3	26	36.5	36.5	36.8	36.6	0.3
DC011	Brain	Female	6	1.08	17	14.57	18	36.5	36.4	36.7	36.5	0.2
DC012	Brain	Female	15	1.5	60	26.67	20	36.5		36.7		0.2
DC013	Brain	Male	8	1.4	22	11.22	35	36.8	36.6	37	37	0.2
DC014	Brain	Male	12	1.3	36	21.3	20	36.1		36.5		0.4

HPT	REGION	SEX	AGE	HEIGHT	Weight	BMI	SD	TBS	TAS	TBR	TAR	ΔT
DC015	Brain	Male	13	1.41	33	16.6	29	36.8		37		0.2
DC016	Brain	Female	0.9	0.86	8	10.82	25	36.5	36.4	36.7	36.5	0.7
DC017	Brain	Female	10	1.35	30	16.46	32	36.8		37.2		0.4
DC018	Brain	Male	6	1.19	25	17.65	28	36.6		36.9		0.3
DC019	Brain	Male	7	1.29	27.5	16.53	34	36.7		37.9		1.2
DC020	Brain	Female	6	1	19	19	20	36	36.4	36.6	36	0.6
DC021	Brain	Male	8	1.05	28	25.4	30	36.7	36.6	37	36.9	0.3
DC022	Brain	Male	4	0.89	16	20.2	28	36	36.5	36.7	36	0.7
DC023	Brain	Female	11	1.28	38	23.19	20	36.5		36.9		0.4
DC024	Brain	Emale	14	1.57	55	22.31	43	36.6		37		0.4
DC025	Brain	Female	16	1.48	70	31.96	22	36.8		37		0.2
DC026	Brain	Male	13	1.5	45	20	28	37		37		0
DC027	Brain	Male	2	0.75	12	21.33	35	36.6	36.5	36.9	36.6	0.3
DC028	Brain	Male	13	1.48	36	16.44	25	36.7		36.8		0.1
DC029	Brain	Female	5	1.11	18	14.61	25	36.7	36.4	37	36.6	0.3

HPT	REGION	SEX	AGE	HEIGHT	Weight	BMI	SD	TBS	TAS	TBR	TAR	ΔT
DC030	Brain	Male	2	0.79	11.5	18.43	44	36.8	36.7	36.9	36.5	0.1
DC031	Knee	Female	16	1.6	50	19.53	29	37		37.1		0.1
DC032	Brain	Female	5	0.96	15	16.28	38	36	36	36.7	36.6	0.7
DC033	Brain	Female	3	0.8	14.8	23.13	30	36.2	36	36.5	36.5	0.3
DC034	Brain	Female	12	0.84	38	53.85	20	36.3	36	36.4	36.2	0.1
DC035	Brain	Female	16	1.5	48.9	21.73	40	36.6		36.9		0.3
DC036	Brain	Male	3	1.03	14	13.2	41	36.7	36.4	36.9	36.8	0.2
DC037	Brain	Female	12	1.65	89	32.69	42	36.7	36	36.7	36.7	0
DC038	Brain	Male	3	1.03	14	13.2	37	36.6	36	36.9	36.8	0.3
DC039	Brain	Male	6	0.89	17.5	22.09	40	36.6	36.1	36.7	36.6	0.1
DC040	Brain	Male	8	1.11	20	16.23	36	36	36	36.4	36.4	0.4
DC041	Brain	Female	4	0.84	16	22.68	46	36.5	36.2	36.7	36.6	0.2
DC042	Brain	Male	3	0.78	25	41.09	36	36.5	36.6	36.7	36.5	0.2
DC043	Brain	Male	1	0.8	9	14.06	44	36.9	37.3	37	37	0.1
DC044	Brain	Male	6	0.9	18	22.22	43	37	37.2	37	37	0

APPENDIX D-3: ADULTS DATA FROM MRI OF FIELD STRENGTH OF 1.5 T AND 0.3 T.

WEIGHT (kg)	HEIGHT (m)	TYMPANIC TBS (°C)	FH TBS (°C)	TYMPANIC TAS (°C)	FH TDS (°C)	FH TDS-34 (°C)	41-TDS (°C)	SCAN TIME (m)	NSA	Δ FHT (°C)	ΔTT (°C)	BMI	FH TDS-7.5 (°C)	FH TDS-33.5 (°C)
58	1.6	36	37	36.5	39	5	2	21	12	2	0.5	22.7	31.5	5.5
60.5	1.65	36	36	37.9	37	3	4	22	13	1	1.9	22.2	29.5	3.5
66.2	1.6	36.8	37	37.8	37	3	4	22	14	0	1	25.9	29.5	3.5
67	1.69	36.9	37	37.9	38	4	3	28	18	1	1	23.5	30.5	4.5
67.7	1.6	36	36	36.9	39	5	2	25	17	3	0.9	26.4	31.5	5.5
69.8	1.5	36.6	37	36.6	38	4	3	25	17	1	0	31.0	30.5	4.5
70.4	1.59	36.5	37	37.6	39	5	2	25	17	2	1.1	27.8	31.5	5.5
74	1.6	36.7	37	37.6	39	5	2	26	17	2	0.9	28.9	31.5	5.5
75	1.72	36.2	36	36.7	39	5	2	26	16	3	0.5	25.4	31.5	5.5
78	1.6	36	36	36.4	38	4	3	21	11	2	0.4	30.5	30.5	4.5
78	1.65	36.5	37	36.6	39	5	2	28	18	2	0.1	28.7	31.5	5.5
80	1.7	36	36	36.9	39	5	2	22	12	3	0.9	27.7	31.5	5.5
80	1.7	36	36	36.5	40	6	1	25	16	4	0.5	27.7	32.5	6.5
86	1.6	36.7	37	37	40	6	1	25	18	3	0.3	33.6	32.5	6.5
86.9	1.69	36	36	36.5	40	6	1	28	20	4	0.5	30.4	32.5	6.5
90	1.75	36.3	36	37.1	40	6	1	28	19	4	0.8	29.4	32.5	6.5

WEIGHT (kg)	HEIGHT (m)	TYMPANIC TBS (°C)	FH TBS (°C)	TYMPANIC TAS (°C)	FH TDS (°C)	FH TDS-34 (°C)	41-TDS (°C)	SCAN TIME (m)	NSA	Δ FHT (°C)	ΔTT (°C)	BMI	FH TDS-7.5 (°C)	FH TDS-33.5 (°C)
98.5	1.82	36	36	37.8	40	6	1	28	19	4	1.8	29.7	32.5	6.5
98.6	1.77	36	36	36.9	40	6	1	28	21	4	0.9	31.5	32.5	6.5
110.6	1.7	36.7	37	37.1	40	6	1	30	20	3	0.4	38.3	32.5	6.5
113	1.6	36.9	38	37.7	40	6	1	30	19	2	0.8	44.1	32.5	6.5
115	1.5	36	36	36.8	40	6	1	25	16	4	0.8	51.1	32.5	6.5
79	1.76	36	36	36.8	38	4	3	25	17	2	0.8	25.5	30.5	4.5
57.5	1.6	36	36	36.4	38	4	3	25	17	2	0.4	22.5	30.5	4.5
115	1.56	36	36	37	40	6	1	28	19	4	1	47.3	32.5	6.5
101	1.8	36.4	36	37	38	4	3	26	17	2	0.6	31.2	30.5	4.5
81	1.6	36.2	37	36.4	39	5	2	25	17	2	0.2	31.6	31.5	5.5
53.1	1.56	35.8	37	36.9	39	5	2	25	17	2	1.1	21.8	31.5	5.5
69.5	1.4	36.7	36	37	39	5	2	25	16	3	0.3	35.5	31.5	5.5
58	1.6	36.8	37	37	40	6	1	26	17	3	0.2	22.7	32.5	6.5
98.5	1.85	37	36	37	40	6	1	30	21	4	0	28.8	32.5	6.5
100.6	1.75	36.8	37	36.9	39	5	2	30	20	2	0.1	32.8	31.5	5.5
80	1.7	36.4	36	36.8	40	6	1	30	20	4	0.4	27.7	32.5	6.5
86	1.69	36.6	36	37	37	3	4	28	19	1	0.4	30.1	29.5	3.5

WEIGHT (kg)	HEIGHT (m)	TYMPANIC TBS (°C)	FH TBS (°C)	TYMPANIC TAS (°C)	FH TDS (°C)	FH TDS-34 (°C)	41-TDS (°C)	SCAN TIME (m)	NSA	Δ FHT (°C)	ΔTT (°C)	BMI	FH TDS-7.5 (°C)	FH TDS-33.5 (°C)
60	1.6	36.8	36	36.9	40	6	1	30	21	4	0.1	23.4	32.5	6.5
69	1.7	35.8	36	37	39	5	2	30	21	3	1.2	23.9	31.5	5.5
80	1.68	36.9	36	37	40	6	1	28	19	4	0.1	28.3	32.5	6.5
89	1.65	36.3	36	37	37	3	4	30	21	1	0.7	32.7	29.5	3.5
65	1.6	36.5	36	37	41	7	0	28	14	5	0.5	25.4	33.5	7.5
98.9	1.8	36.1	36	36.8	40	6	1	30	20	4	0.7	30.5	32.5	6.5
90	1.78	36.4	36	37	38	4	3	26	20	2	0.6	28.4	30.5	4.5
60	1.56	37	37	37	41	7	0	30	18	4	0	24.7	33.5	7.5
110.6	1.7	36.8	36	37	38	4	3	28	20	2	0.2	38.3	30.5	4.5
70	1.59	36	36	37	38	4	3	28	19	2	1	27.7	30.5	4.5
76	1.62	36	36	37	41	7	0	30	19	5	1	29.0	33.5	7.5
113	1.6	36.8	36	36.9	39	5	2	30	20	3	0.1	44.1	31.5	5.5
86	1.6	36	36	36.4	39	5	2	30	20	3	0.4	33.6	31.5	5.5
60	1.7	35.9	37	36.4	38	4	3	28	20	1	0.5	20.8	30.5	4.5
80	1.8	36	36	36.3	37	3	4	26	19	1	0.3	24.7	29.5	3.5
67	1.7	36	36	36.2	38	4	3	28	18	2	0.2	23.2	30.5	4.5
70	1.7	36	36	37	38	4	3	28	19	2	1	24.2	30.5	4.5

134

APPENDIX E

Steady State Temperature Distribution in Three Dimensions

The code of equation (45) where, $T\left[\left(i,j,k\right),\left(SAR=0,t=0\right)\right]$ was used

Tmax = 38;

Tb = 36;

L = 0.1;

[y,x] = meshgrid(-L/2:0.0005:L/2)%x = linspace(-L/2,L/2);

%y = linspace(-L/2,L/2);

*%if x.^2 + y.^2 <= (9/64)*L^2*

  *z = Tmax + (Tb - Tmax)*sin((x.^2 + y.^2)/((9/37)*L^2));*

%else

 % z = Tb;

%end

% plot(x,beta1,x,beta2, x,beta3,x,beta4,x,beta5); grid; shg

% Z = peaks(x,y)

%mesh(z)

contour(z,4000)

ylabel('y (mm)')

xlabel('x (mm)')

%zlabel('TEMPERATURE T(^{o}C)')

%title('Temperature Distribution in 3D')

title('Brain Temperature Distribution Before EMR Exposure')

%xlabel('input value/ X')

The code of Equation (40) where, $T\left[\left(i,j,k\right),\left(SAR=3.2,t=0\right)\right]$ was used

Tmax = 40;

Tb = 36.5;

135

L = 0.1;

[y,x] = meshgrid(-L/2:0.0005:L/2)%x = linspace(-L/2,L/2);

%y = linspace(-L/2,L/2);

*%if x.^2 + y.^2 <= (9/64)*L^2*

   *z = Tmax + (Tb - Tmax)*sin((x.^2 + y.^2)/((9/64)*L^2));*

%else

 %   z = Tb;

%end

% plot(x,beta1,x,beta2, x,beta3,x,beta4,x,beta5); grid; shg

% Z = peaks(x,y)

%mesh(z)

contour(z,4000)

ylabel('y (mm)')

xlabel('x (mm)')

%zlabel('TEMPERATURE T(^{o}C)')

%title('Temperature Distribution in 3D')

title('Brain Temperature Distribution After EMR Exposure')

%xlabel('input value/ X')

Code of equation (44) where $(x, y, z) \in \Gamma : T(x, y, z, t)\big|_{t \neq 0} = T_{art}(x, y, z) = 37^o C$

and $T\big[(i, j, k, t),(SAR = 3.2)\big]$

Tmax = 40;

Tb = 38;

L = 0.01;

[x,y] = meshgrid(-L/2:0.0005:L/2)%x = linspace(-L/2,L/2);

%y = linspace(-L/2,L/2);

*%if x.^2 + y.^2 <= (9/64)*L^2*

*z = Tmax + (Tb - Tmax)*cos((x.^2 + y.^2)/((9/64)*L^2));*

%else

%   z = Tb;

%end

% plot(x,beta1,x,beta2, x,beta3,x,beta4,x,beta5); grid; shg

% Z = peaks(x,y)

%mesh(z)

contour(z,6000)

ylabel('x (cm)')

xlabel('y (cm)')

%zlabel('TEMPERATURE T(oC)')

%title('Temperature Distribution in 3D')

title('Head Temperature Distribution During MRI')

%xlabel('input value/ X')

Transient State Temperature Distribution

To analyze equation (42) where

$$(x, y, z) \in \Gamma : T(x, y, z, t)\big|_{t=20.62\text{sec.}} = T_{art}(x, y, z) \neq 37^o C \text{ and}$$

$T\big[(i, j, k, t), (SAR = 3.2)\big]$ the following code was used

%%% Tiny_FDTD

Tmax =43;

Tb = 37;

L = 0.01;

SAR=3.2

%%% FDTD loop - comment out plot lines for speed

137

for n = 1:20.62;

uy = uy + coU.*(p(1:end-1, :) - p(2:end, :)); %calculate velocity in y

plane

ux = ux + coU.*(p(:, 1:end-1) - p(:, 2:end)); %calculate velocity in x

plane

p = p + coP.*([zeros(1,xDim); uy] - [uy; zeros(1,xDim)] ...

+ [zeros(yDim,1) ux] - [ux zeros(yDim,1)]);   %calculate pressure

from xy velocity

p(ceil(yDim/2),ceil(xDim/2)) = (Tb - Tmax).*cos(((xDim.*(n-t0)).^2 +

yDim.*(n-t0).^2)./((9/64).*L^2));

% exp(-.5 * ((n-t0)/width).^2); %insert hard source

surf(p); shading interp; lighting phong; colormap jet; axis off; zlim([0 1]);

%set(gcf,'Color', [0 0 0], sprintf('Tiny FDTD, step = %i', n));

title(sprintf('FDTD Time = %.2f sec',n*dt*1e3),'Color',[1 0 0],'FontSize',

22); drawnow;

end

To analyze equation (43) where

$$(x,y,z) \in \Gamma : T(x,y,z,t)\big|_{t=60.92\,\text{sec.}} = T_{art}(x,y,z) \neq 37^o C$$

and $T\big[(i,j,k,t),(SAR=3.2)\big]$ the following code was used

%% Tiny_FDTD

Tmax =43;

Tb = 37;

L = 0.01;

SAR=3.2

%% FDTD loop - comment out plot lines for speed

138

for n = 1:60.92;

uy = uy + coU.*(p(1:end-1, :) - p(2:end, :)); %calculate velocity in y

plane

ux = ux + coU.*(p(:, 1:end-1) - p(:, 2:end)); %calculate velocity in x

plane

p = p + coP.*([zeros(1,xDim); uy] - [uy; zeros(1,xDim)] ...

+ [zeros(yDim,1) ux] - [ux zeros(yDim,1)]);   %calculate pressure

from xy velocity

p(ceil(yDim/2),ceil(xDim/2)) = (Tb - Tmax).*cos(((xDim.*(n-t0)).^2 +

yDim.*(n-t0).^2)./((9/64).*L^2));

% exp(-.5 * ((n-t0)/width).^2); %insert hard source

surf(p); shading interp; lighting phong; colormap jet; axis off; zlim([0 1]);

%set(gcf,'Color', [0 0 0], sprintf('Tiny FDTD, step = %i', n));

title(sprintf('FDTD Time = %.2f sec',n*dt*1e3),'Color',[1 0 0],'FontSize',

22); drawnow;

end

To analyze equation (42) where

$(x, y, z) \in \Gamma : T(x, y, z, t)\big|_{t=1.03\min.} = T_{art}(x, y, z) \neq 37^{o}C$ and

$T\big[(i, j, k, t), (SAR = 3.2)\big]$ the following code was used

%% Tiny_FDTD

Tmax =43;

Tb = 37;

L = 0.01;

SAR=3.2

%% FDTD loop - comment out plot lines for speed

139

for n = 1:1.03;

uy = uy + coU.*(p(1:end-1, :) - p(2:end, :)); %calculate velocity in y plane

ux = ux + coU.*(p(:, 1:end-1) - p(:, 2:end)); %calculate velocity in x plane

p = p + coP.*([zeros(1,xDim); uy] - [uy; zeros(1,xDim)] ...

   + [zeros(yDim,1) ux] - [ux zeros(yDim,1)]);   %calculate pressure from xy velocity

p(ceil(yDim/2),ceil(xDim/2)) = (Tb - Tmax).*cos(((xDim.*(n-t0)).^2 + yDim.*(n-t0).^2)./((9/64).*L^2));

% exp(-.5 * ((n-t0)/width).^2); %insert hard source

surf(p); shading interp; lighting phong; colormap jet; axis off; zlim([0 1]);

%set(gcf,'Color', [0 0 0], sprintf('Tiny FDTD, step = %i', n));

title(sprintf('FDTD Time = %.2f min',n*dt*1e3),'Color',[1 0 0],'FontSize', 22); drawnow;

end

To analyze equation (42) where

$(x, y, z) \in \Gamma : T(x, y, z, t)\big|_{t=2.06\text{min.}} = T_{art}(x, y, z) \neq 37^o C$ and

$T\big[(i, j, k, t), (SAR = 3.2)\big]$ the following code was used

%% Tiny_FDTD

Tmax =43;

Tb = 37;

L = 0.01;

SAR=3.2

%% FDTD loop - comment out plot lines for speed

140

for n = 1:2.06;

   uy = uy + coU.(p(1:end-1, :) - p(2:end, :)); %calculate velocity in y*

plane

   ux = ux + coU.(p(:, 1:end-1) - p(:, 2:end)); %calculate velocity in x*

plane

   p = p + coP.([zeros(1,xDim); uy] - [uy; zeros(1,xDim)] ...*

          + [zeros(yDim,1) ux] - [ux zeros(yDim,1)]);   %calculate pressure

from xy velocity

   *p(ceil(yDim/2),ceil(xDim/2)) = (Tb - Tmax).*cos(((xDim.*(n-t0)).^2 +*

yDim.(n-t0).^2)./((9/64).*L^2));*

  *% exp(-.5 * ((n-t0)/width).^2); %insert hard source*

   surf(p); shading interp; lighting phong; colormap jet; axis off; zlim([0 1]);

   %set(gcf,'Color', [0 0 0], sprintf('Tiny FDTD, step = %i', n));

   *title(sprintf('FDTD Time = %.2f sec',n*dt*1e3),'Color',[1 0 0],'FontSize',*

22); drawnow;

end

To analyze equation (44) where

$$(x, y, z) \in \Gamma : T(x, y, z, t)\big|_{t=5.15\min.} = T_{art}(x, y, z) \neq 37^{o}C \text{ and}$$

$$T\big[(i, j, k, t), (SAR = 3.2)\big]$$

%% Tiny_FDTD

Tmax =43;

Tb = 37;

L = 0.01;

SAR=3.2

%% FDTD loop - comment out plot lines for speed

141

```
for n = 1:5.15;

    uy = uy + coU.*( p(1:end-1, :) - p(2:end, :) ); %calculate velocity in y
plane

    ux = ux + coU.*( p(:, 1:end-1) - p(:, 2:end) ); %calculate velocity in x
plane

    p = p + coP.*( [zeros(1,xDim); uy] - [uy; zeros(1,xDim)] ...
            + [zeros(yDim,1) ux] - [ux zeros(yDim,1)] );   %calculate pressure
from xy velocity

    p(ceil(yDim/2),ceil(xDim/2)) = (Tb - Tmax).*cos(((xDim.*(n-t0)).^2 +
yDim.*(n-t0).^2 )./((9/64).*L^2));

    % exp(-.5 * ((n-t0)/width).^2); %insert hard source

    surf(p); shading interp; lighting phong; colormap jet; axis off; zlim([0 1]);

    %set(gcf,'Color', [0 0 0], sprintf('Tiny FDTD, step = %i', n));

    title(sprintf('FDTD Time = %.2f sec',n*dt*1e3),'Color',[1 0 0],'FontSize',
22); drawnow;

end
```

Polynomial Fitting Codes

```
[data, textdata]=xlsread('book2.xlsx')

TBS =data(:,1);
TBR = data(:,2);
n= 1:114;
figure(1)
plot(n,TBR,'r')

hold on

plot(n,TBS,'b')
```

CURRICULUM VITAE

BIOGRAPHY OF Ms. CHRISTIANA SUBAAR

Ms. Christiana Subaar is a PhD student in Health and Radiation Physics at University of Cape Coast (UCC), Ghana but however, was employed by the Ghana Educational Service as an Assistant Director II. Born to an underprivileged family in Rural Ghana, Ms. Christiana Subaar is the first of six siblings to Mr and Mrs Gerald Suurbaar who themselves did not undergo any formal education, but saw the promising prospective of education in the then young independent Ghana under severe military rule amidst political chaos. Having to combine agronomical activities with formal education, the young Christiana survived through basic and secondary education under several financial challenges.

After enrolling into the Teacher Training College, Ms. Subaar finally had the opportunity to contribute to the educational development of other underprivileged kids like her. It was not surprising she accepted postings to Islamic basic school to help address not only the literacy gap in the Islamic community but all other girl child challenges in this minority group. Her interest in pursuing higher education rejuvenated after contributing her quota to close the minority gap. She joined the University for Development Studies to study Applied Physics, a rare field for underdeveloped African women. Her unflinching hard work and dedication saw her graduating among the best of her class. The Bachelor's degree in Physics propelled her to pursue a research carrier. Under her mentorship, she helps several undergraduate students with practical and theoretical lessons in her capacity as a Research and Teaching Assistant at the Department of Applied Physics in 2010-2011. With significant

Knowledge in statistical analysis, data manipulation and logical reasoning, it resulted in her first Journal Paper titled;

"C. Subaar, J. K. Amoako, E.O. Darko, T. Ansah-Narh and T. B. Dery, "Finite Difference Time Domain Approach of Thermal Effects on Paediatric Patients Undergoing Magnetic Resonance Imaging in Ghana", *Research Journal in Engineering and Applied Sciences (RJEAS), 2014; 3(2): 93-97"*.

Ms Subaar's research carrier led her to pursue a Master's of philosophy in Medical Physics. Prior to enrolling in the University of Ghana, Legon, she resumed her teaching role at the St. John Bosco's College of education. She worked as a tutor at the Physics department, taking theoretical and practical classes. Her research carrier was boosted after attaining her MPhiL from Legon, she has continued to research in NMRI relation to thermal effect in vulnerable patients' diagnostics. Under the mentorship of Dr. J. K. Amoako and Dr. A Owusu, she is always carrying out cutting-edge research papers both published and unpublished in a male dominant field with financing challenges. She supervised over forty (40) diploma students in educational research improvement and development. Ms. Subaar has participated in various professional research conferences at the Ghana Atomic Energy Commission, the School of Graduate Studies, University of Ghana, CSIR-EDCTP, the graduate School of Nuclear and Allied Sciences and the Ghana Education service.

Ms. Subaar is currently researching on an analytic project covering *the temperature changes in the brain during magnetic resonance imaging*, an instrumental parameter in the safety of radiation diagnosis.

A Copy of Published Paper from the Thesis

145